




26

The kinetics of complex reactions



Chain reactions

- 26.1 The structure of chain reactions
- 26.2 Explosions
- 26.3 Photochemical reactions

Polymerization kinetics

- 26.4 Chain polymerization
- 26.5 Stepwise polymerization

Catalysis and oscillation

- 26.6 Homogeneous catalysis
- 26.7 Autocatalysis
- 26.8 Oscillating reactions
- 26.9 Chemical chaos

Checklist of key ideas

Further reading

Exercises

Problems

This chapter extends the material introduced in Chapter 25 by showing how complex reaction mechanisms are treated. In particular, we deal with chain reactions, and see that either complicated or simple rate laws can be obtained, depending on the conditions. Under certain circumstances, a chain reaction can become explosive, and we see some of the reasons for this behaviour. An important application of these more complicated techniques is to the kinetics of polymerization reactions. Here we shall see that there are two major classes of polymerization process, and the average molar mass of the product varies with time in distinctive ways. Finally, we consider reactions in which the concentrations of the intermediates and products oscillate in time: although their rate laws may be well known, under certain circumstances the composition of a system may be unpredictable.

Many reactions take place by mechanisms that involve several elementary steps, and some take place at a useful rate only if a catalyst is present. Certain other reactions take place by mechanisms in which there is positive or negative feedback, in which the products of the reaction influence the rate at which more products are produced. In this chapter we see how to develop the ideas introduced in Chapter 25 to deal with these special kinds of reactions.

Chain reactions

Many gas-phase reactions and liquid-phase polymerization reactions are chain reactions. In a chain reaction, an intermediate produced in one step generates an intermediate in a subsequent step; then that intermediate generates another intermediate, and so on.

25.1 The structure of chain reactions

The intermediates in a chain reaction are called chain carriers. In a radical chain reaction the chain carriers are radicals (species with unpaired electrons). Ions may also act as chain carriers. In nuclear fission the chain carriers are neutrons.

(a) The classification of reaction steps

Chain carriers are initially formed in the initiation step of the reaction. For example, Cl atoms are formed by the dissociation of Cl₂ molecules either as a result of vigorous intermolecular collisions in a **thermolysis**, a reaction initiated by heat, or as a result of absorption of a photon in a **photolysis**, a reaction stimulated by the absorption of electromagnetic radiation. The chain carriers produced in the initiation step attack other reactant molecules in the **propagation steps**, and each attack gives rise to a new carrier. An example is the attack of a methyl radical on ethane:



(The dot signifies the unpaired electron and marks the radical.) In some cases the attack results in the production of more than one chain carrier. An example of such a **branching step** is

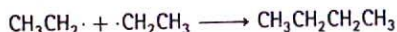


where the attack of one O atom on an H₂O molecule forms two ·OH radicals (recall that an O atom has the ground-state configuration [He]2s²2p⁴, with two unpaired electrons).

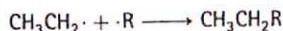
A chain carrier might attack a product molecule formed earlier in the reaction. Because this attack reduces the net rate of formation of product, it is called a **retardation step**. For example, in a photochemical reaction in which HBr is formed from H₂ and Br₂, an H atom might attack an HBr molecule, leading to H₂ and Br·:



Retardation does not end the chain, because one radical (·H) gives rise to another (·Br), but it does deplete the concentration of the product. Elementary reactions in which radicals combine and end the chain are called **termination steps**, as in



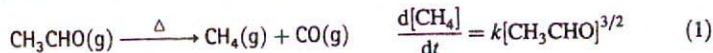
In an **inhibition step**, radicals are removed other than by chain termination, such as by reaction with the walls of the vessel or with foreign radicals:



An NO molecule has an unpaired electron and is a very efficient chain inhibitor. The observation that a reaction is quenched when NO is introduced is a good indication that a radical chain mechanism is in operation.

(b) The rate laws of chain reactions

A chain reaction can have a simple rate law. As a first example, consider the pyrolysis, or thermal decomposition in the absence of air, of acetaldehyde (ethanal, CH₃CHO), which is found to be three-halves order in CH₃CHO:



Some ethane is also detected. The Rice-Herzfeld mechanism for this reaction is as follows:

- (a) Initiation: $\text{CH}_3\text{CHO} \longrightarrow \cdot\text{CH}_3 + \cdot\text{CHO} \quad v = k_a[\text{CH}_3\text{CHO}]$
 (b) Propagation: $\text{CH}_3\text{CHO} + \cdot\text{CH}_3 \longrightarrow \text{CH}_4 + \text{CH}_3\text{CO}\cdot$
 $v = k_b[\text{CH}_3\text{CHO}][\cdot\text{CH}_3]$
 (c) Propagation: $\text{CH}_3\text{CO}\cdot \longrightarrow \cdot\text{CH}_3 + \text{CO} \quad v = k_c[\text{CH}_3\text{CO}\cdot]$
 (d) Termination: $\cdot\text{CH}_3 + \cdot\text{CH}_3 \longrightarrow \text{CH}_3\text{CH}_3 \quad v = k_d[\cdot\text{CH}_3]^2$

As we shall see, this mechanism captures the principal features of the reaction; however, it does not accommodate the formation of various by-products, such as propanone (CH_3COCH_3) and propanal ($\text{CH}_3\text{CH}_2\text{CHO}$).

To test the proposed mechanism we need to show that it leads to the observed rate law. According to the steady-state approximation (Section 25.7c), the net rate of change of the intermediates ($\cdot\text{CH}_3$ and $\text{CH}_3\text{CO}\cdot$) may be set equal to zero:

$$\begin{aligned} \frac{d[\cdot\text{CH}_3]}{dt} &= k_a[\text{CH}_3\text{CHO}] - k_b[\cdot\text{CH}_3][\text{CH}_3\text{CHO}] + k_c[\text{CH}_3\text{CO}\cdot] \\ &\quad - 2k_d[\cdot\text{CH}_3]^2 = 0 \\ \frac{d[\text{CH}_3\text{CO}\cdot]}{dt} &= k_b[\cdot\text{CH}_3][\text{CH}_3\text{CHO}] - k_c[\text{CH}_3\text{CO}\cdot] = 0 \end{aligned}$$

The sum of the two equations is

$$k_a[\text{CH}_3\text{CHO}] - 2k_d[\cdot\text{CH}_3]^2 = 0$$

which implies that the steady-state concentration of $\cdot\text{CH}_3$ radicals is

$$[\cdot\text{CH}_3] = \left(\frac{k_a}{2k_d}\right)^{1/2} [\text{CH}_3\text{CHO}]^{1/2} \quad (2)$$

It follows that the rate of formation of CH_4 is

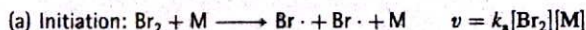
$$\frac{d[\text{CH}_4]}{dt} = k_b[\cdot\text{CH}_3][\text{CH}_3\text{CHO}] = k_b \left(\frac{k_a}{2k_d}\right)^{1/2} [\text{CH}_3\text{CHO}]^{3/2} \quad (3)$$

which is in agreement with the three-halves order observed experimentally (eqn 1). However, as already indicated, the true mechanism must be more complicated because other products are formed in significant quantities.

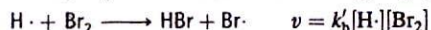
In many cases, a chain reaction leads to a complicated rate law. An example is the reaction between H_2 and Br_2 for which the empirical rate law is

$$\text{H}_2(\text{g}) + \text{Br}_2(\text{g}) \longrightarrow 2\text{HBr}(\text{g}) \quad \frac{d[\text{HBr}]}{dt} = \frac{k[\text{H}_2][\text{Br}_2]^{3/2}}{[\text{Br}_2] + k'[\text{HBr}]} \quad (4)$$

The following mechanism has been proposed to account for this rate law (Fig. 26.1):



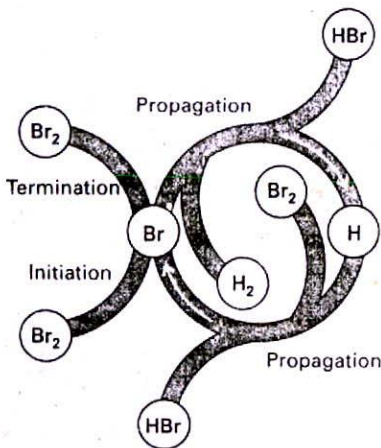
where M is either Br_2 or H_2 .



The third body M removes the energy of recombination. Other possible termination steps include the combination of H atoms to form H_2 and the combination of H and Br atoms; however, it turns out that only Br atom recombination is important. The net rate of formation of the product HBr is

$$\frac{d[\text{HBr}]}{dt} = k_b[\text{Br}\cdot][\text{H}_2] + k'_b[\text{H}\cdot][\text{Br}_2] - k_c[\text{H}\cdot][\text{HBr}]$$

We can now either analyse the rate equations numerically or look for approximate solutions and see if they agree with the empirical rate law. The latter approach is illustrated in the following example.



26.1 A schematic representation of the mechanism of the reaction between hydrogen and bromine. Note how the reactants and products are shown as arms to the circle, but the intermediates (H and Br) occur only within the circle. Similar diagrams are used to depict the action of catalysts.

Example 26.1 Deriving the rate equation of a chain reaction

Derive the rate law for the formation of HBr according to the mechanism given above.

Method Make the steady-state approximation for the concentrations of any intermediates (H· and Br· in the present case) and set the net rates of change of their concentrations equal to zero. Begin by writing down the net rates of formation of the intermediates. Set these expressions equal to zero, solve the resulting equations for the concentrations of the intermediates, and then use the resulting expressions in the equation for the net rate of formation of HBr.

Answer The net rates of formation of the two intermediates are

$$\begin{aligned}\frac{d[\text{H}\cdot]}{dt} &= k_b[\text{Br}\cdot][\text{H}_2] - k'_b[\text{H}\cdot][\text{Br}_2] - k_c[\text{H}\cdot][\text{HBr}] = 0 \\ \frac{d[\text{Br}\cdot]}{dt} &= 2k_a[\text{Br}_2][\text{M}] - k_b[\text{Br}\cdot][\text{H}_2] + k'_b[\text{H}\cdot][\text{Br}_2] + k_c[\text{H}\cdot][\text{HBr}] \\ &\quad - 2k_d[\text{Br}\cdot]^2[\text{M}] = 0\end{aligned}$$

The steady-state concentrations of the intermediates are obtained by solving these two simultaneous equations and are

$$\begin{aligned}[\text{Br}\cdot] &= \left(\frac{k_a}{k_d}\right)^{1/2} [\text{Br}_2]^{1/2} \\ [\text{H}\cdot] &= \frac{k_b(k_a/k_d)^{1/2}[\text{H}_2][\text{Br}_2]^{1/2}}{k'_b[\text{Br}_2] + k_c[\text{HBr}]}\end{aligned}$$

Note that [M] has cancelled. When we substitute these concentrations into the expression for $d[\text{HBr}]/dt$, we obtain

$$\frac{d[\text{HBr}]}{dt} = \frac{2k_b(k_a/k_d)^{1/2}[\text{H}_2][\text{Br}_2]^{3/2}}{[\text{Br}_2] + (k_c/k'_b)[\text{HBr}]}$$

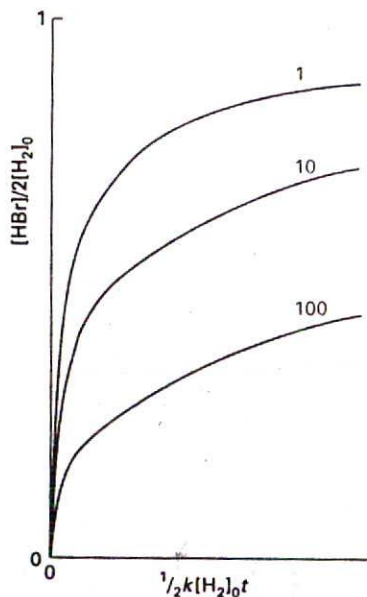
This equation has the same form as the empirical rate law (eqn 4), so the two empirical rate constants can be identified as

$$k = 2k_b \left(\frac{k_a}{k_d}\right)^{1/2} \quad k' = \frac{k_c}{k'_b}$$

Comment The presence of [HBr] in the denominator is a sign that HBr is acting as an inhibitor, and reducing the rate of formation of product. Likewise, the presence of [Br₂] stems from the role of Br₂ in the removal of the reactive ·H radicals from the chain.

Self-test 26.1 Deduce the rate law for the production of HBr when the initiation step is a photochemical process in which $\text{Br}_2 \rightarrow \text{Br}\cdot + \cdot\text{Br}$ with rate $v = I_{\text{abs}}$, where I_{abs} is the intensity of absorbed radiation.

[See eqn 6, below]



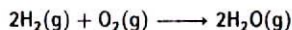
26.2 The numerical integration of the the HBr rate law, Example 26.1, can be used to explore how the concentration of HBr changes with time. These runs began with stoichiometric proportions of H₂ and Br₂; the curves are labelled with the value of $2k' - 1$.

In the examples we have considered, the observed rate laws are reproduced by the mechanisms. That used to be essentially the end of the calculation (but not of the experimental investigation). Now, though, we can make use of computers to integrate the approximate rate law numerically, and hence predict the time dependence of the HBr concentration (Fig. 26.2). Mathematical software may also be used to integrate the original coupled rate laws without needing to invoke the steady-state approximation.

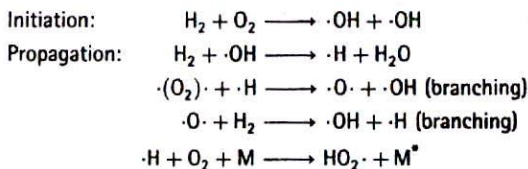
26.2 Explosions

A thermal explosion is due to the rapid increase of reaction rate with increasing temperature. If the energy released by an exothermic reaction cannot escape, the temperature of the system rises and the reaction goes faster. The acceleration of the rate results in a faster rise of temperature, so the reaction goes even faster ... catastrophically fast. A chain-branching explosion may occur when there are chain-branching steps in a reaction, for then the number of chain centres grows exponentially and the rate of reaction may cascade into an explosion.

An example of both types of explosion is provided by the reaction between hydrogen and oxygen:



Although the net reaction is very simple, the mechanism is very complex. A chain reaction is involved, and the chain carriers include $\cdot\text{H}$, $\cdot\text{O}$, $\cdot\text{OH}$, and $\cdot\text{O}_2\text{H}$. Some steps are:

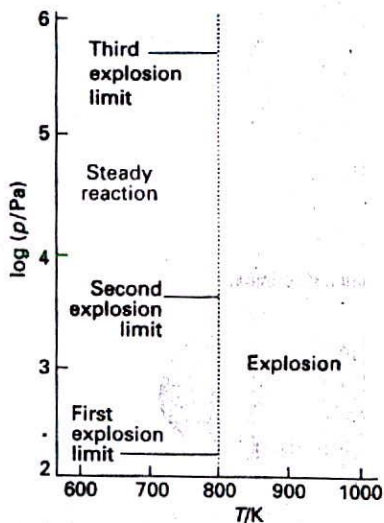


The two branching steps can lead to a chain-branching explosion. The $\text{HO}_2\cdot$ radicals are eliminated by collisions with the walls.

The occurrence of an explosion depends on the temperature and pressure of the system, and the explosion regions for the reaction are shown in Fig. 26.3. At very low pressures the system is outside the explosion region and the mixture reacts smoothly. At these pressures the chain carriers produced in the branching steps can reach the walls of the container where they combine. Increasing the pressure (along a vertical line in the illustration) takes the system through the first explosion limit (if the temperature is greater than about 730 K). The mixture then explodes because the chain carriers react before reaching the walls and the branching reactions are explosively efficient. The reaction is smooth when the pressure is above the second explosion limit. The concentration of molecules in the gas is then so great that the radicals produced in the branching reaction combine in the body of the gas, and reactions such as $\text{O}_2 + \cdot\text{H} \rightarrow \cdot\text{O}_2\text{H}$ can occur. Recombination reactions like this one are facilitated by three-body collisions because the third body (M) can remove the excess energy. At low pressures three-particle collisions are unimportant and recombination is much slower. At higher pressures, when three-particle collisions are important, the explosive propagation of the chain by the radicals is partially quenched because the branching steps are diverted into simple propagation steps (see the following example). When the pressure is increased to above the third explosion limit, the reaction rate increases so much that a thermal explosion occurs. In this limit the reaction



dominates the elimination of $\text{HO}_2\cdot$ by the walls.



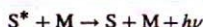
26.3 The explosion limits of the $\text{H}_2 + \text{O}_2$ reaction. In the explosive regions the reaction proceeds explosively when heated homogeneously.

Table 26.1 Photochemical processes†

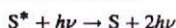
Primary absorption $S \rightarrow S^*$
followed by vibrational and rotational relaxation

Physical processesFluorescence: $S^* \rightarrow S + h\nu$

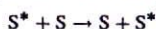
Collision-induced emission:



Stimulated emission:

Intersystem crossing (ISC): $S^* \rightarrow T^*$ Phosphorescence: $T^* \rightarrow S + h\nu$ Internal conversion (IC): $S^* \rightarrow S'$

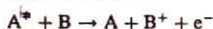
Singlet electronic energy transfer:

Energy pooling: $S^* + S^* \rightarrow S^{**} + S$

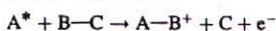
Triplet electronic energy transfer:

Triplet-triplet absorption: $T^* + h\nu \rightarrow T^{**}$ **Ionization**

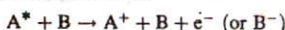
Penning ionization:



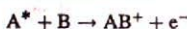
Dissociative ionization:



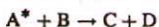
Collisional ionization:



Associative ionization:

**Chemical processes**Dissociation: $A-B^* \rightarrow A + B$ Addition or insertion: $A^* + B \rightarrow AB$

Abstraction or fragmentation:



Isomerization:



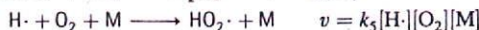
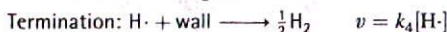
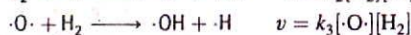
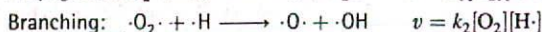
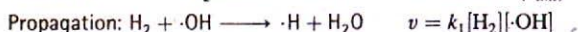
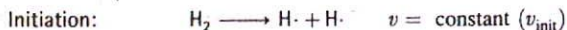
Dissociative excitation:



† S denotes a singlet state and T a triplet state; A, B, and M are arbitrary.

Example 26.2 Examining the explosion behaviour of a chain reaction

Consider the following mechanism for the reaction of hydrogen and oxygen in the fuel-rich regime:



The generic form of this reaction mechanism is



where X is a radical. Show that an explosion occurs when the rate of chain branching exceeds that of chain termination.

Method Identify the onset of explosion with the rapid increase in the concentration of radicals. Set up the rate equation for the concentration of X, and integrate it. Be alert for different behaviour depending on the branching ratio, ε , and the propagation and termination rate constants.

Answer The rate of formation of radicals is

$$\frac{d[X]}{dt} = I + \varepsilon k_a[X] - k_a[X] - k_b[X]$$

$$= I + \phi[X]$$

where

$$\phi = (\varepsilon - 1)k_a - k_b$$

The solution of this simple differential equation is

$$[X](t) = \frac{I}{\phi} (e^{\phi t} - 1)$$

When $\phi < 0$, corresponding to $k_b > (\varepsilon - 1)k_a$ (dominant termination), the concentration of X varies as

$$[X](t) = \frac{I}{k_b - k_a(\varepsilon - 1)} (1 - e^{-(k_b - k_a(\varepsilon - 1))t})$$

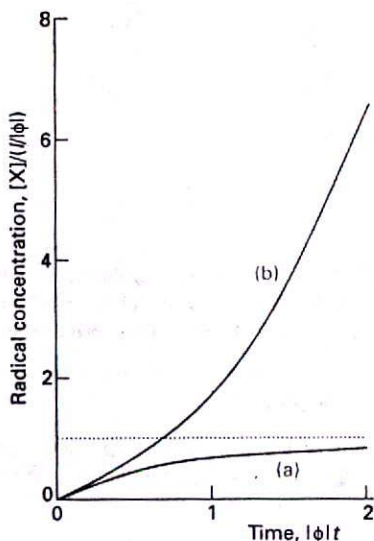
and settles into a steady state as $t \rightarrow \infty$:

$$[X](\infty) = \frac{I}{k_b - k_a(\varepsilon - 1)}$$

See Fig. 26.4a. In contrast, when $\phi > 0$, corresponding to $k_b < (\varepsilon - 1)k_a$ (dominant propagation/branching), the concentration of X increases exponentially without limit. That is, there is an explosion:

$$[X](t) = \frac{I}{k_a(\varepsilon - 1) - k_b} (e^{(k_a(\varepsilon - 1) - k_b)t} - 1)$$

This behaviour is shown in Fig. 26.4b.



26.4 The concentration of radicals (a) when termination is dominant, (b) when propagation and branching are dominant.

Comment This calculation gives an indication of the basis for the transition from smooth combustion to explosive reaction conditions.

Self-test 26.2 Calculate the variation in radical composition when the rates of propagation/branching and termination are equal.

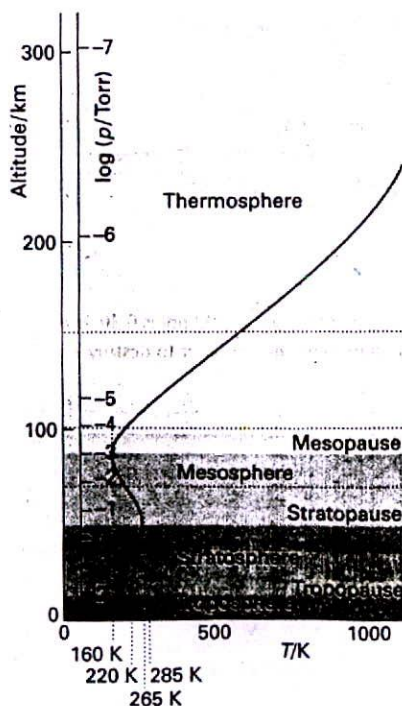
$$[[X](t) = \mathcal{I}t]$$

26.3 Photochemical reactions

Many reactions can be initiated by the absorption of light by one of the mechanisms described in Section 17.2. The most important of all are the photochemical processes that capture the radiant energy of the Sun. Some of these reactions lead to the heating of the atmosphere during the daytime by absorption of ultraviolet radiation (Fig. 26.5). Others include the absorption of red and blue light by chlorophyll and the subsequent use of the energy to bring about the synthesis of carbohydrates from carbon dioxide and water. Without photochemical processes, the world would be simply a warm, sterile, rock. A summary of the processes that can occur following photochemical excitation is given in Table 26.1.

(a) Quantum yield

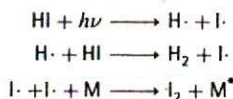
Even though a reactant molecule absorbs a photon, the excited molecule might not form products: there are many ways in which the excitation may be lost. We therefore speak of the **primary quantum yield**, ϕ , the number of reactant molecules producing specified



Production	Reaction	Loss
$\text{O} + h\nu \rightarrow \text{O}^* + e^-$	$\text{O}^* + \text{O}_2 \rightarrow \text{O}_2^* + \text{O}$	$\text{O}^* + e^- \rightarrow \text{O} + \text{O}$
$\text{N} + h\nu \rightarrow \text{N}^* + e^-$	$\text{O}^* + \text{N}_2 \rightarrow \text{NO}^* + \text{N}$	
$\text{O}_2 + h\nu \rightarrow \text{O}_2^* + e^-$	$\text{O}_2^* + \text{N}_2 \rightarrow \text{NO} + \text{NO}^*$	$\text{NO}^* + e^- \rightarrow \text{N} + \text{O}$
$\text{N}_2 + h\nu \rightarrow \text{N}_2^* + e^-$	$\text{N}_2^* + \text{O} \rightarrow \text{N} + \text{NO}^*$	
	$\text{N}_2^* + \text{O}_2 \rightarrow \text{N}_2 + \text{O}_2^*$	
$\text{O}_2 + h\nu \rightarrow \text{O}_2^* + e^-$	$\text{O}_2^* + \text{N}_2 \rightarrow \text{NO} + \text{NO}^*$	$\text{H}^+(\text{H}_2\text{O})_n + e^-$
$\text{N}_2 + h\nu \rightarrow \text{N}_2^* + e^-$	$\text{N}_2^* + \text{O} \rightarrow \text{N} + \text{NO}^*$	
	$\text{N}_2^* + \text{O}_2 \rightarrow \text{N}_2 + \text{O}_2^*$	
$\text{NO} + h\nu \rightarrow \text{NO}^* + e^-$		
$\text{O}_2 + h\nu \rightarrow \text{O} + \text{O}$	$\text{NO}^*, n\text{H}_2\text{O} \rightarrow \text{H}^+(\text{H}_2\text{O})_n$	
$\text{O}_3 + h\nu \rightarrow \text{O}_2 + \text{O}$		

26.5 The temperature profile through the atmosphere and some of the reactions that occur. The temperature peak at about 50 km is due to the absorption of solar radiation by the O_2 and N_2 ionization reactions.

primary products (atoms or ions, for instance) for each photon absorbed. As a result of one successful initiation, many reactant molecules might be consumed. The overall quantum yield, Φ , is the number of reactant molecules that react for each photon absorbed. In the photolysis of HI, for example, the processes are



The overall quantum yield is 2 because the absorption of one photon leads to the destruction of two HI molecules. In a chain reaction, Φ may be very large, and values of about 10^4 are common. In such cases the chain acts as a chemical amplifier of the initial dissociation step.

Example 26.3 Determining the quantum yield

When a sample of 4-heptanone was irradiated with 313 nm light with a power output of 50 W under conditions of total absorption for 100 s, it was found that 2.8×10^{-3} mol C_2H_4 was formed. What is the quantum yield for the formation of ethene?

Method First, calculate the amount of photons generated in an interval Δt : see Example 11.1. Then divide the amount of ethene molecules formed by the amount of photons absorbed.

Answer From Example 11.1, the amount (in moles) of photons absorbed is

$$n = \frac{P\Delta t}{(hc/\lambda)N_A}$$

If $n_{\text{C}_2\text{H}_4}$ is the amount of ethene molecule formed, the quantum yield is

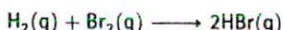
$$\begin{aligned} \Phi &= \frac{n_{\text{C}_2\text{H}_4}}{n} = \frac{n_{\text{C}_2\text{H}_4} N_A hc}{\lambda P \Delta t} \\ &= \frac{(2.8 \times 10^{-3} \text{ mol}) \times (6.022 \times 10^{23} \text{ mol}^{-1}) \times (6.626 \times 10^{-34} \text{ J s}) \times (2.997 \times 10^8 \text{ m s}^{-1})}{(50 \text{ J s}^{-1}) \times (3.13 \times 10^{-7} \text{ m}) \times (100 \text{ s})} \\ &= 0.21 \end{aligned}$$

Self-test 26.3 The overall quantum yield for another reaction at 290 nm is 0.30. For what length of time must irradiation with a 100 W source continue in order to destroy 1.0 mol of molecules?

[3.8 h]

(b) Photochemical rate laws

As an example of how to incorporate the photochemical activation step into a mechanism, consider the photochemical activation of the reaction



In place of the first step in the thermal reaction we have



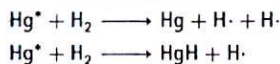
where \mathcal{I}_{abs} is the rate at which photons of the appropriate frequency are absorbed divided by the volume in which absorption occurs. It follows that \mathcal{I}_{abs} should take the place of $k_a[\text{Br}_2][\text{M}]$ in the thermal reaction scheme, so from Example 26.1 we can write

$$\frac{d[\text{HBr}]}{dt} = \frac{2k_b(1/k_d[\text{M}])^{1/2}[\text{H}_2][\text{Br}_2]\mathcal{I}_{\text{abs}}^{1/2}}{[\text{Br}_2] + (k_c/k'_b)[\text{HBr}]} \quad (6)$$

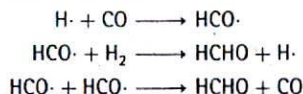
Equation 6 predicts that the reaction rate should depend on the square root of the absorbed light intensity, which is confirmed experimentally.

(c) Photosensitization

The reactions of a molecule that does not absorb directly can be stimulated if another absorbing molecule is present, because the latter may be able to transfer its energy during a collision. An example of this photosensitization is the reaction often used to generate atomic hydrogen, the irradiation of hydrogen gas containing a trace of mercury vapour using radiation of wavelength 254 nm from a mercury discharge lamp. The Hg atoms are excited (to Hg^*) by resonant absorption of the radiation, and then collide with H_2 molecules. Two reactions then take place:



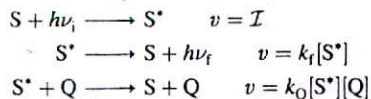
The latter reaction is the initiation step for other mercury photosensitized reactions, such as the synthesis of formaldehyde from carbon monoxide and hydrogen:



Note that the last step is termination by disproportionation rather than by combination. Photosensitization also plays an important role in solution kinetics, and molecules containing the carbonyl chromophore (such as benzophenone, $\text{C}_6\text{H}_5\text{COC}_6\text{H}_5$) are often used to trap the incident light and transfer it to some potentially reactive species.

(d) Quenching

Some photochemical reactions can be slowed down by the addition of a species that removes energy from the excited species, and its effect may be studied by monitoring the fluorescence from the excited state. Consider, for example, the scheme



in which S is an absorbing species, S^* an excited singlet state, Q a quenching agent, and $h\nu_i$ and $h\nu_f$ represent the incident and fluorescent photons, respectively. The steady-state approximation for the concentration of S^* implies that

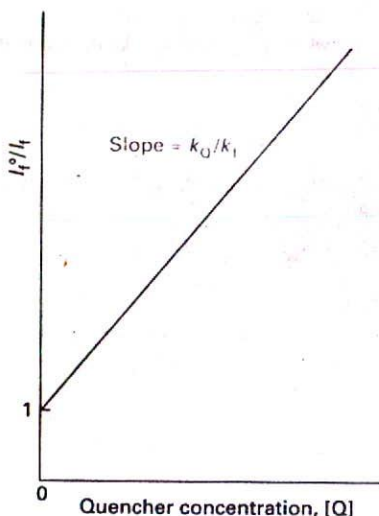
$$\frac{d[\text{S}^*]}{dt} = \mathcal{I} - (k_f + k_Q[\text{Q}])[\text{S}^*] = 0 \quad (7)$$

and hence that

$$[\text{S}^*] = \frac{\mathcal{I}}{k_f + k_Q[\text{Q}]} \quad (8)$$

The fluorescence intensity is proportional to $k_f[\text{S}^*]$, so

$$\mathcal{I}_f \propto \frac{k_f\mathcal{I}}{k_f + k_Q[\text{Q}]} \quad (9)$$



26.6 The format of a Stern–Volmer plot and the interpretation of the slope in terms of the rate constants for quenching and fluorescence.

If we denote the fluorescence intensity in the absence of Q as I_f^0 , it follows that

$$\frac{I_f^0}{I_f} = 1 + \frac{k_Q}{k_f} [Q] \quad (10)$$

Therefore, a plot of the left-hand side of this expression against $[Q]$ should be a straight line with slope k_Q/k_f . Such a plot is called a Stern–Volmer plot (Fig. 26.6); it is used to determine the rate constant for quenching.

We need to disentangle k_Q/k_f to obtain the two rate constants. To do so, the time constant of the decay can be measured in a pulse experiment. The rate law immediately after a brief flash of radiation has formed an initial concentration of S^* is

$$\frac{d[S^*]}{dt} = -(k_f + k_Q[Q])[S^*] \quad (11)$$

with the solution

$$[S^*]_t = [S^*]_0 e^{-t/\tau_f} \quad \frac{1}{\tau_f} = k_f + k_Q[Q] \quad (12)$$

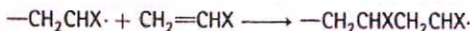
Therefore, a plot of $1/\tau_f$ (which can be obtained from the shape of the fluorescence intensity curve as a function of time) against $[Q]$ gives k_f as the intercept at $[Q] = 0$ and k_Q as the slope.

Polymerization kinetics

In chain polymerization an activated monomer, M, attacks another monomer, links to it, then that unit attacks another monomer, and so on. The monomer is used up slowly through the reaction by linking to the growing chains (Fig. 26.7). High polymers are formed rapidly and, as we shall see in detail later, only the yield and not the average molar mass of the polymer is increased by allowing long reaction times. In step polymerization any two monomers present in the reaction mixture can link together at any time (Fig. 26.8), and growth is not confined to chains that are already forming. As a result, monomers are removed early in the reaction and (as we shall see) the average molar mass of the product grows with time.

26.4 Chain polymerization

Chain polymerization results in the rapid growth of an individual polymer chain for each activated monomer. It commonly occurs by addition, often by a radical chain process. Examples include the addition polymerizations of ethene, methyl methacrylate, and styrene, as in



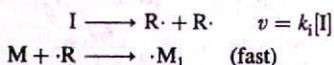
and subsequent reactions. The central feature of the kinetic analysis (which is summarized in the *Justification* below), is that the rate of polymerization is proportional to the square root of the initiator concentration:

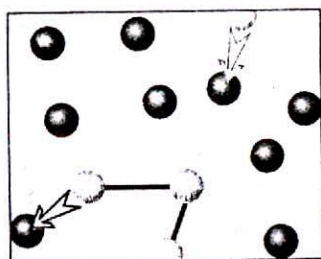
$$v = k[I]^{1/2}[M] \quad (13)$$

Justification 26.1

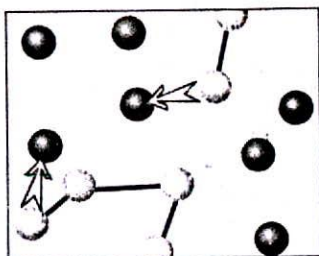
There are three basic types of reaction step in a chain polymerization process:

(a) Initiation:

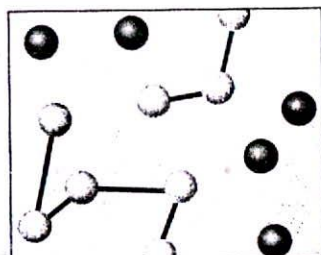




(a)

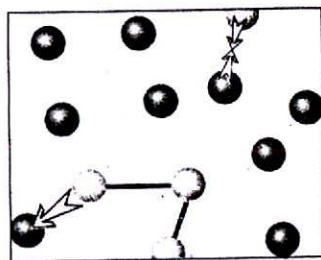


(b)

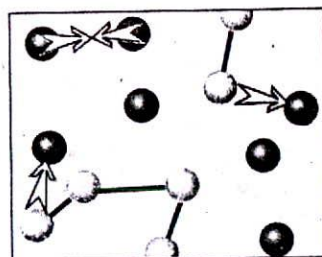


(c)

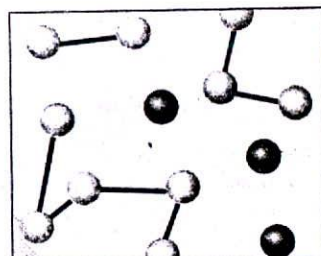
26.7 The process of chain polymerization. Chains grow as each chain acquires additional monomers.



(a)



(b)

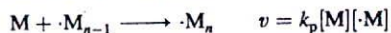
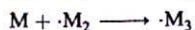
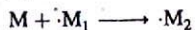


(c)

26.8 In step polymerization, growth can start at any pair of monomers, and so new chains begin to form throughout the reaction.

where I is the initiator, $R\cdot$ the radicals I forms, and $\cdot M_1$ is a monomer radical. We have shown a reaction in which a radical is produced, but in some polymerizations the initiation step leads to the formation of an ionic chain carrier. The rate-determining step is the formation of the radicals $R\cdot$ by homolysis of the initiator, so the rate of initiation is equal to the v given above.

(b) Propagation:

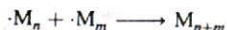


The rate at which the total concentration of radicals grows as a result of these steps is equal to the rate of the rate-determining initiation step. It follows that

$$\left(\frac{d[M]}{dt}\right)_{\text{production}} = 2\phi k_i[I] \quad (14)$$

where ϕ is the yield of the initiation step, the fraction of radicals $R\cdot$ that successfully initiate a chain.

(c) Termination:



If we suppose that the rate of termination is independent of the length of the chain, the rate law for termination is

$$v = k_t [\cdot M]^2 \quad (15)$$

and the rate of change of radical concentration by this process is

$$\left(\frac{d[\cdot M]}{dt}\right)_{\text{termination}} = -2k_t [\cdot M]^2 \quad (16)$$

In practice, other termination steps may intervene. Side reactions may also occur, such as **chain transfer**, in which the reaction



initiates a new chain at the expense of the one currently growing.

The total radical concentration is approximately constant throughout the main part of the polymerization, so the net rate of formation can be set equal to zero:

$$\frac{d[\cdot M]}{dt} = 2\phi k_i [I] - 2k_t [\cdot M]^2 = 0$$

The steady-state concentration of radical chains is therefore

$$[\cdot M] = \left(\frac{\phi k_i}{k_t}\right)^{1/2} [I]^{1/2} \quad (17)$$

Because the rate of propagation of the chains (the rate at which the monomer is consumed) is

$$\frac{d[M]}{dt} = -k_p [\cdot M][M] \quad (18)$$

it follows that

$$\frac{d[M]}{dt} = -k_p \left(\frac{\phi k_i}{k_t}\right)^{1/2} [I]^{1/2} [M] \quad (19)$$

which has the form of eqn 13.

The kinetic chain length, ν , is a measure of the efficiency of the chain propagation mechanism. It is defined as the ratio of the number of monomer units consumed per active centre produced in the initiation step:

$$\nu = \frac{\text{number of monomer units consumed}}{\text{number of active centres produced}} \quad (20)$$

The kinetic chain length is therefore equal to the ratio of the propagation and initiation rates:

$$\nu = \frac{\text{propagation rate}}{\text{initiation rate}} \quad (21)$$

Because the initiation rate is equal to the termination rate, we can write this expression (using the rate constants introduced in the *Justification*) as

$$\nu = \frac{k_p [\cdot M][M]}{2k_t [M\cdot]^2} = \frac{k_p [M]}{2k_t [\cdot M]} \quad (22)$$

When the steady-state expression, eqn 17, is substituted for the radical concentration, we obtain

$$\nu = k [\cdot M][I]^{-1/2} \quad k = \frac{1}{2} k_p (\phi k_i k_t)^{-1/2} \quad (23)$$

We see that, the slower the initiation of the chain (the smaller the initiator concentration and the smaller the initiation rate constant), the greater the kinetic chain length.

Example 26.4 Using the kinetic chain length

Estimate the average number of units in a polymer produced by a chain mechanism in which termination occurs by combination of radicals.

Method Because termination occurs by the combination of two radicals, the average number of monomers in a polymer molecule, $\langle n \rangle$, produced by the reaction is the sum of the numbers in the two combining polymer chains. The latter are both, on average, equal to ν .

Answer The average number of monomers in a product molecule is

$$\langle n \rangle = 2\nu = 2k[M][I]^{-1/2}$$

with k given in eqn 23.

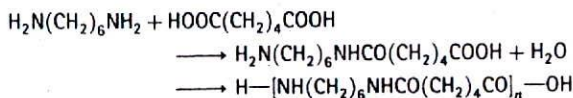
Comment We see that, the slower the initiation (as expressed by the rate constant k_i and the initiator concentration $[I]$), the longer the average chain length, and therefore the higher the average molar mass of the polymer. Some of the consequences of molar mass for polymers were explored in Chapter 23: now we see how we can exercise kinetic control over them.

Self-test 26.4 Another termination mechanism is a disproportionation reaction of the form $M\cdot + \cdot M \rightarrow M + :M$. Calculate the average polymer length.

$$[\langle n \rangle = k[\cdot M][I]^{-1/2}]$$

26.5 Stepwise polymerization

Stepwise polymerization commonly proceeds by a condensation reaction, in which a small molecule (typically H_2O) is eliminated in each step. Stepwise polymerization is the mechanism of production of polyamides, as in the formation of nylon-66:



Polyesters and polyurethanes are formed similarly (the latter without elimination). A polyester, for example, can be regarded as the outcome of the stepwise condensation of a hydroxyacid $HO-M-COOH$. We shall consider the formation of a polyester from such a monomer, and measure its progress in terms of the concentration of the $-COOH$ groups in the sample (which we denote A), for these groups gradually disappear as the condensation proceeds. Because the condensation reaction can occur between molecules containing any

number of monomer units, chains of many different lengths can grow in the reaction mixture. We shall show how to use the reaction scheme to predict molar mass distributions.

(a) The rate law of stepwise polymerization

The condensation can be expected to be overall second-order in the concentration of the -OH and -COOH (or A) groups:

$$\frac{d[A]}{dt} = -k[\text{OH}][A] \quad (24a)$$

However, because there is one -OH group for each -COOH group, this equation is the same as

$$\frac{d[A]}{dt} = -k[A]^2 \quad (24b)$$

If it is assumed that the rate constant for the condensation is independent of the chain length, then k remains constant throughout the reaction. The solution of this rate law is given by eqn 25.12, and is

$$[A] = \frac{[A]_0}{1 + kt[A]_0} \quad (25)$$

The fraction, p , of -COOH groups that have condensed at time t is

$$p = \frac{[A]_0 - [A]}{[A]_0} = \frac{kt[A]_0}{1 + kt[A]_0} \quad (26)$$

Example 26.5 Calculating the degree of polymerization

Find an expression for the growth with time of the degree of polymerization of a polymer formed by a stepwise process.

Method The number of monomers per polymer molecule is the ratio of the initial concentration of A, $[A]_0$, to the number of end groups, $[A]$, at the time of interest, because there is one A group per polymer molecule. For example, if there were initially 1000 A groups and there are now only 10, each polymer must be 100 units long on average. The value of $[A]$ can be expressed in terms of p , and hence in terms of the time by using eqn 26.

Answer The average number of monomers per polymer molecule is

$$\langle n \rangle = \frac{[A]_0}{[A]} = \frac{1}{1 - p}$$

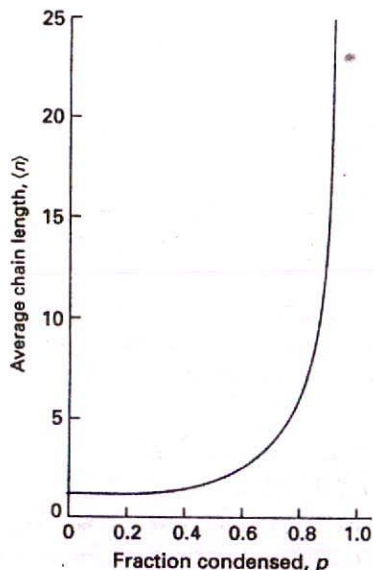
This result is illustrated in Fig. 26.9. When we substitute the value for p given in eqn 26, we find

$$\langle n \rangle = 1 + kt[A]_0$$

Comment The average length grows linearly with time so, the longer a stepwise polymerization proceeds, the higher the average molar mass of the product.

Self-test 26.5 Derive the expression for the time dependence of p for a stepwise polymerization in which the reaction is acid-catalysed by the -COOH acid functional group. The rate law is $d[A]/dt = -k[A]^2[\text{OH}]$.

$$[p = 1 - \alpha^{-1/2}, \alpha = 1 + 2kt[A]_0^2]$$



26.9 The average chain length of a polymer as a function of the fraction of reacted monomers, p . Note that p must be very close to 1 for the chains to be long.

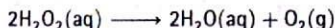
Catalysis and oscillation

If the activation energy of a reaction is high, at normal temperatures only a small proportion of molecular encounters result in reaction. A catalyst is a substance that accelerates a reaction but undergoes no net chemical change. It functions by lowering the activation energy of the reaction by providing an alternative path that avoids the slow, rate-determining step of the uncatalysed reaction, and results in a higher reaction rate at the same temperature. Catalysts can be very effective; for instance, the activation energy for the decomposition of hydrogen peroxide in solution is 76 kJ mol^{-1} , and the reaction is slow at room temperature. When a little iodide is added, the activation energy falls to 57 kJ mol^{-1} , and the rate constant increases by a factor of 2000. Enzymes, which are biological catalysts, are very specific and can have a dramatic effect on the reaction they control. The activation energy for the acid hydrolysis of sucrose is 107 kJ mol^{-1} , but the enzyme saccharase reduces it to 36 kJ mol^{-1} , corresponding to an acceleration of the reaction by a factor of 10^{12} at body temperature (310 K).

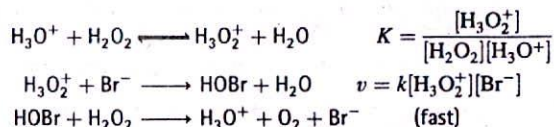
A **homogeneous catalyst** is a catalyst that is in the same phase as the reaction mixture (for example, an acid added to an aqueous solution). A **heterogeneous catalyst** is in a different phase (for example, a solid catalyst for a gas-phase reaction). We examine heterogeneous catalysis in Chapter 28 and consider only homogeneous catalysis here.

26.6 Homogeneous catalysis

Some idea of the mode of action of homogeneous catalysts can be obtained by examining the kinetics of the bromide-catalysed decomposition of hydrogen peroxide:



The reaction is believed to proceed through the following pre-equilibrium:



(In the equilibrium constant, the activity of H_2O has been set equal to 1.) Because the second step is rate-determining, the rate law of the overall reaction is obtained by setting the overall rate equal to the rate of the second step and using the equilibrium constant to express the concentration of H_3O_2^+ in terms of the reactants:

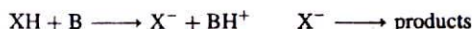
$$\frac{d[\text{O}_2]}{dt} = k_{\text{eff}}[\text{H}_2\text{O}_2][\text{H}_3\text{O}^+][\text{Br}^-] \quad k_{\text{eff}} = kK \quad (27)$$

in agreement with the observed dependence of the rate on the Br^- concentration and the pH of the solution. The observed activation energy is that of the effective rate coefficient kK . In the absence of Br^- ions the reaction cannot proceed through the path set out above, and a different and much higher activation energy is observed.

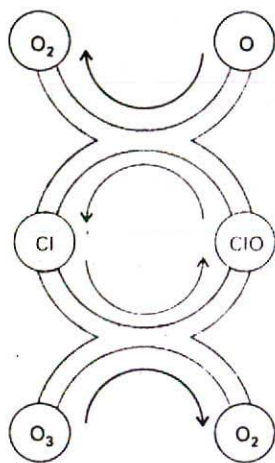
In acid catalysis the central step is the transfer of a proton to the substrate:



and is the primary process in the solvolysis of esters and keto-enol tautomerism. In base catalysis, a hydrogen ion is transferred from the substrate to a base:



It is the primary step in the isomerization and halogenation of organic compounds, and of the Claisen and aldol reactions.



26.10 A catalytic cycle showing the propagation of ozone decomposition by chlorine atoms. Note how the Cl atoms are recycled.

Homogeneous catalytic cycles play a role in atmospheric chemistry. For instance, the presence of chlorine atoms resulting from the photolysis of CFCs (chlorofluorocarbons) can participate in the decomposition of ozone in the stratosphere (Fig. 26.10):

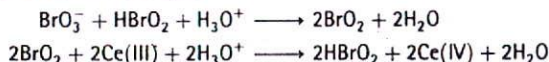


26.7 Autocatalysis

The phenomenon of autocatalysis is the catalysis of a reaction by the products. For example, in a reaction $\text{A} \rightarrow \text{P}$ it may be found that the rate law is

$$v = k[\text{A}][\text{P}] \quad (28)$$

so the reaction rate increases as products are formed. The reaction gets started because there are usually other reaction routes for the formation of some P initially, which then takes part in the autocatalytic reaction proper. An example of autocatalysis is provided by two steps in the Belousov-Zhabotinskii reaction (BZ reaction), which will figure in discussions later in the chapter:



The product HBrO_2 is a reactant in the first step.

The industrial importance of autocatalysis (which occurs in a number of reactions, such as oxidations) is that the rate of the reaction can be maximized by ensuring that the optimum concentrations of reactant and product are always present.

Example 26.6 Calculating concentrations in an autocatalytic reaction

Integrate the rate equation for the $\text{A} \rightarrow \text{P}$ autocatalytic reaction in eqn 28.

Method The rate law is given in eqn 28, with $v = -d[\text{A}]/dt$. It is convenient to write $[\text{A}] = [\text{A}]_0 - x$, $[\text{P}] = [\text{P}]_0 + x$ and then to write down the expression for the rate of change of either species in terms of x .

Answer With the substitution indicated, the rate law becomes

$$\frac{dx}{dt} = k([\text{A}]_0 - x)([\text{P}]_0 + x)$$

Integration by partial fractions, using the relation

$$\frac{1}{([\text{A}]_0 - x)([\text{P}]_0 + x)} = \frac{1}{[\text{A}]_0 + [\text{P}]_0} \left(\frac{1}{[\text{A}]_0 - x} + \frac{1}{[\text{P}]_0 + x} \right)$$

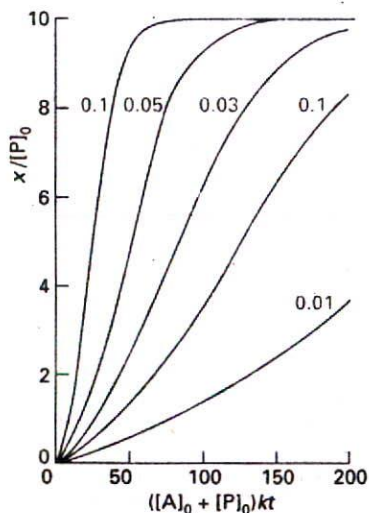
gives

$$\frac{1}{[\text{A}]_0 + [\text{P}]_0} \ln \left(\frac{([\text{P}]_0 + x)[\text{A}]_0}{([\text{P}]_0)([\text{A}]_0 - x)} \right) = kt$$

This expression can be rearranged into

$$\frac{x}{[\text{P}]_0} = \frac{e^{at} - 1}{1 + be^{at}} \quad a = ([\text{A}]_0 + [\text{P}]_0)k \quad b = \frac{[\text{P}]_0}{[\text{A}]_0}$$

Comment The solution is plotted in Fig. 26.11. The rate of reaction is slow initially (little P present), then fast (when P and A are both present), and finally slow again (when A has disappeared).



26.11 The concentration of product during the autocatalysed $\text{A} \rightarrow \text{P}$ reaction discussed in Example 26.6. Individual curves are labelled with the value of b .

Self-test 26.6 At what time is the reaction rate a maximum?

$$[t_{\text{max}} = -(1/ka) \ln b]$$



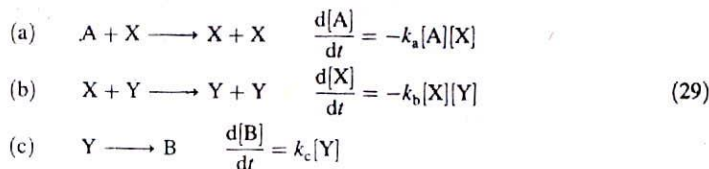
26.12 Some reactions show oscillations in time; some show spatially periodic variations. This sequence of photographs shows the emergence of a spatial pattern.

26.8 Oscillating reactions

One consequence of autocatalysis is the possibility that the concentrations of reactants, intermediates, and products will vary periodically either in space or in time (Fig. 26.12). Chemical oscillation is the analogue of electrical oscillation, with autocatalysis playing the role of positive feedback. Oscillating reactions are much more than a laboratory curiosity. While they are known to occur in only a few cases in industrial processes, there are many examples in biochemical systems where a cell plays the role of a chemical reactor. Oscillating reactions, for example, maintain the rhythm of the heartbeat. They are also known to occur in the glycolytic cycle, in which one molecule of glucose is used to produce (through enzyme-catalysed reactions involving ATP) two molecules of ATP. The concentrations of all the metabolites in the chain oscillate under some conditions, and do so with the same period but with different phases.

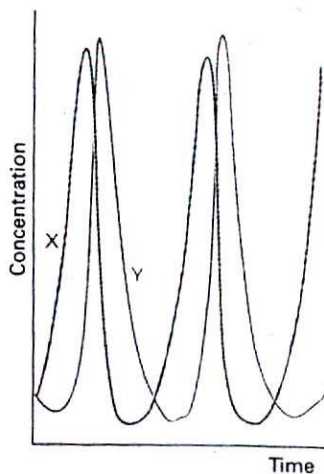
(a) The Lotka–Volterra mechanism

We shall use an autocatalytic reaction of a particularly simple form that illustrates how these oscillations may occur. The actual chemical examples that have been discovered so far have a different mechanism, as we shall see. The Lotka–Volterra mechanism is as follows:

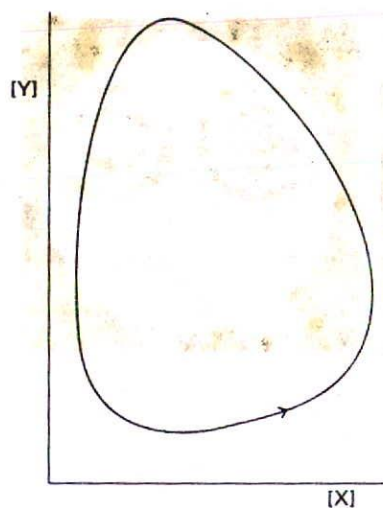


Steps (a) and (b) are autocatalytic. The concentration of A is held constant by supplying it to the reaction vessel as needed. (B plays no part in the reaction once it has been produced, so it is unnecessary to remove it; in practice, though, it would normally be removed.) These constraints leave [X] and [Y], the concentrations of the intermediates, as variables. Note that we are considering a steady-state condition, which is maintained by the flow of A into the reactor. This steady-state condition must not be confused with the steady-state approximation made earlier: in the present case we solve the rate equations exactly for the variable concentrations of X and Y, but hold [A] at an arbitrary but constant value.

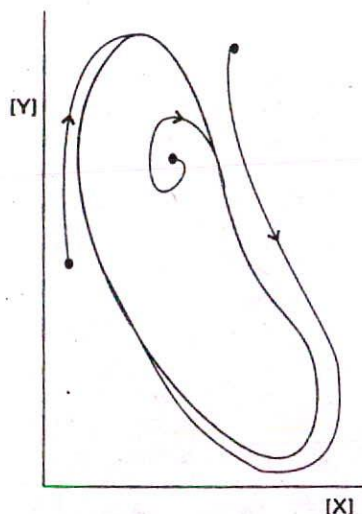
The Lotka–Volterra equations can be solved numerically, and the results can be depicted in two ways. One way is to plot [X] and [Y] against time (Fig. 26.13). The same information



26.13 The periodic variation of the concentrations of the intermediates X and Y in a Lotka–Volterra reaction. The system is in a steady state, but not at equilibrium.



26.14 An alternative representation of the periodic variation of [X] and [Y] is to plot one against the other. Then the system describes closed orbits; different orbits are obtained with different starting conditions.



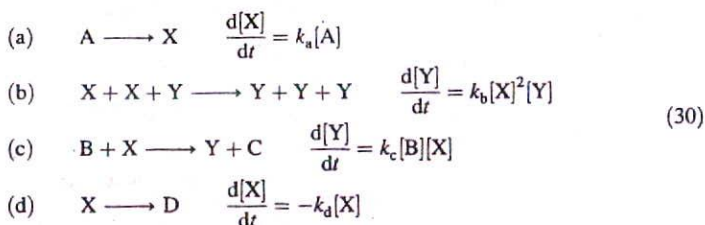
26.15 Some oscillating reactions approach a closed trajectory whatever their starting conditions. The closed trajectory (shown here in green) is called a limit cycle.

can be displayed more succinctly by plotting one concentration against the other (Fig. 26.14).

The periodic variation of the concentrations of the intermediates can be explained as follows. At some stage there may be only a little X present, but reaction (a) provides more, and the production of X autocatalyses the production of even more X. There is therefore a surge of X. However, as X is formed, reaction (b) can begin. It occurs slowly initially, because [Y] is small, but autocatalysis leads to a surge of Y. This surge, though, removes X, and so reaction (a) slows, and less X is produced. Because less X is now available, reaction (b) slows. As less Y becomes available to remove X, X has a chance to surge forward again, and so on.

(b) The brusselator

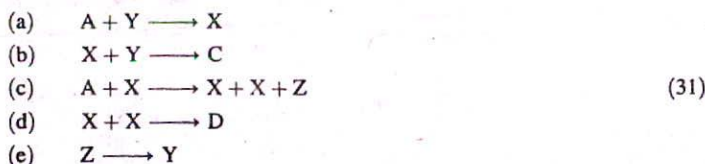
Another very interesting set of equations is called the brusselator (because it is an oscillator that originated with Ilya Prigogine's group in Brussels):



Because the reactants (A and B) are maintained at constant concentration, the two variables are the concentrations of X and Y. These two concentrations may be calculated by solving the rate equations numerically, and the results are plotted in Fig. 26.15. The interesting feature is that, whatever the initial concentrations of X and Y, the system settles down into the same periodic variation of concentrations. The common trajectory to which the system migrates is called a limit cycle, and its period depends on the values of the rate constants. A limit cycle is an example of a structure called by mathematicians an *attractor* because it appears to attract to itself trajectories in its vicinity. In conventional chemistry, which deals with closed systems of reactants and products, the equilibrium state is an attractor determined by the minimum value of the Gibbs energy at a given temperature and pressure. In open systems maintained far from equilibrium, a limit cycle may act as an attractor.

(c) The oregonator

One of the first oscillating reactions to be reported and studied systematically was the BZ reaction mentioned earlier, which takes place in a mixture of potassium bromate, malonic acid, and a cerium(IV) salt in an acidic solution. The mechanism has been elucidated by Richard Noyes, and involves 18 elementary steps and 21 different chemical species. The main features of this awesomely complex mechanism can be reproduced by the following oregonator (so called because Noyes and his group work in Oregon), where A stands for BrO_3^- , C for HBrO , D for a product, X for HBrO_2 , Y for Br^- , and Z for Ce^{4+} :



A, B, C, and D are held constant (in the model) by maintaining an influx of reactants and removal of products. The oscillations arise in a similar way to the brusselator, and can be

traced to the autocatalysis in step (c) and the linkage between the reactions provided by the other steps.

(d) Bistability

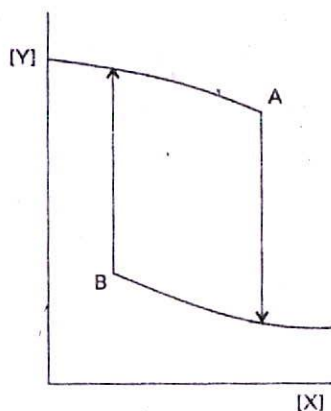
Attempts have been made to discover the underlying causes of oscillation more deeply than by simply recognizing the role of autocatalysis. It appears that in one class of systems three conditions must be fulfilled in order to obtain oscillations:

1. The reactions must be far from equilibrium.
2. The reactions must have autocatalytic steps.
3. The system must be able to exist in two steady states.

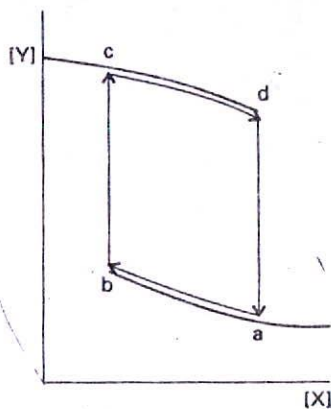
The last criterion is called **bistability**, and is a property that takes us well beyond what is familiar from the equilibrium properties of systems.

Consider a reaction in which there are two intermediates X and Y. If the concentration of Y is at some high value in a reactor, and X is added, then the concentration of Y might decrease as shown by the upper line in Fig. 26.16. If X is at some high value, then as Y is added the reaction might result in the slow increase of Y as shown by the lower line. However, in each case, a concentration may be reached at which the concentration will jump from one curve to the other (just as a supercooled liquid might suddenly solidify). The two curves represent the two stable states of the bistable system. Neither state is an equilibrium state in the thermodynamic sense: they occur in steady states that are well removed from equilibrium, and the concentrations of X and Y represent the consequences of reactants continuously flowing into and of products flowing out of the reactor.

Now consider what happens when a third type of intermediate, Z, is present. Suppose Z reacts with both X and Y. In the absence of Z the flows of material might correspond to the stable state on the upper curve of Fig. 26.17. However, as Z reacts with Y to produce X the state of the system moves along the curve (to the right, as Y decreases and X increases) until the sudden transition occurs to the lower curve. Then Z reacts with X and produces Y, which means that the composition moves to the left along the lower curve. There comes a point, however, when the concentration of X has been reduced so much, and that of Y has risen so



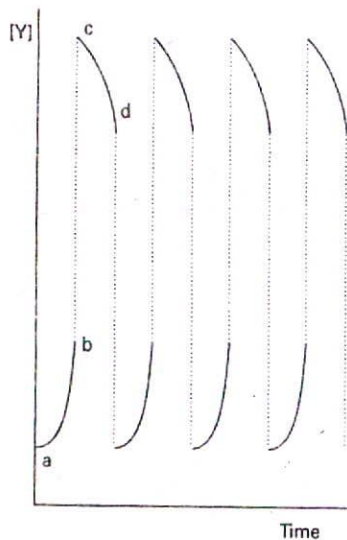
26.16 A system showing bistability. As the concentration of X is increased (by adding it to a reactor) the concentration of Y decreases along the upper curve but at A drops sharply to a low value. If X is then decreased, the concentration increases along the lower curve, but rises sharply to a high value at B.



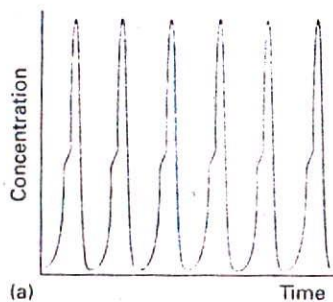
26.17 Chemical oscillation in a bistable system occurs as a result of the effect of a third substance Z which can react with X to produce Y and with Y to produce X. As a result, the system switches periodically between the upper and lower curves.

much, that there is a sudden transition to the upper curve, when the process begins again. The leaping from one stable state to another is manifest as the sudden surge or depletion of the concentration of a species (Fig. 26.18).

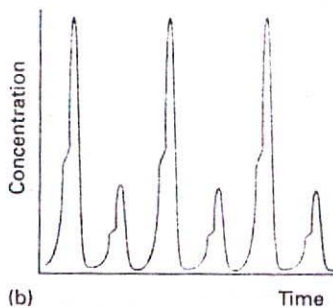
By studying the regions of concentrations and the rate constants for the individual steps of a reaction it is now becoming possible to predict the occurrence of bistable chemical systems and to anticipate the occurrence of oscillations. We are still far, however, from being able to use these ideas to account for gene expression, the patterns on tigers and butterflies, and the oscillation of cool flames, in all of which it is thought that these processes play a part.



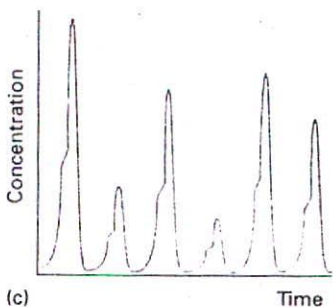
26.18 The leaping from one branch to another of a bistable system appears to the observer as a periodic surge and depletion of concentration.



(a)

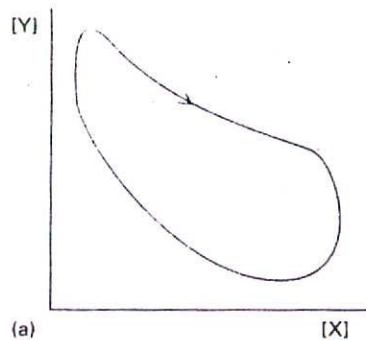


(b)

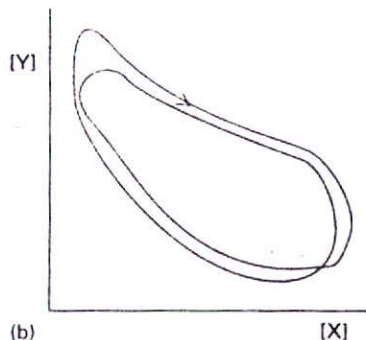


(c)

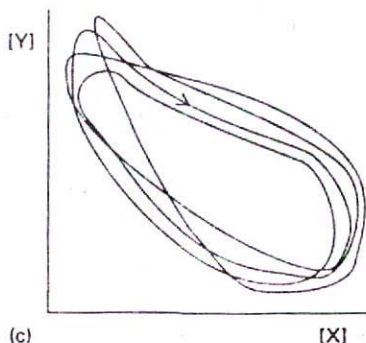
26.19 The onset of chaos as a result of period-doubling. (a) Steady-state oscillation, (b) the oscillation after one period-doubling step, (c) the chaotic regime after many period-doubling steps.



(a)

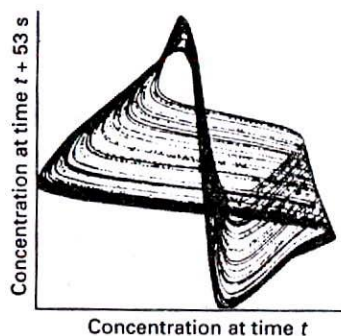


(b)



(c)

26.20 Successive trajectories in concentration space (a) before period-doubling, (b) after one period-doubling step, (c) after several period-doubling steps.



26.21 A representation of a strange attractor for a system showing chemical chaos.

26.9 Chemical chaos

A remarkable development of chemical kinetics in recent years has been the discovery of rate laws for complex reactions that have innately chaotic solutions. Specifically, it is found that the solutions of certain sets of rate laws, although fully determined by the structure of the equations, cannot be used to predict the composition of the system from its initial composition. The kinetic equations that we have been considering are of such richness that it should be hardly surprising that they, or minor elaborations of them, can display such chaotic solutions. Instead of a reaction showing periodic oscillatory behaviour, the concentrations burst into chaotic oscillation, and the concentrations of the intermediates show unpredictable amplitudes or unpredictable frequencies (Fig. 26.19). Such behaviour can be literally a matter of life and death for, should the heartbeat become chaotic, death may result. The type of chaos that stems from the structure of well-defined (and often quite simple) nonlinear differential equations is called *deterministic chaos*, for the behaviour of the solutions is predictable but infinitely sensitive to the initial conditions.

There are several ways in which a reaction can be steered into a chaotic regime. For example, in certain systems the change in a parameter (such as a flow rate through the reaction vessel or the rate of stirring) may result in the successive doubling of the period of the limit cycle (Fig. 26.20). When this period-doubling occurs, the system must circulate twice round the cycle before an initial pair of concentrations is restored. Then, after a further modification of the parameter, the period doubles again, and the limit cycle circulates four times before repeating itself. As each period doubles, the periodicity of the motion becomes less apparent, and finally appears like random fluctuations. The trajectory of the composition of the system is now highly complex, and may take a path that never retraces its path or crosses itself. Such a path is called a *strange attractor* (Fig. 26.21).

It should be understood, however, that the term 'chaos' is in some respects misleading. First, the conditions under which certain systems of differential equations display period-doubling can be specified exactly, and the progression through period-doubling cycles shows considerable regularity that is common to many classes of systems. In so far as the composition can be specified exactly, then a later composition can be predicted. Our inability to predict the composition of a system that is in a chaotic regime stems from our inability experimentally to know the initial conditions exactly or make a later determination of the composition at an exact later instant. The unpredictability of a chaotic system lies not in the formulation or solution of the differential equations that describe the rates of processes, but in our ability to relate those solutions to the practical system of interest given the inherent imprecision of experimental observations.

Checklist of key ideas

Chain reactions

- chain reaction

26.1 The structure of chain reactions

- chain carrier
 radical chain reaction
 initiation step
 thermolysis
 photolysis
 propagation step
 branching step
 retardation step

- termination step
 inhibition step
 pyrolysis
 Rice-Herzfeld mechanism
 hydrogen-bromine reaction

26.2 Explosions

- thermal explosion
 chain-branching explosion
 explosion region
 first explosion limit
 second explosion limit
 third explosion limit

26.3 Photochemical reactions

- primary quantum yield
 overall quantum yield
 photochemical rate law
 photosensitization
 Stern-Volmer plot (10)

Polymerization kinetics

- chain polymerization
 step polymerization

26.4 Chain polymerization

- chain transfer
 kinetic chain length (20)

- rate law for chain polymerization (23)

26.5 Stepwise polymerization

- fraction polymerized (26)

Catalysis and oscillation

- catalyst
 homogeneous catalyst
 heterogeneous catalyst

26.6 Homogeneous catalysis

- acid catalysis
 base catalysis

26.7 Autocatalysis

- autocatalysis
 Belousov-Zhabotinskii (BZ) reaction

26.8 Oscillating reactions

- Lotka-Volterra mechanism
 steady-state condition
 brusselator

- limit cycle
 attractor
 Oregonator
 bistability

26.9 Chemical chaos

- deterministic chaos
 period-doubling
 strange attractor

Further reading

Articles of general interest

- K.J. Laidler, Rate-controlling step: a necessary or useful concept? *J. Chem. Educ.* **65**, 250 (1988).
- A.F. Shaaban, The integrated rate equation of the nitric oxide-oxygen reaction. *J. Chem. Educ.* **67**, 869 (1990).
- J.N. Spencer, Competitive and coupled reactions. *J. Chem. Educ.* **69**, 281 (1992).
- R.T. Raines and D.E. Hansen, An intuitive approach to steady-state kinetics. *J. Chem. Educ.* **65**, 757 (1988).
- P. Engelking, Laser photochemistry. In *Encyclopedia of applied physics* (ed. G.L. Trigg), **8**, 283. VCH, New York (1994).
- G.F. Swiegers, Applying the principles of chemical kinetics to population growth problems. *J. Chem. Educ.* **70**, 364 (1993).
- J.G. Eberhardt and E. Levin, A simplified integration technique for reaction rate laws of integral order in several substances. *J. Chem. Educ.* **72**, 193 (1995).
- X. Tan, S. Lindenbaum, and N. Meltzer, A unified equation for chemical kinetics. *J. Chem. Educ.* **71**, 566 (1994).
- G.I. Gellene, Application of kinetic approximations to the $A + B \rightleftharpoons C$ reaction system. *J. Chem. Educ.* **72**, 196 (1995).
- S. Bluestone and K.Y. Yan, A method to find the rate constants in chemical kinetics of a complex reaction. *J. Chem. Educ.* **72**, 884 (1995).
- F. Mata-Perez and J.F. Perez-Benito, The kinetic rate law for autocatalytic reactions. *J. Chem. Educ.* **64**, 925 (1987).
- L.J. Soltzberg, Self-organization in chemistry. *J. Chem. Educ.* **66**, 187 (1989).
- R.J. Field, The language of dynamics. *J. Chem. Educ.* **66**, 188 (1989).
- K.L. Stevenson and O. Horváth, Reactions induced by light. In *Encyclopedia of applied physics* (ed. G.L. Trigg), **16**, 117. VCH, New York (1996).
- C.L. McCormick, Polymerization and polymer reactions. In *Encyclopedia of applied physics* (ed. G.L. Trigg), **14**, 445. VCH, New York (1996).
- R.M. Noyes, Some models of chemical oscillators. *J. Chem. Educ.* **66**, 190 (1989).
- I.R. Epstein, The role of flow systems in far-from-equilibrium dynamics. *J. Chem. Educ.* **66**, 191 (1989).
- R.J. Field and F.W. Schneider, Oscillating chemical reactions and nonlinear dynamics. *J. Chem. Educ.* **66**, 195 (1989).
- E. Hughes, Jr, Solving differential equations in kinetics by using power series. *J. Chem. Educ.* **66**, 46 (1989).
- W. Jahnke and A.T. Winfree, Recipes for Belousov-Zhabotinsky reagents. *J. Chem. Educ.* **68**, 320 (1991).
- S.K. Scott, Oscillations in simple models of chemical systems. *Acc. Chem. Res.* **20**, 186 (1987).
- P. Brumer and M. Shapiro, Coherence chemistry: controlling chemical reactions with lasers. *Acc. Chem. Res.* **22**, 407 (1989).
- H.G. Schuster, Chaotic phenomena. In *Encyclopedia of applied physics* (ed. G.L. Trigg), **3**, 189. VCH, New York (1992).

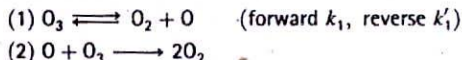
Texts and sources of data and information

- M.J. Pilling and P.W. Seakins, *Reaction kinetics*. Oxford University Press (1995).
- S.R. Logan, *Chemical kinetics*. Longman, Harlow (1996).
- F.W. Billmeyer, *Textbook of polymer science*. Wiley-Interscience, New York (1984).
- M. Kucera, *Comprehensive chemical kinetics: mechanism and kinetics of addition polymerizations*, Vol. 31. Elsevier, Amsterdam (1992).
- R.P. Wayne, *Principles and applications of photochemistry*. Oxford University Press (1988).
- R.P. Wayne, *Chemistry of atmospheres*. Clarendon Press, Oxford (1991).
- C.H. Bamford and C.F. Tipper (ed.), *Comprehensive chemical kinetics*, Vols 1-26. Elsevier, Amsterdam (1969-86).
- R.G. Compton (ed.), *Comprehensive chemical kinetics*, Vols 27-33. Elsevier, Amsterdam (1987-92).
- S.K. Scott, *Oscillations, waves, and chaos in chemical kinetics*, Oxford Chemistry Primers. Oxford University Press (1994).
- M. Boudart, *Kinetics of chemical processes*. Butterworth, London (1991).
- P. Gray and S.K. Scott, *Chemical oscillations and instabilities*. Clarendon Press, Oxford (1990).

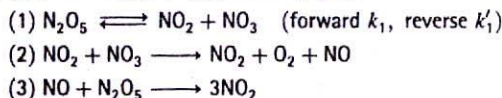
Exercises

In the following exercises and problems, it is recommended that rate constants be labelled with the number of the step in the proposed reaction mechanism, and any reverse steps be labelled similarly but with a prime.

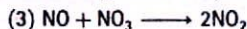
26.1 (a) Derive the rate law for the decomposition of ozone in the reaction $2\text{O}_3(\text{g}) \rightarrow 3\text{O}_2(\text{g})$ on the basis of the following proposed mechanism:



26.1 (b) On the basis of the following proposed mechanism, account for the experimental fact that the rate law for the decomposition $2\text{N}_2\text{O}_5(\text{g}) \rightarrow 4\text{NO}_2(\text{g}) + \text{O}_2(\text{g})$ is $v = k[\text{N}_2\text{O}_5]$.

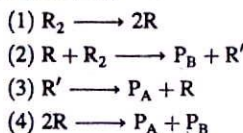


26.2 (a) A slightly different mechanism for the decomposition of N_2O_5 from that in Exercise 26.1b has also been proposed. It differs only in the last step, which is replaced by



Show that this mechanism leads to the same overall rate law.

26.2 (b) Consider the following mechanism for the thermal decomposition of R_2 :



where R_2 , P_A , P_B are stable hydrocarbons and R and R' are radicals. Find the dependence of the rate of decomposition of R_2 on the concentration of R_2 .

26.3 (a) Refer to Fig. 26.3 and determine the pressure range for a chain-branching explosion in the hydrogen-oxygen reaction at 800 K.

26.3 (b) Refer to Fig. 26.3 and determine the pressure range for a chain-branching explosion in the hydrogen-oxygen reaction at (a) 700 K, (b) 900 K.

26.4 (a) In a photochemical reaction $\text{A} \rightarrow 2\text{B} + \text{C}$, the quantum efficiency with 500 nm light is $2.1 \times 10^2 \text{ moleinstein}^{-1}$. After exposure of 300 mmol of A to the light, 2.28 mmol of B is formed. How many photons were absorbed by A?

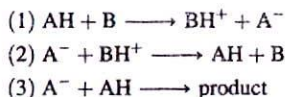
26.4 (b) In a photochemical reaction $\text{A} \rightarrow \text{B} + \text{C}$, the quantum efficiency with 500 nm light is $1.2 \times 10^2 \text{ moleinstein}^{-1}$. After exposure of 200 mmol A to the light, 1.77 mmol B is formed. How many photons were absorbed by A?

26.5 (a) In an experiment to measure the quantum efficiency of a photochemical reaction, the absorbing substance was exposed to 490 nm light from a 100 W source for 45 min. The intensity of the

transmitted light was 40 per cent of the intensity of the incident light. As a result of irradiation, 0.344 mol of the absorbing substance decomposed. Determine the quantum efficiency.

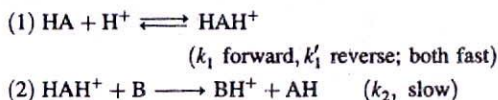
26.5 (b) In an experiment to measure the quantum efficiency of a photochemical reaction, the absorbing substance was exposed to 320 nm radiation from a 87.5 W source for 28.0 min. The intensity of the transmitted light was 0.257 that of the incident light. As a result of irradiation, 0.324 mol of the absorbing substance decomposed. Determine the quantum efficiency.

26.6 (a) The condensation reaction of propanone, $(\text{CH}_3)_2\text{CO}$, in aqueous solution is catalysed by bases, B, which react reversibly with propanone to form the carbanion $\text{C}_3\text{H}_5\text{O}^-$. The carbanion then reacts with a molecule of propanone to give the product. A simplified version of the mechanism is



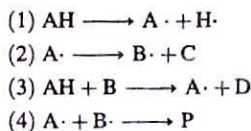
where AH stands for propanone and A^- denotes its carbanion. Use the steady-state approximation to find the concentration of the carbanion and derive the rate equation for the formation of the product.

26.6 (b) Consider the acid-catalysed reaction



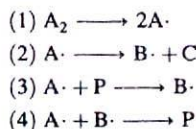
Deduce the rate law and show that it can be made independent of the specific term $[\text{H}^+]$.

26.7 (a) Consider the following chain mechanism:



Identify the initiation, propagation, and termination steps, and use the steady-state approximation to deduce that the decomposition of AH is first-order in AH.

26.7 (b) Consider the following chain mechanism:

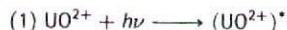


Identify any initiation, propagation, retardation, inhibition, and termination steps, and use the steady-state approximation to deduce the rate law for the consumption of A_2 .

Problems

Numerical problems

26.1 The number of photons falling on a sample can be determined by a variety of methods, of which the classical one is chemical actinometry. The decomposition of oxalic acid $(\text{COOH})_2$, in the presence of uranyl sulfate, $(\text{UO}_2)\text{SO}_4$, proceeds according to the sequence

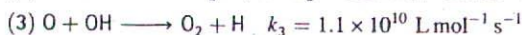
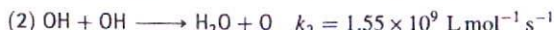
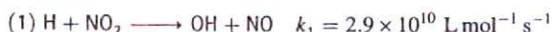


with a quantum efficiency of 0.53 at the wavelength used. The amount of oxalic acid remaining after exposure can be determined by titration (with KMnO_4) and the extent of decomposition used to find the number of incident photons. In a particular experiment, the actinometry solution consisted of 5.232 g anhydrous oxalic acid, 25.0 cm^3 water (together with the uranyl salt). After exposure for 300 s the remaining solution was titrated with 0.212 M $\text{KMnO}_4(\text{aq})$, and 17.0 cm^3 were required for complete oxidation of the remaining oxalic acid. What is the rate of incidence of photons at the wavelength of the experiment? Express the answer in photons/second and einstein/second.

26.2 When benzophenone is illuminated with ultraviolet light it is excited into a singlet state. This singlet changes rapidly into a triplet, which phosphoresces. Triethylamine acts as a quencher for the triplet. In an experiment in methanol as solvent, the phosphorescence intensity varied with amine concentration as shown below. A flash photolysis experiment had also shown that the half-life of the fluorescence in the absence of quencher is 29 μs . What is the value of k_q ?

$[Q]/(\text{mol L}^{-1})$	0.0010	0.0050	0.0100
$I_f/(\text{arbitrary units})$	0.41	0.25	0.16

26.3 Studies of combustion reactions depend on knowing the concentrations of H atoms and HO radicals. Measurements on a flow system using ESR for the detection of radicals gave information on the reactions



(J.N. Bradley, W. Hack, K. Hoyerermann, and H.G. Wagner, *J. Chem. Soc. Faraday Trans. 1*, 1889 (1973)). Using initial H atom and NO_2 concentrations of $4.5 \times 10^{-10} \text{ mol cm}^{-3}$ and $5.6 \times 10^{-10} \text{ mol cm}^{-3}$, respectively, compute and plot curves showing the O, O_2 , and OH concentrations as a function of time in the range 0–10 ns.

26.4 In a flow study of the reaction between O atoms and Cl_2 (J.N. Bradley, D.A. Whytock, and T.A. Zaleski, *J. Chem. Soc. Faraday Trans. 1*, 1251 (1973)) at high chlorine pressures, plots of $\ln([O]_0/[O])$ against distances l along the flow tube, where $[O]_0$ is the oxygen concentration at zero chlorine pressure, gave straight lines. Given the flow velocity as 6.66 ms^{-1} and the data below, find the rate coefficient for the reaction $\text{O} + \text{Cl}_2 \rightarrow \text{ClO} + \text{Cl}$.

l/cm	0	2	4	6	8	10	12	14	16	18
$\ln([O]_0/[O])$	0.27	0.31	0.34	0.38	0.45	0.46	0.50	0.55	0.56	0.60

with $[O]_0 = 3.3 \times 10^{-8} \text{ mol L}^{-1}$, $[\text{Cl}_2] = 2.54 \times 10^{-7} \text{ mol L}^{-1}$, and $p = 1.70 \text{ Torr}$.

26.5 Models of population growth are analogous to chemical reaction rate equations. In the model due to Malthus (1798) the rate of change of the population N of the planet is assumed to be given by $dN/dt = \text{births} - \text{deaths}$. The numbers of births and deaths are proportional to the population, with proportionality constants b and d . Obtain the integrated rate law. How well does it fit the (very approximate) data below on the population of the planet as a function of time?

Year	1750	1825	1922	1960	1974	1987
$N/10^9$	0.5	1	2	3	4	5

Theoretical problems

26.6 An autocatalytic reaction $\text{A} \rightarrow \text{P}$ is observed to have the rate law $d[\text{P}]/dt = k[\text{A}]^2[\text{P}]$. Solve the rate law for initial concentrations $[\text{A}]_0$ and $[\text{P}]_0$. Calculate the time at which the rate reaches a maximum.

26.7 Another reaction with the stoichiometry $\text{A} \rightarrow \text{P}$ has the rate law $d[\text{P}]/dt = k[\text{A}][\text{P}]^2$; integrate the rate law for initial concentrations $[\text{A}]_0$ and $[\text{P}]_0$. Calculate the time at which the rate reaches a maximum.

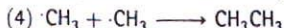
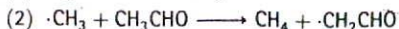
26.8 The Rice–Herzfeld mechanism for the dehydrogenation of ethane is specified in Section 26.1b, and it is noted there that it led to first-order kinetics. Confirm this remark, and find the approximations that lead to the rate law quoted there. How may the conditions be changed so that the reaction shows different orders?

26.9 Photolysis of $\text{Cr}(\text{CO})_6$ in the presence of certain molecules M, can give rise to the following reaction sequence:



Suppose that the absorbed light intensity is so weak that $I \ll k_4[\text{Cr}(\text{CO})_5\text{M}]$. Find the factor f in the equation $d[\text{Cr}(\text{CO})_5\text{M}]/dt = -f[\text{Cr}(\text{CO})_5\text{M}]$. Show that a graph of $1/f$ against $[\text{M}]$ should be a straight line.

26.10 The following mechanism has been proposed for the thermal decomposition of acetaldehyde (ethanal):



Find an expression for the rate of formation of methane and the rate of disappearance of acetaldehyde.

26.11 Express the root mean square deviation, $\{ \langle M^2 \rangle - \langle \bar{M} \rangle^2 \}^{1/2}$, of the molar mass of a condensation polymer in terms of p , and deduce its time dependence.

26.12 Calculate the ratio of the mean cube molar mass to the mean square molar mass in terms of (a) the fraction p , (b) the chain length.

26.13 Derive an expression for the rate of disappearance of a species A in a photochemical reaction for which the mechanism is:

- (1) initiation with light of intensity I , $A \xrightarrow{h\nu} 2R\cdot$
- (2) propagation, $A + R\cdot \longrightarrow R\cdot + B$
- (3) termination, $R\cdot + R\cdot \longrightarrow R_2$

Hence, show that rate measurements will give only a combination of k_2 and k_3 if a steady state is reached, but that both may be obtained if a steady state is not reached.

26.14 The photochemical chlorination of chloroform in the gas phase has been found to follow the rate law $d[CCl_3]/dt = k[Cl_2]^{1/2}I^{1/2}$. Devise a mechanism that leads to this rate law when the chlorine pressure is high.

26.15 Conventional equilibrium considerations do not apply when a reaction is being driven by light absorption. Thus the steady-state concentration of products and reactants might differ significantly from equilibrium values. For instance, suppose the reaction $A \rightarrow B$ is driven by light absorption, and that its rate is I_a , but that the reverse reaction $B \rightarrow A$ is bimolecular and second-order with a rate $k[B]^2$. What is the stationary state concentration of B? Why does this 'photostationary state' differ from the equilibrium state?

26.16 Write a program for the integration of the Lotka-Volterra equations and arrange for it to plot the concentration of Y against that of X. Explore the consequences of varying the starting concentrations for the integration. Identify the conditions (the concentrations of X and Y) corresponding to the steady state of the Lotka-Volterra equations (the point at the centre of the orbits).

26.17 Set up the overall rate equations for the concentrations of X and Y in terms of the Oregonator and explore the periodic properties of the solutions.

26.18 Many biological and biochemical processes involve autocatalytic steps. In the SIR model of the spread and decline of infectious diseases the population is divided into three classes; the susceptibles, S, who can catch the disease, the infectives, I, who have the disease and can transmit it, and the removed class, R, who have either had the disease and recovered, are dead, or are immune or isolated. The model mechanism for this process implies the following rate laws:

$$\frac{dS}{dt} = -rSI \quad \frac{dI}{dt} = rSI - aI \quad \frac{dR}{dt} = aI$$

What are the autocatalytic steps of this mechanism? Find the conditions on the ratio a/r that decide whether the disease will spread (an epidemic) or die out. Show that a constant population is built into this system, namely that $S + I + R = N$, meaning that the timescales of births, deaths by other causes, and migration are assumed large compared to that of the spread of the disease.

Additional problems supplied by Carmen Giunta and Charles Trapp

26.19 J.D. Chapple-Sokol, C.J. Giunta, and R.G. Gordon (*J. Electrochem. Soc.* 136, 2993 (1989)) proposed the following radical chain mechanism for the initial stages of the gas-phase oxidation of silane by nitrous oxide:

- (1) $N_2O \longrightarrow N_2 + O$
- (2) $O + SiH_4 \longrightarrow SiH_3 + OH$
- (3) $OH + SiH_4 \longrightarrow SiH_3 + H_2O$
- (4) $SiH_3 + N_2O \longrightarrow SiH_3O + N_2$
- (5) $SiH_3O + SiH_4 \longrightarrow SiH_3OH + SiH_3$
- (6) $SiH_3 + SiH_3O \longrightarrow (H_3Si)_2O$

Label each step with its role in the chain. Use the steady-state approximation to show that this mechanism predicts the following rate law for SiH_4 consumption (provided k_1 and k_6 are in some sense small):

$$\frac{d[SiH_4]}{dt} = -k[N_2O][SiH_4]^{1/2}$$

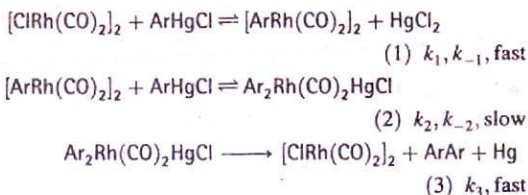
26.20 Ultraviolet radiation photolyses O_3 to O_2 and O. Determine the rate at which ozone is consumed by 305 nm radiation in a layer of the stratosphere of thickness 1 km. The quantum efficiency is 0.94 at 220 K, the concentration about $8 \times 10^{-9} \text{ mol L}^{-1}$, the molar absorption coefficient $260 \text{ L mol}^{-1} \text{ cm}^{-1}$, and the flux of 305 nm radiation about $1 \times 10^{14} \text{ photons cm}^{-2} \text{ s}^{-1}$. Data from W.B. DeMore, S.P. Sander, D.M. Golden, R.F. Hampson, M.J. Kurylo, C.J. Howard, A.R. Ravishankara, C.E. Kolb, and M.J. Molina, *Chemical kinetics and photochemical data for use in stratospheric modeling: Evaluation Number 11*, JPL Publication 94-26 (1994).

26.21 Arylmercury compounds have played an ever-increasing role in organic synthesis in recent years because of their ability to accommodate almost all important organic functional groups and their chemical and thermal stability. Y. Wang (*Int. J. Chem. Kinet.* 25, 91 (1993)) has studied the kinetics and mechanism of the dimerization of arylmercurials (A), with formulas XC_6H_4HgCl (X = H, p-CH₃, m-CH₃, o-CH₃, p-Cl, and others) catalysed by $[CIRh(CO)_2]_2$ (C) in hexamethylphosphoramide (HMPA). The observed dimerization in each case is represented by the equation $2ArHgCl \rightarrow ArAr + HgCl_2 + Hg$, and plots of $x/([A]_0 - x)$, where x is the molar concentration of the arylmercury compound reacted and $[A]_0$ the initial concentration, was found to be a linear function of time. In each case, $[A]_0 = 0.100 \text{ mol L}^{-1}$ and $[C] = 5.00 \times 10^{-4} \text{ mol L}^{-1}$. Concentration data as a function of time at 60°C for the compounds with X = H and Cl are

X = H	$x/([A]_0 - x)$	0.14	0.48	0.63	0.84	1.12
	t/min	25	85	115	150	205
X = p-Cl	$x/([A]_0 - x)$	0.04	0.27	0.60	1.05	
	t/min	30	123	236	405	

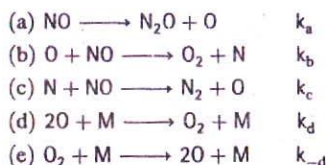
Similar results were obtained for the other compounds in the series. (a) Plot these data and confirm that the reactions are second-order.

Would the first-order integrated rate law fit the data too? (b) The proposed mechanism for these reactions is



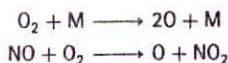
Derive the rate law for the rate of disappearance of ArHgCl and determine the conditions under which this mechanism supports the experimental results.

26.22 Because of its importance in atmospheric chemistry, the thermal decomposition of nitric oxide, $2\text{NO}(\text{g}) \rightarrow \text{N}_2(\text{g}) + \text{O}_2(\text{g})$, has been among the most thoroughly studied of gas phase reactions. The commonly accepted mechanism has been that of H. Wise and M.F. Frech (*J. Chem. Phys.* 22, 1724 (1952)):



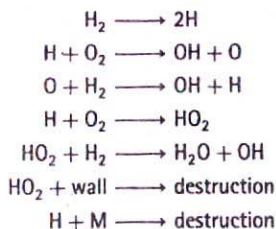
(a) Label the steps of this mechanism as initiation, propagation, etc. (b) Write down the full expression for the rate of disappearance of NO. What does this expression for the rate become on the basis of the assumptions that $v_b = v_c$ when [N] reaches its steady-state concentration, that the rate of the propagation step is more rapid than the rate of the initiation step, and that oxygen atoms are in equilibrium with oxygen molecules? (c) Find an expression for the effective activation energy, $E_{a,\text{eff}}$, for the overall reaction in terms of the activation energies of the individual steps of the reaction. (d) Estimate $E_{a,\text{eff}}$ from the bond energies of the species involved. (e) It has been pointed out by R.J. Wu and C.T. Yeh (*Int. J. Chem. Kinet.* 28, 89 (1996)) that the reported experimental values of $E_{a,\text{eff}}$ obtained by different authors have varied from 253 to 357 kJ mol^{-1} . They suggest that the assumption of oxygen atoms and oxygen molecules being in equilibrium is unwarranted and that the steady-state approximation needs to be applied to the entire mechanism. Obtain the overall rate law based on the steady-state approximation and find the forms that it assumes for low NO conversion (low O_2 concentration). (f) When the

reaction conversion becomes significant, Wu and Yeh suggest that two additional elementary steps,



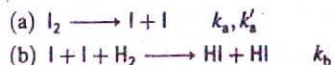
start to compete with step (a) as the initiation step. Obtain the rate laws based on these alternative mechanisms and again estimate the apparent activation energies. Is the range of these different theoretically estimated values for $E_{a,\text{eff}}$ consistent with the range of values obtained experimentally?

26.23 The water formation reaction has been studied many times and continues to be of interest. Despite the many studies there is not uniform agreement on the mechanism. But, as explosions are known to occur at certain critical values of the pressure, any proposed mechanism that is to be considered plausible must be consistent with the existence of these critical explosion limits. One such plausible mechanism is that of Example 26.2. Another is the following:



In a manner similar to that in Example 26.2, determine whether or not this mechanism can lead to explosions under appropriate conditions.

26.24 For many years the reaction $\text{H}_2(\text{g}) + \text{I}_2(\text{g}) \rightarrow 2\text{HI}(\text{g})$ and its reverse were assumed to be elementary bimolecular reactions. However, J.H. Sullivan (*J. Chem. Phys.* 46, 73 (1967)) suggested that the following mechanism for the reaction, originally proposed by M. Bodenstein (*Z. physik. Chem.* 29, 56 (1898)), provides a better explanation of the experimental results:




Obtain the expression for the rate of formation of HI based on this mechanism. Under what conditions does this rate law reduce to the one for the originally accepted mechanism?



27

Molecular reaction dynamics



Reactive encounters

- 27.1 Collision theory
- 27.2 Diffusion-controlled reactions
- 27.3 The material balance equation

Activated complex theory

- 27.4 The reaction coordinate and the transition state
- 27.5 The Eyring equation
- 27.6 Thermodynamic aspects

The dynamics of molecular collisions

- 27.7 Reactive collisions
- 27.8 Potential energy surfaces
- 27.9 Some results from experiments and calculations

Checklist of key ideas

Further reading

Exercises

Problems

The simplest quantitative account of reaction rates is in terms of collision theory, which can be used only for the discussion of reactions between simple species in the gas phase. Reactions in solution can be classified into two types: diffusion-controlled and activation-controlled. The former can be expressed quantitatively in terms of the diffusion equation. In activated complex theory, it is assumed that the reactant molecules form a complex that can be discussed in terms of the population of its energy levels. Activated complex theory inspires a thermodynamic approach to reaction rates, in which the rate constant is expressed in terms of thermodynamic parameters. This approach is useful for parametrizing the rates of reactions in solution. The highest level of sophistication is in terms of potential energy surfaces and the motion of molecules through these surfaces. As we shall see, such an approach gives a very intimate picture of the events that occur when reactions occur, and is open to experimental study.

Now we are at the heart of chemistry. Here we examine the details of what happens to molecules at the climax of reactions. Extensive changes of structure are taking place and energies the size of dissociation energies are being redistributed among bonds: old bonds are being ripped apart and new bonds are being formed.

As may be imagined, the calculation of the rates of such processes from first principles is very difficult. Nevertheless, like so many intricate problems, the broad features can be established quite simply, and only when we enquire more deeply do the complications emerge. In this chapter we look at three levels of approach to the calculation of a rate constant for an elementary bimolecular reaction. Although a great deal of information can be obtained from gas-phase reactions, many reactions of interest take place in solution, and we shall also see to what extent their rates can be predicted.

Reactive encounters

In this section we consider two elementary approaches to the calculation of reaction rates, one relating to gas-phase reactions and the other to reactions in solution. Both approaches

are based on the view that reactant molecules must meet, and that reaction takes place only if they have a certain minimum energy. In the collision theory of bimolecular gas-phase reactions, which we mentioned briefly in Section 25.5b, products are formed only if the collision is sufficiently energetic; otherwise the colliding reactant molecules separate again. In solution, the reactant molecules may simply diffuse together and then acquire energy from their immediate surroundings while they are in contact.

27.1 Collision theory

We shall consider the bimolecular elementary reaction



where P denotes products, and aim to calculate the second-order rate constant k_2 .

We can anticipate the general form of the expression for k_2 by considering the physical requirements for reaction. We can expect the rate v to be proportional to the rate of collisions, and therefore to the mean speed of the molecules, $\bar{c} \propto (T/M)^{1/2}$ where M is the molar mass of the molecules, their collisional cross-section, σ , and the number densities of A and B:

$$v \propto \sigma \left(\frac{T}{M}\right)^{1/2} N_A N_B \propto \sigma \left(\frac{T}{M}\right)^{1/2} [A][B]$$

However, a collision will be successful only if the kinetic energy exceeds a minimum value, the activation energy, E_a , of the reaction. This requirement suggests that the rate constant should also be proportional to a Boltzmann factor of the form $e^{-E_a/RT}$. So we can anticipate, by writing the reaction rate in the form given in eqn 1, that

$$k_2 \propto \sigma \left(\frac{T}{M}\right)^{1/2} e^{-E_a/RT}$$

However, not every collision will lead to reaction even if the energy requirement is satisfied, because the reactants may need to collide in a certain relative orientation. This 'steric requirement' suggests that a further factor, P , should be introduced, and that

$$k_2 \propto P \sigma \left(\frac{T}{M}\right)^{1/2} e^{-E_a/RT} \quad (2)$$

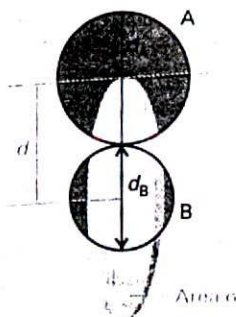
As we shall see in detail below, this expression has the form predicted by collision theory. It reflects three aspects of a successful collision:

$$k_2 \propto \text{steric requirement} \times \text{encounter rate} \\ \times \text{minimum energy requirement}$$

(a) Collision rates in gases

We have anticipated that the reaction rate, and hence k_2 , depends on the frequency with which molecules collide. The collision density, Z_{AB} , is the number of (A, B) collisions in a region of the sample in an interval of time divided by the volume of the region and the duration of the interval. The frequency of collisions of a single molecule in a gas was calculated in Section 1.3b. As shown in the *Justification* on the following page, that result can be adapted to deduce that

$$Z_{AB} = \sigma \left(\frac{8kT}{\pi\mu}\right)^{1/2} N_A^2 [A][B] \quad (3)$$



27.1 The collision cross-section for two molecules can be regarded to be the area within which the centre of the projectile molecule (A) must enter around the target molecule (B) in order for a collision to occur. If the diameters of the two molecules are d_A and d_B , the radius of the target area is $d = \frac{1}{2}(d_A + d_B)$ and the cross-section is πd^2 .

where σ is the collision cross-section (Fig. 27.1):

$$\sigma = \pi d^2 \quad d = \frac{1}{2}(d_A + d_B) \quad (4)$$

and μ is the reduced mass,

$$\mu = \frac{m_A m_B}{m_A + m_B} \quad (5)$$

Similarly, the collision density for like molecules at a molar concentration $[A]$ is

$$Z_{AA} = \sigma \left(\frac{4kT}{\pi m_A} \right)^{1/2} N_A^2 [A]^2 \quad (6)$$

Collision densities may be very large. For example, in nitrogen at room temperature and pressure, with $d = 280$ pm, $Z = 5 \times 10^{34} \text{ m}^{-3} \text{ s}^{-1}$.

Justification 27.1

It follows from eqn 1.30 that the collision frequency, z , for a single A molecule of mass m_A in a gas of other A molecules is

$$z = \sigma \bar{c}_{\text{rel}} N_A \quad (7)$$

where N_A is the number density of A molecules and \bar{c}_{rel} is their relative mean speed. As indicated in Section 1.3,

$$\bar{c}_{\text{rel}} = 2^{1/2} \bar{c} \quad \bar{c} = \left(\frac{8kT}{\pi m} \right)^{1/2} \quad (8)$$

For future convenience, it is sensible to introduce $\mu = \frac{1}{2}m$ (for like molecules of mass m), and then to write

$$\bar{c}_{\text{rel}} = \left(\frac{8kT}{\pi \mu} \right)^{1/2} \quad (9)$$

This expression also applies to the mean relative speed of dissimilar molecules, provided that μ is interpreted as the reduced mass in eqn 5.

The total collision density is the collision frequency multiplied by the number density of A molecules:

$$Z_{AA} = \frac{1}{2} z N_A = \frac{1}{2} \sigma \bar{c}_{\text{rel}} N_A^2 \quad (10)$$

The factor of $\frac{1}{2}$ has been introduced to avoid double counting of the collisions (so one A molecule colliding with another A molecule is counted as one collision regardless of their actual identities). For collisions of A and B molecules present at number densities N_A and N_B , the collision density is

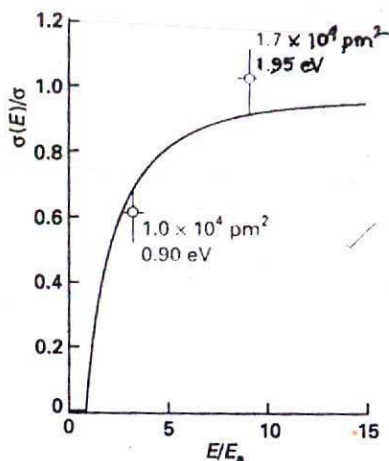
$$Z_{AB} = \sigma \bar{c}_{\text{rel}} N_A N_B \quad (11)$$

Note that we have discarded the factor of $\frac{1}{2}$ because now we are considering an A molecule colliding with any of the B molecules as a collision.

The number density of a species J is $N_J = N_A [J]$, where $[J]$ is their molar concentration and N_A is the Avogadro constant. Equations 3 and 6 then follow.

(b) The energy requirement

According to collision theory, the rate of change in the molar concentration of A molecules is the product of the collision density and the probability that a collision occurs with sufficient energy. The latter condition can be incorporated by writing the collision cross-



27.2 The variation of the reactive cross-section with energy as expressed by eqn 15. The data points are from experiments on the reaction $\text{H} + \text{D}_2 \rightarrow \text{HD} + \text{D}$. (K. Tsukiyama, B. Katz, and R. Bersohn, *J. Chem. Phys.* 84, 1934 (1986).)

section as a function of the kinetic energy of approach of the two colliding species, and setting the cross-section, $\sigma(\varepsilon)$, equal to zero if the kinetic energy of approach is below a certain threshold value, ε_a . Later, we shall identify $N_A \varepsilon_a$ as E_a , the (molar) activation energy of the reaction. Then, for a collision with a specific relative speed of approach v_{rel} (not, at this stage, a mean value),

$$\frac{d[A]}{dt} = -\sigma(\varepsilon)v_{\text{rel}}N_A[A][B] \quad (12)$$

The relative kinetic energy, ε , and the relative speed are related by $\varepsilon = \frac{1}{2}\mu v_{\text{rel}}^2$, so $v_{\text{rel}} = (2\varepsilon/\mu)^{1/2}$. At this point we recognize that a wide range of approach energies is present in a sample, so we should average the expression just derived over a Boltzmann distribution of energies, write

$$\frac{d[A]}{dt} = -\left\{ \int_0^\infty \sigma(\varepsilon)v_{\text{rel}}f(\varepsilon) d\varepsilon \right\} N_A[A][B] \quad (13)$$

and hence recognize the rate constant as

$$k_2 = N_A \int_0^\infty \sigma(\varepsilon)v_{\text{rel}}f(\varepsilon) d\varepsilon \quad (14)$$

Now suppose that the reactive collision cross-section is zero below ε_a and that above that energy it varies as

$$\sigma(\varepsilon) = \left(1 - \frac{\varepsilon_a}{\varepsilon}\right)\sigma \quad (15)$$

This form of the energy dependence is broadly consistent with experimental determinations of the reaction between H and D_2 as determined by molecular beam measurements of the kind described later (Fig. 27.2). Then, in the *Justification* below, we show that

$$k_2 = N_A \sigma \bar{v}_{\text{rel}} e^{-E_a/RT} \quad (16)$$

Justification 27.2

The Maxwell-Boltzmann distribution of molecular speeds is given in Section 1.3a. It may be expressed in terms of the kinetic energy, ε , by writing $\varepsilon = \frac{1}{2}mv^2$, then $dv = d\varepsilon/(2m\varepsilon)^{1/2}$ and eqn 1.22 becomes

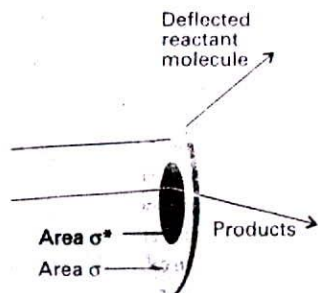
$$\begin{aligned} f(v) dv &= 4\pi \left(\frac{m}{2\pi kT}\right)^{3/2} \left(\frac{2\varepsilon}{m}\right) e^{-\varepsilon/kT} \frac{d\varepsilon}{(2m\varepsilon)^{1/2}} \\ &= 2\pi \left(\frac{1}{\pi kT}\right)^{3/2} \varepsilon^{1/2} e^{-\varepsilon/kT} d\varepsilon \\ &= f(\varepsilon) d\varepsilon \end{aligned} \quad (17)$$

The integral we need to evaluate is therefore

$$\begin{aligned} \int_0^\infty \sigma(\varepsilon)v_{\text{rel}}f(\varepsilon) d\varepsilon &= 2\pi \left(\frac{1}{\pi kT}\right)^{3/2} \int_0^\infty \sigma(\varepsilon) \left(\frac{2\varepsilon}{\mu}\right)^{1/2} \varepsilon^{1/2} e^{-\varepsilon/kT} d\varepsilon \\ &= \left(\frac{8}{\pi\mu kT}\right)^{1/2} \left(\frac{1}{kT}\right) \int_0^\infty \varepsilon \sigma(\varepsilon) e^{-\varepsilon/kT} d\varepsilon \end{aligned}$$

Now we introduce the approximation for $\sigma(\varepsilon)$ in eqn 15, and evaluate

$$\int_0^\infty \varepsilon \sigma(\varepsilon) e^{-\varepsilon/kT} d\varepsilon = \sigma \int_{\varepsilon_a}^\infty \varepsilon \left(1 - \frac{\varepsilon_a}{\varepsilon}\right) e^{-\varepsilon/kT} d\varepsilon = (kT)^2 \sigma e^{-\varepsilon_a/kT}$$



27.3 The collision cross-section is the target area that results in simple deflection of the projectile molecule; the reaction cross-section is the corresponding area for chemical change to occur on collision.

We have made use of the fact that $\sigma = 0$ for $\epsilon < \epsilon_a$. It follows that

$$\int_0^{\infty} \sigma(\epsilon) v_{\text{rel}} f(\epsilon) d\epsilon = \sigma \left(\frac{8kT}{\pi\mu} \right)^{1/2} e^{-\epsilon_a/kT}$$

as in eqn 16 (with $\epsilon_a/kT = E_a/RT$).

Equation 16 has the Arrhenius form $k_2 = Ae^{-E_a/RT}$ provided the exponential temperature dependence dominates the weak square-root temperature dependence of the pre-exponential factor.¹ It follows that the activation energy, E_a , can be identified with the minimum kinetic energy along the line of approach that is needed for reaction, and that the pre-exponential factor is a measure of the rate at which collisions occur in the gas.

(c) The steric requirement

The simplest procedure for calculating k_2 is to use for σ the values obtained for non-reactive collisions (for example, typically those obtained from viscosity measurements) or from tables of molecular radii. Table 27.1 compares some values of the pre-exponential factor calculated in this way with values obtained from Arrhenius plots (Section 25.5a). One of the reactions shows fair agreement between theory and experiment, but for others there are major discrepancies. In some cases the experimental values are orders of magnitude smaller than those calculated, which suggests that the collision energy is not the only criterion for reaction and that some other feature, such as the relative orientation of the colliding species, is important. Moreover, one reaction in the table has a pre-exponential factor larger than theory, which seems to indicate that the reaction occurs more quickly than the particles collide!

We can express the disagreement between experiment and theory by introducing a steric factor, P , and expressing the reactive cross-section, σ^* , as a multiple of the collision cross-section, $\sigma^* = P\sigma$ (Fig. 27.3). Then the rate constant becomes

$$k_2 = P\sigma \left(\frac{8kT}{\pi\mu} \right)^{1/2} N_A e^{-E_a/RT} \quad (18)$$

This expression has the form we anticipated in eqn 2. The steric factor is normally found to be several orders of magnitude smaller than 1.

Table 27.1* Arrhenius parameters for gas-phase reactions

	$A/(\text{L mol}^{-1} \text{s}^{-1})$		$E_a/(\text{kJ mol}^{-1})$	P
	Experiment	Theory		
$2\text{NOCl} \rightarrow 2\text{NO} + 2\text{Cl}$	9.4×10^9	5.9×10^{10}	102.0	0.16
$2\text{ClO} \rightarrow \text{Cl}_2 + \text{O}_2$	6.3×10^7	2.5×10^{10}	0.0	2.5×10^{-3}
$\text{H}_2 + \text{C}_2\text{H}_4 \rightarrow \text{C}_2\text{H}_6$	1.24×10^6	7.3×10^{11}	180.0	1.7×10^{-6}
$\text{K} + \text{Br}_2 \rightarrow \text{KBr} + \text{Br}$	1.0×10^{12}	2.1×10^{11}	0.0	4.8

* More values are given in the Data section.

¹ From the general definition of activation energy in eqn 25.25 and eqn 18:

$$RT^2 \frac{d \ln k}{dT} = E_a + \frac{1}{2} RT$$

so the activation energy is weakly temperature-dependent. Commonly, $E_a \gg RT$, and the $\frac{1}{2} RT$ can be neglected.

Example 27.1 Estimating a steric factor (1)

Estimate the steric factor for the reaction $\text{H}_2 + \text{C}_2\text{H}_4 \rightarrow \text{C}_2\text{H}_6$ at 628 K given that the pre-exponential factor is $1.24 \times 10^6 \text{ L mol}^{-1} \text{ s}^{-1}$.

Method To calculate P , we need to calculate the pre-exponential factor, A , by using eqn 16 and then compare the answer with experiment: the ratio is P . Collision cross-sections for non-reactive encounters are listed in Table 1.3. The best way to estimate the collision cross-section for dissimilar spherical species is to calculate the collision diameter for each one (from $\sigma = \pi d^2$), to calculate the mean of the two diameters, and then to calculate the cross-section for that mean diameter. However, as neither species is spherical, a simpler but more approximate procedure is just to take the average of the two collision cross-sections.

Answer The reduced mass of the colliding pair is

$$\mu = \frac{m_1 m_2}{m_1 + m_2} = 3.15 \times 10^{-27} \text{ kg}$$

because $m_1 = 2.016 \text{ u}$ for H_2 and $m_2 = 28.05 \text{ u}$ for C_2H_4 (the atomic mass unit, 1 u, is defined inside the front cover). Hence

$$\left(\frac{8kT}{\pi\mu}\right)^{1/2} = 2.65 \times 10^3 \text{ m s}^{-1}$$

From Table 1.3, $\sigma(\text{H}_2) = 0.27 \text{ nm}^2$ and $\sigma(\text{C}_2\text{H}_4) = 0.64 \text{ nm}^2$, giving a mean collision cross-section of $\sigma = 0.46 \text{ nm}^2$. Therefore,

$$A = \sigma \left(\frac{8kT}{\pi\mu}\right)^{1/2} N_A = 7.33 \times 10^{11} \text{ L mol}^{-1} \text{ s}^{-1}$$

Experimentally $A = 1.24 \times 10^6 \text{ L mol}^{-1} \text{ s}^{-1}$, so it follows that $P = 1.7 \times 10^{-6}$.

Comment The very small value of P is one reason why catalysts are needed to bring this reaction about at a reasonable rate. As a general guide, the more complex the molecules, the smaller the value of P .

Self-test 27.1 It is found for the reaction $\text{NO} + \text{Cl}_2 \rightarrow \text{NOCl} + \text{Cl}$ that $A = 4.0 \times 10^9 \text{ L mol}^{-1} \text{ s}^{-1}$ at 298 K. Use $\sigma(\text{NO}) = 0.42 \text{ nm}^2$ and $\sigma(\text{Cl}_2) = 0.93 \text{ nm}^2$ to estimate the P factor for the reaction.

[0.018]

An example of a reaction for which it is possible to estimate the steric factor is $\text{K} + \text{Br}_2 \rightarrow \text{KBr} + \text{Br}$, for which the experimental value of P is 4.8. In this reaction, the distance of approach at which reaction occurs appears to be considerably larger than the distance needed for deflection of the path of the approaching molecules in a non-reactive collision. It has been proposed that the reaction proceeds by a **harpoon mechanism**. This brilliant name is based on a model of the reaction which pictures the K atom as approaching a Br_2 molecule; when the two are close enough an electron (the harpoon) flips across from K to Br_2 . In place of two neutral particles there are now two ions, and so there is a Coulombic attraction between them: this attraction is the line on the harpoon. Under its influence the ions move together (the line is wound in), the reaction takes place, and $\text{KBr} + \text{Br}$ emerge. The harpoon extends the cross-section for the reactive encounter, and the reaction rate is greatly underestimated by taking for the collision cross-section the value for simple mechanical contact between $\text{K} + \text{Br}_2$.

Example 27.2 Estimating a steric factor (2)

Estimate the value of P for the harpoon mechanism by calculating the distance at which it is energetically favourable for the electron to leap from K to Br_2 .

Method We should begin by identifying all the contributions to the energy of interaction between the colliding species. There are three contributions to the energy of the process $\text{K} + \text{Br}_2 \rightarrow \text{K}^+ + \text{Br}_2^-$. The first is the ionization energy, I , of K. The second is the electron affinity, E_{ea} , of Br_2 . The third is the Coulombic interaction energy between the ions when they have been formed: when their separation is R this energy is $-e^2/4\pi\epsilon_0 R$. The electron flips across when the sum of these three contributions changes from positive to negative (that is, when the sum is zero).

Answer The net change in energy when the transfer occurs at a separation R is

$$E = I - E_{\text{ea}} - \frac{e^2}{4\pi\epsilon_0 R}$$

The ionization energy I is larger than E_{ea} , so E becomes negative only when R has decreased to less than some critical value R^* given by

$$\frac{e^2}{4\pi\epsilon_0 R^*} = I - E_{\text{ea}}$$

When the particles are at this separation, the harpoon shoots across from K to Br_2 , so we can identify the reactive cross-section as $\sigma^* = \pi R^{*2}$. This value of σ^* implies that the steric factor is

$$P = \frac{\sigma^*}{\sigma} = \frac{R^{*2}}{d^2} = \left\{ \frac{e^2}{4\pi\epsilon_0 d(I - E_{\text{ea}})} \right\}^2$$

where $d = R(\text{K}) + R(\text{Br}_2)$. With $I = 420 \text{ kJ mol}^{-1}$ (corresponding to $7.0 \times 10^{-19} \text{ J}$), $E_{\text{ea}} \approx 250 \text{ kJ mol}^{-1}$ (corresponding to $4.2 \times 10^{-19} \text{ J}$), and $d = 400 \text{ pm}$, we find $P = 4.2$, in good agreement with the experimental value (4.8).

Self test 27.2 Estimate the value of P for the harpoon reaction between Na and Cl_2 for which $d \approx 350 \text{ pm}$; take $E_{\text{ea}} \approx 230 \text{ kJ mol}^{-1}$.

[2.2]

Example 27.2 illustrates two points about steric factors. First, the concept of a steric factor is not wholly useless because in some cases its numerical value can be estimated. Second (and more pessimistically) most reactions are much more complex than $\text{K} + \text{Br}_2$, and we cannot expect to obtain P so easily. What we need is a more powerful theory that lets us calculate, and not merely guess, its value. We go some way to setting up that theory in Section 27.4 and the sections that follow.

27.2 Diffusion-controlled reactions

Encounters between reactants in solution occur in a very different manner from encounters in gases. Reactant molecules have to jostle their way through the solvent, so their encounter frequency is considerably less than in a gas. However, because a molecule also migrates only slowly away from a location, two reactant molecules that encounter each other stay near each other for much longer than in a gas. This lingering of one molecule near another on account of the hindering presence of solvent molecules is called the cage effect. Such an encounter pair may accumulate enough energy to react even though it does not have

enough energy to do so when it is first formed. The activation energy of a reaction is a much more complicated quantity in solution than in a gas because the encounter pair is surrounded by solvent and the energy of the entire local assembly of reactant and solvent molecules must be considered.

(a) Classes of reaction

The complicated overall process can be divided into simpler parts by setting up a simple kinetic scheme. We suppose that the rate of formation of an encounter pair AB is first-order in each of the reactants A and B:



As we shall see, k_d (where the *d* signifies diffusion) is determined by the diffusional characteristics of A and B. The encounter pair can break up without reaction or it can go on to form products P. If we suppose that both processes are pseudofirst-order reactions (with the solvent perhaps playing a role), then we can write



and



The concentration of AB can now be found from the equation for the net rate of change of concentration of AB:

$$\frac{d[AB]}{dt} = k_d[A][B] - k'_d[AB] - k_a[AB] \approx 0 \quad (22)$$

This expression solves to

$$[AB] \approx \frac{k_d[A][B]}{k_a + k'_d} \quad (23)$$

The rate of formation of products is therefore

$$\frac{d[P]}{dt} \approx k_a[AB] = k_2[A][B] \quad k_2 = \frac{k_a k_d}{k_a + k'_d} \quad (24)$$

Two limits can now be distinguished. If the rate of separation of the unreacted encounter pair is much slower than the rate at which it forms products, then $k'_d \ll k_a$ and the effective rate constant is

$$k_2 \approx \frac{k_a k_d}{k_a} = k_d \quad (25)$$

In this diffusion-controlled limit, the rate of reaction is governed by the rate at which the reactant molecules diffuse through the solvent. An indication that a reaction is diffusion-controlled is that its rate constant is of the order of $10^9 \text{ L mol}^{-1} \text{ s}^{-1}$ or greater. Because the combination of radicals involves very little activation energy, radical and atom recombination reactions are often diffusion-controlled.

An activation-controlled reaction arises when a substantial activation energy is involved in the reaction of AB. Then $k_a \ll k'_d$ and

$$k_2 \approx \frac{k_a k_d}{k'_d} = k_a K \quad (26)$$

where K is the equilibrium constant for $A + B \rightleftharpoons AB$. In this limit, the reaction proceeds at the rate at which energy accumulates in the encounter pair from the surrounding solvent. Some experimental data are given in Table 27.2.

Table 27.2. Arrhenius parameters for reactions in solution

	Solvent	$A/(\text{L mol}^{-1} \text{s}^{-1})$	$E_a/(\text{kJ mol}^{-1})$
$(\text{CH}_3)_3\text{CCl}$ solvolysis	Water	7.1×10^{16}	100
	Ethanol	3.0×10^{13}	112
	Chloroform	1.4×10^4	45
$\text{CH}_3\text{CH}_2\text{Br} + \text{OH}^-$	Ethanol	4.3×10^{11}	89.5

*More values are given in the Data section.

(b) Diffusion and reaction

The rate of a diffusion-controlled reaction is calculated by considering the rate at which the reactants diffuse together. As shown in the *Justification* below, the rate constant for a reaction in which the two reactant molecules react if they come within a distance R^* of one another is

$$k_d = 4\pi R^* D N_A \quad (27)$$

where D is the sum of the diffusion coefficients of the two reactant species in the solution.

Justification 27.3

According to the diffusion equation ($D_B \nabla^2[B] = \partial[B]/\partial t$, Section 24.11), the concentration of B when the system has reached a steady state ($\partial[B]/\partial t = 0$) satisfies $\nabla^2[B]_r = 0$, where the subscript r signifies a quantity that varies with the distance r . For a spherically symmetrical system, ∇^2 can be replaced by radial derivatives alone (see Table 11.1), so the equation satisfied by $[B]_r$ is

$$\frac{d^2[B]_r}{dr^2} + \frac{2}{r} \frac{d[B]_r}{dr} = 0 \quad (28)$$

The general solution of this equation is

$$[B]_r = a + \frac{b}{r} \quad (29)$$

We need two boundary conditions to pin down the values of the two constants. One condition is that $[B]_r$ has its bulk value $[B]$ as $r \rightarrow \infty$. The second condition is that the concentration of B is zero at $r = R^*$, the distance at which reaction occurs. It follows that $a = [B]$ and $b = -R^*[B]$, and hence that (for $r \geq R^*$)

$$[B]_r = \left(1 - \frac{R^*}{r}\right)[B] \quad (30)$$

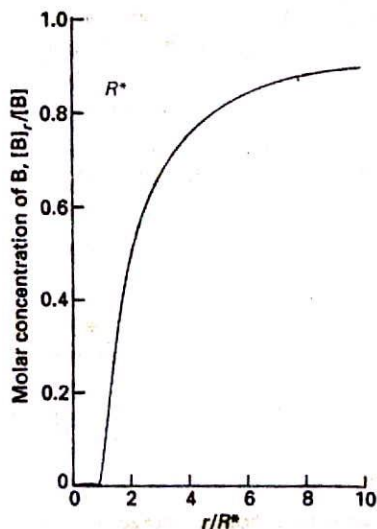
The variation of concentration expressed by this equation is illustrated in Fig. 27.4.

The rate of reaction is the (molar) flux, J , of the reactant B towards A multiplied by the area of the spherical surface of radius R^* :

$$\text{rate of reaction} = 4\pi R^{*2} J \quad (31)$$

From Fick's first law (eqn 24.8), the flux towards A is proportional to the concentration gradient, so at a radius R^* :

$$J = D_B \left(\frac{d[B]_r}{dr} \right)_{r=R^*} = \frac{D_B [B]}{R^*}$$



27.4 The concentration profile for reaction in solution when a molecule B diffuses towards another reactant molecule and reacts if it reaches R^* .

(A sign change has been introduced because we are interested in the flux towards decreasing values of r .) When this condition is substituted into the previous equation we obtain

$$\text{rate of reaction} = 4\pi R^* D_B [B] \quad (32)$$

The rate of the diffusion-controlled reaction is equal to the average flow of B molecules to all the A molecules in the sample. If the bulk concentration of A is $[A]$, the number of A molecules in the sample of volume V is $N_A[A]V$; the global flow of all B to all A is therefore $4\pi R^* D_B N_A [A][B]V$. It is unrealistic to suppose that all A are stationary; this feature is removed by replacing D_B by the sum of the diffusion coefficients of the two species and writing $D = D_A + D_B$. Then the rate of change of concentration of AB is

$$\frac{d[AB]}{dt} = 4\pi R^* D N_A [A][B] \quad (33)$$

Hence, the diffusion-controlled rate constant is as given in eqn 27.

Equation 27 can be taken further by incorporating the Stokes–Einstein equation (eqn 24.73) relating the diffusion constant and the hydrodynamic radius R_A and R_B of each molecule in a medium of viscosity η :

$$D_A = \frac{kT}{6\pi\eta R_A} \quad D_B = \frac{kT}{6\pi\eta R_B} \quad (34)$$

As these relations are approximate, little extra error is introduced if we write $R_A = R_B = \frac{1}{2}R^*$, which leads to

$$k_d = \frac{8RT}{3\eta} \quad (35)$$

(The R in this equation is the gas constant.) The radii have cancelled because, although the diffusion constants are smaller when the radii are large, the reactive collision radius is larger and the particles need travel a shorter distance to meet. In this approximation, the rate constant is independent of the identities of the reactants, and depends only on the temperature and the viscosity of the solvent.

Illustration

The rate constant for the recombination of I atoms in hexane at 298 K, when the viscosity of the solvent is 0.326 cP (with 1 P = 10^{-1} kg m $^{-1}$ s $^{-1}$) is

$$k_d = \frac{8 \times (8.3145 \text{ JK}^{-1} \text{ mol}^{-1}) \times (298 \text{ K})}{3 \times (3.26 \times 10^{-4} \text{ kg m}^{-1} \text{ s}^{-1})} = 2.0 \times 10^7 \text{ m}^3 \text{ mol}^{-1} \text{ s}^{-1}$$

Because 1 m 3 = 10 3 L, this result corresponds to 2.0×10^{10} L mol $^{-1}$ s $^{-1}$. The experimental value is 1.3×10^{10} L mol $^{-1}$ s $^{-1}$, so the agreement is very good considering the approximations involved.

27.3 The material balance equation

The diffusion of reactants plays an important role in many chemical processes, such as the diffusion of O $_2$ molecules into red blood corpuscles and the diffusion of a gas towards a catalyst. We can have a glimpse of the kinds of calculations involved by considering the diffusion equation (Section 24.11) generalized to take into account the possibility that the diffusing, convecting molecules are also reacting.

(a) The formulation of the equation

Consider a small volume element in a chemical reactor (or a biological cell). The net rate at which J molecules enter the region by diffusion and convection is given by eqn 24.78:

$$\frac{\partial[J]}{\partial t} = D \frac{\partial^2[J]}{\partial x^2} - v \frac{\partial[J]}{\partial x} \quad (36)$$

The net rate of change of molar concentration due to chemical reaction is

$$\frac{\partial[J]}{\partial t} = -k[J] \quad (37)$$

if we suppose that J disappears by a pseudofirst-order reaction. Therefore, the overall rate of change of the concentration of J is

$$\frac{\partial[J]}{\partial t} = D \frac{\partial^2[J]}{\partial x^2} - v \frac{\partial[J]}{\partial x} - k[J] \quad (38)$$

Equation 38 is called the **material balance equation**. If the rate constant is large, then $[J]$ will decline rapidly. However, if the diffusion constant is large, then the decline can be replenished as J diffuses rapidly into the region. The convection term, which may represent the effects of stirring, can sweep material either into or out of the region according to the sign of v .

(b) Solutions of the equation

The material balance equation is a second-order partial differential equation, and it is far from easy to solve in general. Some idea of how it is solved can be obtained by considering the special case in which there is no convective motion (as in an unstirred reaction vessel):

$$\frac{\partial[J]}{\partial t} = D \frac{\partial^2[J]}{\partial x^2} - k[J] \quad (39)$$

If the solution of this equation in the absence of reaction (that is, for $k = 0$) is $[J]$, then the solution in the presence of reaction ($k > 0$) is

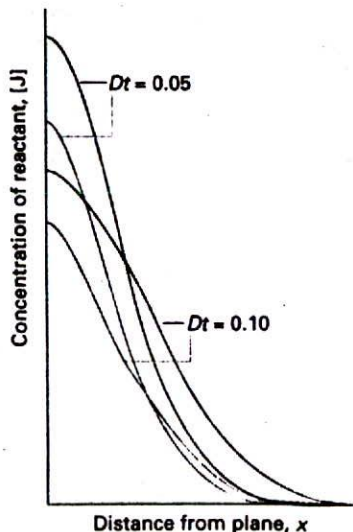
$$[J]^* = k \int_0^t [J] e^{-kt} dt + [J] e^{-kt} \quad (40)$$

We have already met one solution of the diffusion equation in the absence of reaction: eqn 24.79 is the solution for a system in which initially a layer of $n_0 N_A$ molecules is spread over a plane of area A :

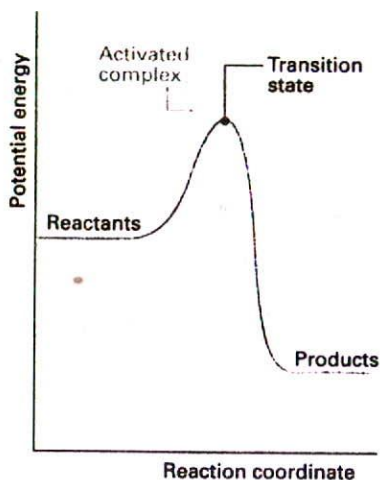
$$[J] = \frac{n_0 e^{-x^2/4Dt}}{A(\pi Dt)^{1/2}} \quad (41)$$

When this expression is substituted into eqn 40 and the integral is evaluated, we obtain the concentration of J as it diffuses away from its initial surface layer and undergoes reaction in the solution above (Fig. 27.5).

Even this relatively simple example has led to an equation that is difficult to solve, and only in some special cases can the full material balance equation be solved analytically. Most modern work on reactor design and cell kinetics uses numerical methods to solve the equation, and detailed solutions for realistic environments can be obtained reasonably easily. Some of the interesting applications include the exploration of the spatial periodicity of autocatalytic reactions mentioned in Section 26.8.



27.5 The concentration profiles for a diffusing, reacting system (for example, a column of solution) in which one reactant is initially in a layer at $x = 0$. In the absence of reaction (grey lines) the concentration profiles are the same as in Fig. 24.24. (Arbitrary values for D and k have been taken.)



27.6 A reaction profile. The horizontal axis is the reaction coordinate, and the vertical axis is potential energy. The activated complex is the region near the potential maximum, and the transition state corresponds to the maximum itself.

Activated complex theory

We now consider a more detailed calculation of rate constants which uses the concepts of statistical thermodynamics developed in Chapter 20. The approach we describe, which is called activated complex theory (ACT), has the advantage that a quantity corresponding to the steric factor appears automatically, and P does not need to be grafted on to an equation as an afterthought. Activated complex theory is an attempt to identify the principal features governing the size of a rate constant in terms of a model of the events that take place during the reaction.

27.4 The reaction coordinate and the transition state

The general features of how the potential energy of the reactants A and B change in the course of a bimolecular elementary reaction are shown in Fig. 27.6. Initially, only the reactants A and B are present. As the reaction event proceeds, A and B come into contact, distort, and begin to exchange or discard atoms. The potential energy rises to a maximum, and the cluster of atoms that corresponds to the region close to the maximum is called the activated complex. After the maximum, the potential energy falls as the atoms rearrange in the cluster, and it reaches a value characteristic of the products. The climax of the reaction is at the peak of the potential energy. Here two reactant molecules have come to such a degree of closeness and distortion that a small further distortion will send them in the direction of products. This crucial configuration is called the transition state of the reaction. Although some molecules entering the transition state might revert to reactants, if they pass through this configuration then it is inevitable that products will emerge from the encounter.²

27.5 The Eyring equation

Activated complex theory pictures a reaction between A and B as proceeding through the formation of an activated complex, C^\ddagger , that falls apart by unimolecular decay into products, P, with a rate constant k^\ddagger :



The concentration of the activated complex is likely to be proportional to the concentrations of the reactants, and later we show explicitly that³

$$[C^\ddagger] = K^\ddagger [A][B] \quad (43)$$

where K^\ddagger is a proportionality constant (with dimensions 1/concentration). It follows that

$$v = k_2 [A][B] \quad k_2 = k^\ddagger K^\ddagger \quad (44)$$

Our task is to calculate the unimolecular rate constant k^\ddagger and the proportionality constant K^\ddagger .

(a) The rate of decay of the activated complex

An activated complex can form products if it passes through the transition state. If its vibration-like motion along the reaction coordinate occurs with a frequency ν , the frequency with which the cluster of atoms forming the complex approaches the transition state is also ν . However, it is possible that not every oscillation along the reaction coordinate

2 The terms activated complex and transition state are often used as synonyms; however, we shall preserve a distinction. Activated complex theory is also widely referred to as transition state theory.

3 This chapter inevitably puts heavy demands on the letter K ; the various meanings are summarized in Table 27.3 at the end of the chapter.

takes the complex through the transition state. For instance, the centrifugal effect of rotations might also be an important contribution to the break-up of the complex, and in some cases the complex might be rotating too slowly, or rotating rapidly but about the wrong axis. Therefore, we suppose that the rate of passage of the complex through the transition state is proportional to the vibrational frequency along the reaction coordinate, and write

$$k^\ddagger = \kappa \nu \quad (45)$$

where κ is the transmission coefficient. In the absence of information to the contrary, κ is assumed to be about 1.

(b) The concentration of the activated complex

The simplest procedure for estimating the concentration of the activated complex is to assume that there is a pre-equilibrium between the reactants and the complex,⁴ and to write

$$A + B \rightleftharpoons C^\ddagger \quad K = \frac{(p_{C^\ddagger}/p^\ominus)}{(p_A/p^\ominus)(p_B/p^\ominus)} = \frac{p_{C^\ddagger} p^\ominus}{p_A p_B}$$

The partial pressures, p_j , can be expressed in terms of the molar concentrations by using $p_j = RT[J]$, which gives

$$[C^\ddagger] = K \frac{RT}{p^\ominus} [A][B] \quad (46)$$

from which it follows that

$$K^\ddagger = K \frac{RT}{p^\ominus} \quad (47)$$

The remaining task is to calculate the equilibrium constant K .

We saw in Section 20.7 how to calculate equilibrium constants from structural data. Equation 20.56 of that section can be used directly, which in this case gives

$$K = \frac{N_A q_{C^\ddagger}^\ominus}{q_A q_B} e^{-\Delta E_0/RT} \quad (48)$$

where

$$\Delta E_0 = E_0(C^\ddagger) - E_0(A) - E_0(B) \quad (49)$$

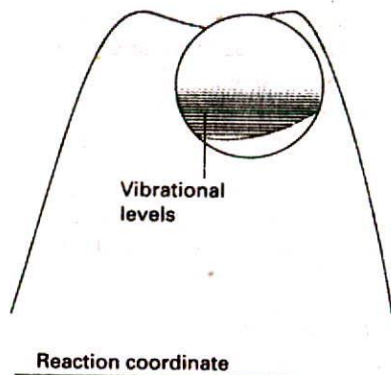
and the q_j^\ominus are the standard molar partition functions, as defined in Section 20.2. Note that the units of N_A and the q_j are mol^{-1} , so K is dimensionless (as is appropriate for an equilibrium constant).

In the final step of this part of the calculation, we focus attention on the partition function of the activated complex. We have already assumed that a vibration of the activated complex C^\ddagger tips it through the transition state. The partition function for this vibration is

$$q = \frac{1}{1 - e^{-h\nu/kT}} \quad (50)$$

where ν is its frequency (the same frequency that determines k^\ddagger). This frequency is much lower than for an ordinary molecular vibration because the oscillation corresponds to the

⁴ In an earlier edition of this text a different line of argument was used: we recognized that almost nothing is known about the populations of the levels of the activated complex. Since nothing is known, the most honest approach is to assume that the populations depend on the energy and not on the identity of the level (that is, whether it belongs to A, B, or C^\ddagger). This 'least-prejudiced' approach leads to the same results as here, but has the advantage that it avoids the presumption of equilibrium between the reactants and their activated complex. Its disadvantage is that it is slightly less direct. The second edition should be consulted for details.



27.7 In an elementary depiction of the activated complex close to the transition state, there is a broad, shallow dip in the potential energy surface along the reaction coordinate. The complex vibrates harmonically and almost classically in this well. However, see footnote 5.

complex falling apart (Fig. 27.7), so the force constant is very low.⁵ Therefore, because $h\nu/kT \ll 1$, the exponential may be expanded and the partition function reduces to

$$q = \frac{1}{1 - (1 - \frac{h\nu}{kT} + \dots)} \approx \frac{kT}{h\nu} \quad (51)$$

We can therefore write

$$q_{C^\ddagger} \approx \frac{kT}{h\nu} \bar{q}_{C^\ddagger} \quad (52)$$

where \bar{q} denotes the partition function for all the other modes of the complex. The constant K^\ddagger is therefore

$$K^\ddagger = \frac{kT}{h\nu} \bar{K} \quad \bar{K} = \left(\frac{RT}{p^\ominus} \right) \left(\frac{N_A \bar{q}_{C^\ddagger}^\ominus}{q_A^\ominus q_B^\ominus} \right) e^{-\Delta E_0/RT} \quad (53)$$

with $(p^\ominus/RT)\bar{K}$ a kind of equilibrium constant, but with one vibrational mode of C^\ddagger discarded.

(c) The rate constant

We can now combine all the parts of the calculation into

$$k_2 = k^\ddagger K^\ddagger = \kappa \nu \frac{kT}{h\nu} \bar{K} \quad (54)$$

At this stage the unknown frequencies ν cancel, and we obtain the Eyring equation:

$$k_2 = \kappa \frac{kT}{h} \bar{K} \quad (55)$$

The factor \bar{K} is given by eqn 53 in terms of the partition functions of A, B, and C^\ddagger , so in principle we now have an explicit expression for calculating the second-order rate constant for a bimolecular reaction in terms of the molecular parameters for the reactants and the activated complex and the quantity κ .

The partition functions for the reactants can normally be calculated quite readily, using either spectroscopic information about their energy levels or the approximate expressions set out in Table 20.2. The difficulty with the Eyring equation, however, lies in the calculation of the partition function of the activated complex: C^\ddagger cannot normally be investigated spectroscopically, and in general we need to make assumptions about the size, shape, and structure of the complex. We shall illustrate what is involved for two simple cases.

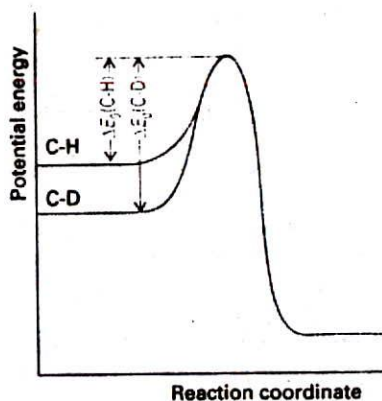
(d) The collision of structureless particles

As a first example, consider the case of two structureless particles, A and B, colliding to give an activated complex that resembles a diatomic molecule. Because the reactants $J = A, B$ are structureless 'atoms', the only contributions to their partition functions are the translational terms:

$$q_J^\ominus = \frac{V_m^\ominus}{\Lambda_J^3} \quad \Lambda_J = \frac{h}{(2\pi m_J kT)^{1/2}} \quad V_m^\ominus = \frac{RT}{p^\ominus} \quad (56)$$

The activated complex is a diatomic cluster of mass $m_C = m_A + m_B$ and moment of inertia I . It has one vibrational mode, but that mode corresponds to motion along the reaction

5 There is a real problem here. Figure 27.7 is probably an oversimplification, for in many cases there is no dip at the top of the barrier, and the curvature of the potential energy, and therefore the force constant, is negative. Formally, the vibrational frequency is then imaginary. We ignore this problem here, but see *Further reading*.



27.8 Changes in the reaction profile when a bond undergoing cleavage is deuterated. The only significant change is to the zero-point energy of the reactants, which is lower for C-D than for C-H. As a result, the activation energy is greater for C-D than for C-H.

coordinate and therefore does not appear in $\bar{q}_{\text{C}^\ddagger}$. It follows that the standard molar partition function of the activated complex is

$$\bar{q}_{\text{C}^\ddagger} = \left(\frac{2IkT}{h^2} \right) \frac{V_m^\ominus}{\Lambda_{\text{C}^\ddagger}^3} \quad (57)$$

The moment of inertia of a diatomic molecule of bond length r is μr^2 , where $\mu = m_A m_B / (m_A + m_B)$ is the effective mass, so the expression for the rate constant is

$$\begin{aligned} k_2 &= \kappa \frac{kT}{h} \frac{RT}{p^\ominus} \left(\frac{N_A \Lambda_A^3 \Lambda_B^3}{\Lambda_{\text{C}^\ddagger}^3 V_m^\ominus} \right) \left(\frac{2IkT}{h^2} \right) e^{-\Delta E_0/RT} \\ &= \kappa \frac{kT}{h} N_A \left(\frac{\Lambda_A \Lambda_B}{\Lambda_{\text{C}^\ddagger}} \right)^3 \left(\frac{2IkT}{h^2} \right) e^{-\Delta E_0/RT} \\ &= \kappa N_A \left(\frac{8kT}{\pi \mu} \right)^{1/2} \pi r^2 e^{-\Delta E_0/RT} \end{aligned} \quad (58)$$

Finally, by identifying the reactive cross-section σ^* as $\kappa \pi r^2$, we arrive at precisely the same expression as that obtained from simple collision theory (eqn 16).

(e) The kinetic isotope effect

As a second example, consider the effect of deuteration on a reaction in which the rate-determining step is the scission of a C-H bond. The experimental observation we seek to explain is the kinetic isotope effect, the decrease in the rate of the reaction on deuteration. We shall demonstrate that the difference lies in the fact that C-H scission has a lower activation energy than C-D scission on account of the former's greater zero-point vibrational energy.

The reaction coordinate corresponds to the stretching of the C-H bond, and the potential energy profile is shown in Fig. 27.8. On deuteration, the dominant change is the reduction of the zero-point energy of the bond (because the deuterium atom is heavier). The whole reaction profile is not lowered, however, because the relevant vibration in the activated complex has a very low force constant, so there is little zero-point energy associated with the reaction coordinate in either the proton or the deuterium forms of the complex.

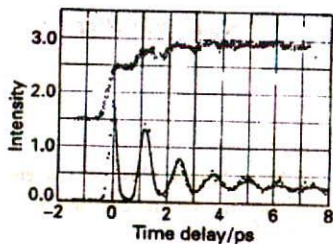
We assume that the deuteration affects only the reaction coordinate, and hence that the partition functions for all the other internal modes remain unchanged. The translational partition functions are changed by deuteration, but the mass of the rest of the molecule is normally so great that the change is insignificant. The value of ΔE_0 changes on account of the change of zero-point energy, and

$$\begin{aligned} \Delta E_0(\text{C-D}) - \Delta E_0(\text{C-H}) &= N_A \left\{ \frac{1}{2} \hbar \omega(\text{C-H}) - \frac{1}{2} \hbar \omega(\text{C-D}) \right\} \\ &= \frac{1}{2} N_A \hbar k_f^{1/2} \left(\frac{1}{\mu_{\text{CH}}^{1/2}} - \frac{1}{\mu_{\text{CD}}^{1/2}} \right) \end{aligned} \quad (59)$$

where k_f is the force constant of the bond and μ the relevant effective mass (Section 16.9). Because all the partition functions are the same (by assumption), the rate constants for the two species should be in the ratio

$$\frac{k(\text{C-D})}{k(\text{C-H})} = e^{-\lambda} \quad \lambda = \frac{\hbar k_f^{1/2}}{2kT} \left(\frac{1}{\mu_{\text{CH}}^{1/2}} - \frac{1}{\mu_{\text{CD}}^{1/2}} \right) \quad (60)$$

Note that $\lambda > 0$ because $\mu_{\text{CD}} > \mu_{\text{CH}}$. This equation predicts that at room temperature C-H cleavage should be about seven times faster than C-D cleavage, other conditions being equal.



27.9 Femtosecond spectroscopic results for the reaction in which NaI separates into Na and I. The full circles are the absorption of the complex and the open circles the absorption of the free Na atoms. (A.H. Zewail, *Science* 242, 1645 (1988).)

(f) The experimental observation of the activated complex

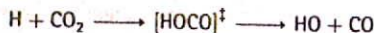
Until very recently there were no direct spectroscopic observations on activated complexes, for they have a very fleeting existence and often survive for only a picosecond or so. However, the development of femtosecond pulsed lasers and their application to chemistry in the form of femtochemistry has made it possible to make observations on species that have such short lifetimes that in a number of respects they resemble an activated complex.

In a typical experiment, a femtosecond pulse is used to excite a molecule to a dissociative state, and then a second femtosecond pulse is fired at an interval after the dissociating pulse. The frequency of the second pulse is set at an absorption of one of the free fragmentation products, so its absorption is a measure of the abundance of the dissociation product. For example, when ICN is dissociated by the first pulse, the emergence of CN from the photoactivated state can be monitored by watching the growth of the free CN absorption (or, more commonly, its laser-induced fluorescence). In this way it has been found that the CN signal remains zero until the fragments have separated by about 600 pm, which takes about 205 fs.

Some sense of the progress that has been made in the study of the intimate mechanism of chemical reactions can be obtained by considering an analogue of the harpoon reaction introduced in Section 27.1c. The decay of the ion pair Na^+X^- , where X is a halogen, has been studied by exciting it with a femtosecond pulse to an excited state that corresponds to a covalently bonded NaX molecule. The second probe pulse examines the system at an absorption frequency either of the free Na atom or at a frequency at which the atom absorbs when it is a part of the complex. The latter frequency depends on the Na-X distance, so an absorption (in practice, a laser-induced fluorescence) is obtained each time the vibration of the complex returns it to that separation.

A typical set of results for NaI is shown in Fig. 27.9. The bound Na absorption intensity shows up as a series of pulses that recur in about 1 ps, showing that the complex vibrates with about that period. The decline in intensity shows the rate at which the complex can dissociate as the two atoms swing away from each other. The complex does not dissociate on every outward-going swing because there is a chance that the I atom can be harpooned again, in which case it fails to make good its escape. The free Na absorption also grows in an oscillating manner, showing the periodicity of the vibration of the complex, each swing of which gives it a chance to dissociate. The precise period of the oscillation in NaI is 1.25 ps, corresponding to a vibrational wavenumber of 27 cm^{-1} (recall that activated complex theory assumes that such a vibration has a very low frequency). The complex survives for about ten oscillations. In contrast, although the oscillation frequency of NaBr is similar, it barely survives one oscillation.

Femtosecond spectroscopy has also been used to examine analogues of the activated complex involved in bimolecular reactions. Thus, a molecular beam can be used to produce a van der Waals molecule (Section 22.5c), such as $\text{IH}\cdots\text{OCO}$. The HI bond can be dissociated by a femtosecond pulse, and the H atom is ejected towards the O atom of the neighbouring CO_2 molecule to form HOCO. Hence, the van der Waals molecule is a source of a species that resembles the activated complex of the reaction



The probe pulse is tuned to the OH radical, which enables the evolution of $[\text{HOCO}]^\ddagger$ to be studied in real time.

27.6 Thermodynamic aspects

The statistical thermodynamic version of activated complex theory rapidly runs into difficulties because only rarely is anything known about the structure of the activated

complex. However, the concepts that it introduces, principally that of an equilibrium between the reactants and the activated complex, have motivated a more general, empirical approach in which the activation process is expressed in terms of thermodynamic functions.

(a) Activation parameters

If we accept that $(p^\ominus/RT)K$ is an equilibrium constant (despite one mode of C^\ddagger having been discarded), we can express it in terms of a Gibbs energy of activation, $\Delta^\ddagger G$, through the definition⁶

$$\Delta^\ddagger G = -RT \ln(p^\ominus/RT)K \quad [61]$$

Then the rate constant becomes

$$k_2 = \kappa \frac{kT}{h} \frac{RT}{p^\ominus} e^{-\Delta^\ddagger G/RT} \quad [62]$$

Because $G = H - TS$, the Gibbs energy of activation can be divided into an entropy of activation, $\Delta^\ddagger S$, and an enthalpy of activation, $\Delta^\ddagger H$, by writing

$$\Delta^\ddagger G = \Delta^\ddagger H - T\Delta^\ddagger S \quad [63]$$

When eqn 63 is used in eqn 62 and κ is absorbed into the entropy term, we obtain

$$k_2 = B e^{\Delta^\ddagger S/R} e^{-\Delta^\ddagger H/RT} \quad B = \frac{kT}{h} \frac{RT}{p^\ominus} \quad [64]$$

The formal definition of activation energy, $E_a = RT^2(\partial \ln k / \partial T)$, then gives $E_a = \Delta^\ddagger H + 2RT$,⁷ so

$$k_2 = e^2 B e^{\Delta^\ddagger S/R} e^{-E_a/RT} \quad [65]$$

from which it follows that the Arrhenius factor A can be identified as

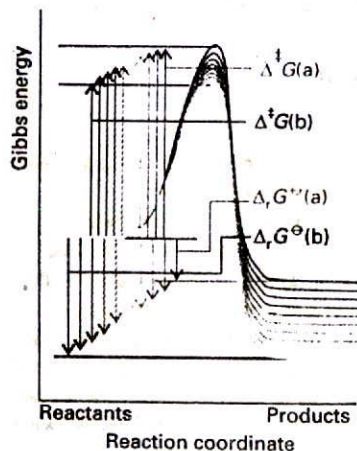
$$A = e^2 B e^{\Delta^\ddagger S/R} \quad [66]$$

The entropy of activation is negative because two reactant species come together to form one species. However, if there is a reduction in entropy below what would be expected for the simple encounter of A and B , then A will be smaller than that expected on the basis of simple collision theory. Indeed, we can identify that additional reduction in entropy, $\Delta^\ddagger S_{\text{steric}}$, as the origin of the steric factor of collision theory, and write

$$P = e^{\Delta^\ddagger S_{\text{steric}}/R} \quad [67]$$

Thus, the more complex the steric requirements of the encounter, the more negative the value of $\Delta^\ddagger S_{\text{steric}}$, and the smaller the value of P .

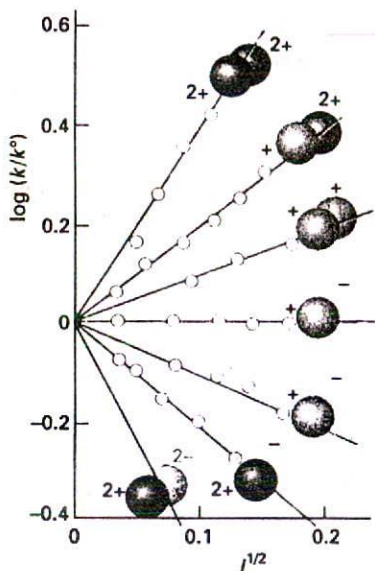
Gibbs energies, enthalpies, and entropies of activation are widely used to report experimental reaction rates, especially for organic reactions in solution. They are encountered when relationships between equilibrium constants and rates of reaction are explored using correlation analysis, in which $\ln K$ (which is equal to $-\Delta_r G^\ominus/RT$) is plotted against $\ln k$ (which is proportional to $-\Delta^\ddagger G/RT$). In many cases the correlation is linear, signifying that, as the reaction becomes thermodynamically more favourable, its rate constant increases (Fig. 27.10). This linear correlation is the origin of the alternative name linear free energy relation (LFER; see *Further reading*).



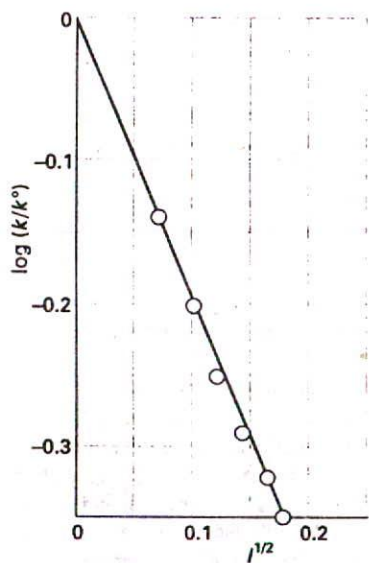
27.10 For a related series of reactions, as the magnitude of the standard reaction Gibbs energy increases, so the activation barrier decreases. The approximate linear correlation between $\Delta^\ddagger G$ and $\Delta_r G^\ominus$ is the origin of linear free energy relations. Note how a high value of $\Delta^\ddagger G$ for reaction a correlates with a low value of $|\Delta_r G^\ominus|$ for that reaction (green), but a smaller value of $\Delta^\ddagger G$, as for reaction b (black) correlates with a larger value of $|\Delta_r G^\ominus|$.

⁶ All the $\Delta^\ddagger X$ in this section are standard thermodynamic quantities, $\Delta^\ddagger X^\ominus$, but we shall omit the standard state sign to avoid overburdening the notation.

⁷ For reactions in solution, $E_a = \Delta^\ddagger H + RT$.



27.11 Experimental tests of the kinetic salt effect for reactions in water at 298 K. The ion types are shown as spheres, and the slopes of the lines are those given by the Debye-Hückel limiting law and eqn 73.



27.12 The experimental ionic strength dependence of the rate constant of a hydrolysis reaction: the slope gives information about the charge types involved in the activated complex of the rate-determining step. See Example 27.3.

(b) Reactions between ions

The thermodynamic version of activated complex theory simplifies the discussion of reactions in solution. The statistical thermodynamic theory is very complicated to apply because the solvent plays a role in the activated complex. In the thermodynamic approach we combine the rate law

$$\frac{d[\text{P}]}{dt} = k^\ddagger [\text{C}^\ddagger] \quad (68)$$

with the thermodynamic equilibrium constant

$$K = \frac{a_{\text{C}^\ddagger}}{a_{\text{A}}a_{\text{B}}} = K_\gamma \frac{[\text{C}^\ddagger]}{[\text{A}][\text{B}]} \quad K_\gamma = \frac{\gamma_{\text{C}^\ddagger}}{\gamma_{\text{A}}\gamma_{\text{B}}} \quad (69)$$

Then

$$\frac{d[\text{P}]}{dt} = k_2 [\text{A}][\text{B}] \quad k_2 = \frac{k^\ddagger K}{K_\gamma} \quad (70)$$

If k_2° is the rate constant when the activity coefficients are 1 (that is, $k_2^\circ = k^\ddagger K$), we can write

$$k_2 = \frac{k_2^\circ}{K_\gamma} \quad (71)$$

At low concentrations the activity coefficients can be expressed in terms of the ionic strength, I , of the solution by using the Debye-Hückel limiting law (Section 10.2c, particularly eqn 10.19) in the form

$$\log \gamma_j = -Az_j^2 I^{1/2} \quad (72)$$

with $A = 0.509$ in aqueous solution at 298 K. Then

$$\begin{aligned} \log k_2 &= \log k_2^\circ - A\{z_{\text{A}}^2 + z_{\text{B}}^2 - (z_{\text{A}} + z_{\text{B}})^2\} I^{1/2} \\ &= \log k_2^\circ + 2Az_{\text{A}}z_{\text{B}} I^{1/2} \end{aligned} \quad (73)$$

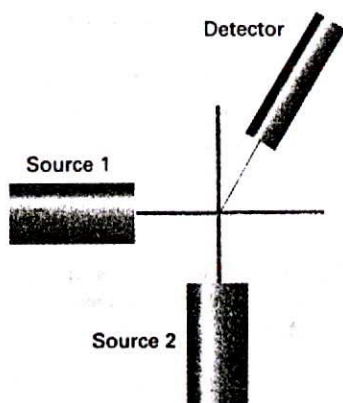
The charge numbers of A and B are z_{A} and z_{B} , so the charge number of the activated complex is $z_{\text{A}} + z_{\text{B}}$; the z_j are positive for cations and negative for anions.

Equation 73 expresses the kinetic salt effect, the variation of the rate constant of a reaction between ions with the ionic strength of the solution (Fig. 27.11). If the reactant ions have the same sign (as in a reaction between cations or between anions), then increasing the ionic strength by the addition of inert ions increases the rate constant. The formation of a single, highly charged ionic complex from two less highly charged ions is favoured by a high ionic strength because the new ion has a denser ionic atmosphere and interacts with that atmosphere more strongly. Conversely, ions of opposite charge react more slowly in solutions of high ionic strength. Now the charges cancel and the complex has a less favourable interaction with its atmosphere than the separated ions.

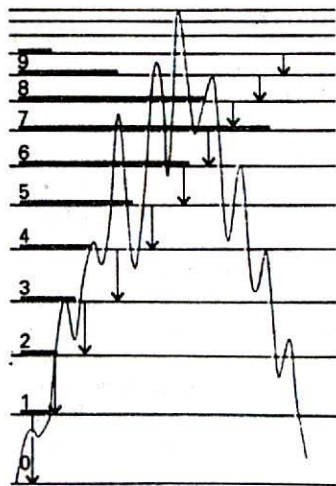
Example 27.3 Analysing the kinetic salt effect

The rate constant for the base hydrolysis of $[\text{CoBr}(\text{NH}_3)_5]^{2+}$ varies with ionic strength as tabulated below. What can be deduced about the charge of the activated complex in the rate-determining stage?

I	0.0050	0.0100	0.0150	0.0200	0.0250	0.0300
k/k°	0.718	0.631	0.562	0.515	0.475	0.447



27.13 In a crossed-beam experiment, state-selected molecules are generated in two separate sources, and are directed perpendicular to one another. The detector responds to molecules (which may be product molecules if chemical reaction occurs) scattered into a chosen direction.



27.14 Infrared chemiluminescence from CO produced in the reaction $O + CS \rightarrow CO + S$ arises from the non-equilibrium populations of the vibrational states of CO and the radiative relaxation to equilibrium.

Method According to eqn 73, plot $\log(k/k^\circ)$ against $I^{1/2}$, when the slope will give $1.02z_A z_B$, from which we can infer the charges of the ions involved in the formation of the activated complex.

Answer Form the following table:

I	0.0050	0.0100	0.0150	0.0200	0.0250	0.0300
$I^{1/2}$	0.071	0.100	0.122	0.141	0.158	0.173
$\log(k/k^\circ)$	-0.14	-0.20	-0.25	-0.29	-0.32	-0.35

These points are plotted in Fig. 27.12. The slope of the (least squares) straight line is -2.04 , indicating that $z_A z_B = -2$. Because $z_A = -1$ for the OH^- ion, if that ion is involved in the formation of the activated complex, then the charge number of the second ion is $+2$. This analysis suggests that the pentaamminebromocobalt(III) cation participates in the formation of the activated complex.

Comment! The rate constant is also influenced by the relative permittivity of the medium.

Self-test 27.3 An ion of charge number $+1$ is known to be involved in the activated complex of a reaction. Deduce the charge number of the other ion from the following data:

I	0.005	0.010	0.015	0.020	0.025	0.030
k/k°	0.930	0.902	0.884	0.867	0.853	0.841

[-1]

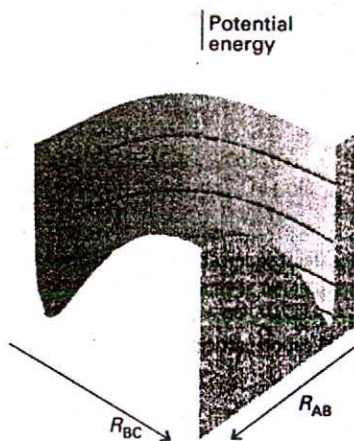
The dynamics of molecular collisions

We now come to the third and most detailed level of our examination of the factors that govern the rates of reactions. Molecular beams allow us to study collisions between molecules in preselected energy states, and can be used to determine the states of the products of a reactive collision. Information of this kind is essential if a full picture of the reaction is to be built, because the rate constant is an average over events in which reactants in different initial states evolve into products in their final states.

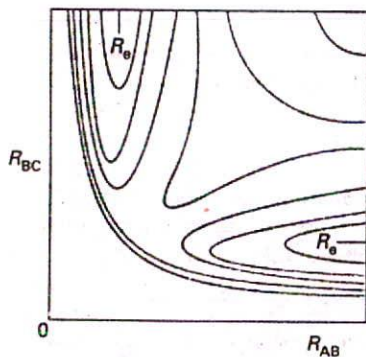
27.7 Reactive collisions

Detailed experimental information about the intimate processes that occur during reactive encounters comes from molecular beams, especially crossed molecular beams (Fig. 27.13). The detector for the products of the collision of two beams can be moved to different angles, so the angular distribution of the products can be determined. Because the molecules in the incoming beams can be prepared with different energies (for example, with different translational energies by using rotating sectors and supersonic nozzles, and with different vibrational energies by using selective excitation with lasers) and with different orientations (by using electric fields), it is possible to study the dependence of the success of collisions on these variables and to study how they affect the properties of the outgoing product molecules.

One method for examining the energy distribution in the products is infrared chemiluminescence, in which vibrationally excited molecules emit infrared radiation as they return to their ground states. By studying the intensities of the infrared emission spectrum, the populations of the vibrational states may be determined (Fig. 27.14). Another method makes use of laser-induced fluorescence. In this technique, a laser is used to excite a product molecule from a specific vibration-rotation level; the intensity of the fluorescence



27.15 The potential energy surface for the $\text{H} + \text{H}_2 \rightarrow \text{H}_2 + \text{H}$ reaction when the atoms are constrained to be collinear.



27.16 The contour diagram (with contours of equal potential energy) corresponding to the surface in Fig. 27.15. R_e marks the equilibrium bond length of an H_2 molecule (strictly, it relates to the arrangement when the third atom is at infinity).

from the upper state is monitored and interpreted in terms of the population of the initial vibration-rotation state.

The concept of collision cross-section was introduced in connection with collision theory in Section 27.1, where we saw that the second-order rate constant, k_2 , can be expressed as a Boltzmann-weighted average of the reactive collision cross-section and the relative speed of approach. We shall write eqn 14 as

$$k_2 = \langle \sigma v_{\text{rel}} \rangle N_A \quad (74)$$

where the angle brackets denote a Boltzmann average. Molecular beam studies provide a more sophisticated version of this quantity, for they provide the state-to-state cross-section, $\sigma_{nn'}$, and hence the state-to-state rate constant, $k_{nn'}$:

$$k_{nn'} = \langle \sigma_{nn'} v_{\text{rel}} \rangle N_A \quad (75)$$

The rate constant k_2 is the sum of the state-to-state rate constant over all final states (because a reaction is successful whatever the final state of the products) and over a Boltzmann-weighted sum of initial states (because the reactants are initially present with a characteristic distribution of populations at a temperature T):

$$k_2 = \sum_{n,n'} k_{nn'}(T) f_n(T) \quad (76)$$

where $f_n(T)$ is the Boltzmann factor at a temperature T .

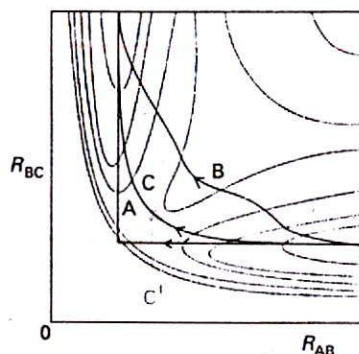
It follows that, if we can determine or calculate the state-to-state cross-sections for a wide range of approach speeds and initial and final states, then we have a route to the calculation of the rate constant for the reaction.

27.8 Potential energy surfaces

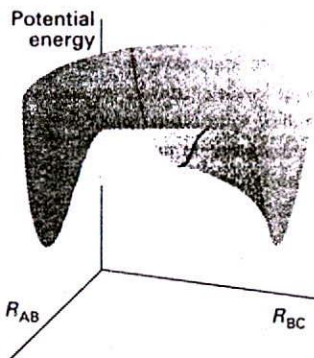
One of the most important concepts for discussing beam results and calculating the state-to-state collision cross-section is the potential energy surface of a reaction, the potential energy as a function of the relative positions of all the atoms taking part in the reaction. For a collision between an H atom and an H_2 molecule, for instance, the potential energy surface is the plot of the potential energy for all relative locations of the three hydrogen nuclei. Detailed calculations show that the approach of an atom along the H-H axis requires less energy for reaction than any other approach, so initially we confine our attention to a collinear approach. Two parameters are required to define the nuclear separations: one is the $\text{H}_A\text{-H}_B$ separation R_{AB} , and the other is the $\text{H}_B\text{-H}_C$ separation R_{BC} .

At the start of the encounter R_{AB} is infinite and R_{BC} is the H_2 equilibrium bond length. At the end of a successful reactive encounter R_{AB} is equal to the equilibrium bond length and R_{BC} is infinite. The total energy of the three-atom system depends on their relative separations, and can be found by doing a molecular orbital calculation. The plot of the total energy of the system against R_{AB} and R_{BC} gives the potential energy surface of this collinear reaction (Fig. 27.15). This surface is normally depicted as a contour diagram (Fig. 27.16).

When R_{AB} is very large, the variation in potential energy represented by the surface as R_{BC} changes are those of an isolated H_2 molecule as its bond length is altered. A section through the surface at $R_{AB} = \infty$, for example, is the same as the H_2 bonding potential energy curve drawn in Fig. 14.18. At the edge of the diagram where R_{BC} is very large, a section through the surface is the molecular potential energy curve of an isolated H_AH_B molecule.



27.17 Various trajectories through the potential energy surface shown in Fig. 27.16. Path A corresponds to a route in which R_{BC} is held constant as H_A approaches; path B corresponds to a route in which R_{BC} lengthens at an early stage during the approach of H_A ; path C is the route along the floor of the potential valley.



27.18 The transition state is a set of configurations (here, marked by the line across the saddle point) through which successful reactive trajectories must pass.

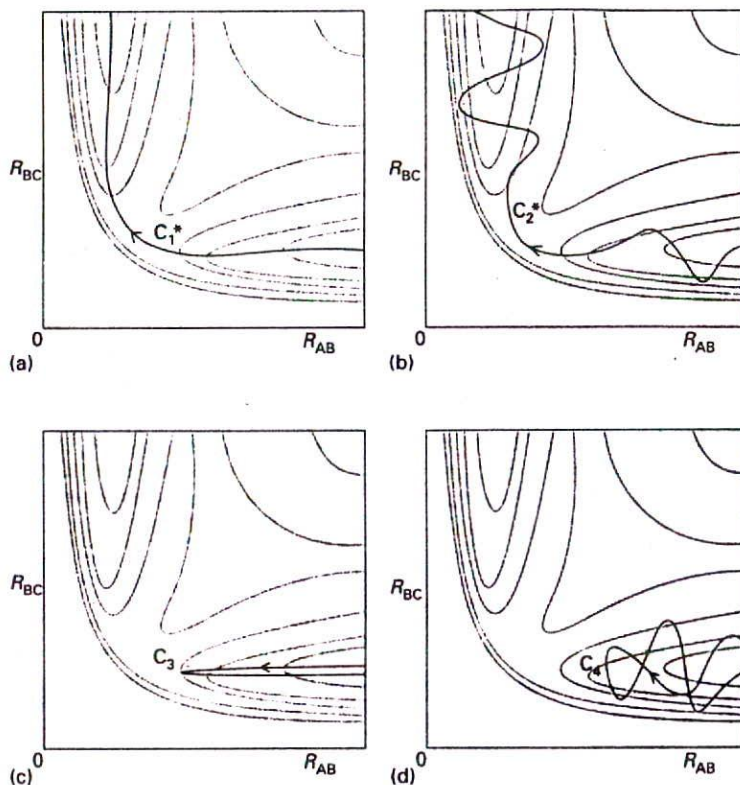
The actual path of the atoms in the course of the encounter depends on their total energy, the sum of their kinetic and potential energies. However, we can obtain an initial idea of the paths available to the system for paths that correspond to least potential energy. For example, consider the changes in potential energy as H_A approaches H_BH_C . If the H_B-H_C bond length is constant during the initial approach of H_A , then the potential energy of the H_3 cluster would rise along the path marked A in Fig. 27.17. We see that the potential energy rises to a high value as H_A is pushed into the molecule, and then decreases sharply as H_C breaks off and separates to a great distance. An alternative reaction path can be imagined (B) in which the H_B-H_C bond length increases while H_A is still far away. Both paths, although feasible if the molecules have sufficient initial kinetic energy, take the three atoms to regions of high potential energy in the course of the encounter.

The path of least potential energy is the one marked C, corresponding to R_{BC} lengthening as H_A approaches and begins to form a bond with H_B . The H_B-H_C bond relaxes at the demand of the incoming atom, and the potential energy climbs only as far as the saddle-shaped region of the surface, to the saddle point marked C^\ddagger . The encounter of least potential energy is one in which the atoms take route C up the floor of the valley, through the saddle point, and down the floor of the other valley as H_C recedes and the new H_A-H_B bond achieves its equilibrium length. This path is the reaction coordinate we met in Section 27.4.

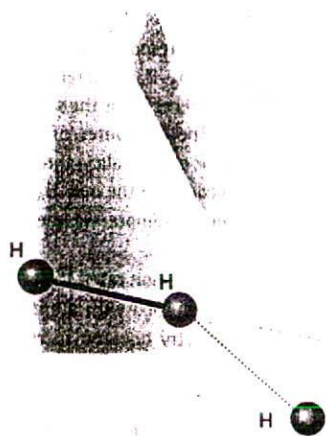
We can now make contact with the activated complex theory of reaction rates. In terms of trajectories on potential surfaces, the transition state can be identified with a critical geometry such that every trajectory that goes through this geometry goes on to react (Fig. 27.18).

27.9 Some results from experiments and calculations

To travel successfully from reactants to products the incoming molecules must possess enough kinetic energy to be able to climb to the saddle point of the potential surface. Therefore, the shape of the surface can be explored experimentally by changing the relative speed of approach (by selecting the beam velocity) and the degree of vibrational excitation and observing whether reaction occurs and whether the products emerge in a vibrationally



27.19 Some successful (*) and unsuccessful (°) encounters. (a) C_1^* corresponds to the path along the foot of the valley; (b) C_2^* corresponds to an approach of H_A to a vibrating H_{BC} molecule, and the formation of a vibrating H_{AB} molecule as H_C departs. (c) C_3 corresponds to H_A approaching a non-vibrating H_{BC} molecule, but with insufficient translational kinetic energy; (d) C_4 corresponds to H_A approaching a vibrating H_{BC} molecule, but still the energy, and the phase of the vibration, is insufficient for reaction.



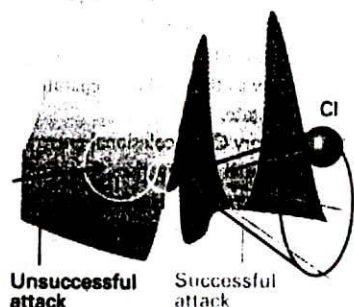
27.20 An indication of the anisotropy of the potential energy changes as H approaches H_2 with different angles of attack. The collinear attack has the lowest potential barrier to reaction. The surface indicates the potential energy profile along the reaction coordinate for each configuration.

excited state (Fig. 27.19). For example, one question that can be answered is whether it is better to smash the reactants together with a lot of translational kinetic energy or to ensure instead that they approach in highly excited vibrational states. Thus, is trajectory C_2^* , where the $H_B H_C$ molecule is initially vibrationally excited, more efficient at leading to reaction than the trajectory C_1^* , in which the total energy is the same but has a high translational kinetic energy?

(a) The direction of attack and separation

Figure 27.20 shows the results of a calculation of the potential energy as an H atom approaches an H_2 molecule from different angles, the H_2 bond being allowed to relax to the optimum length in each case. The potential barrier is least for collinear attack, as we assumed earlier. (But we must be aware that other lines of attack are feasible and contribute to the overall rate.) In contrast, Fig. 27.21 shows the potential energy changes that occur as a Cl atom approaches an HI molecule. The lowest barrier occurs for approaches within a cone of half-angle 30° surrounding the H atom. The relevance of this result to the calculation of the steric factor of collision theory should be noted: not every collision is successful, because not every one lies within the reactive cone.

If the collision is sticky, so that when the reactants collide they orbit around each other, the products can be expected to emerge in random directions because all memory of the approach direction has been lost. A rotation takes about 1 ps, so if the collision is over in less than that time the complex will not have had time to rotate and the products will be thrown off in a specific direction. In the collision of K and I_2 , for example, most of the products are



27.21 The potential energy barrier for the approach of Cl to HI. In this case, successful encounters occur only when Cl approaches within a cone surrounding the H atom.

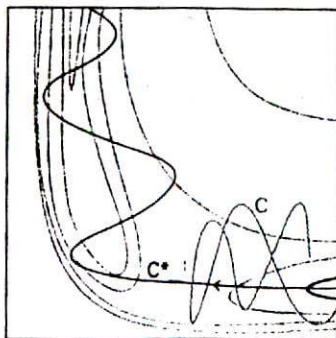
thrown off in the forward direction.⁸ This product distribution is consistent with the harpoon mechanism (Section 27.1c) because the transition takes place at long range. In contrast, the collision of K with CH_3I leads to reaction only if the molecules approach each other very closely. In this mechanism, K effectively bumps into a brick wall, and the KI product bounces out in the backward direction. The detection of this anisotropy in the angular distribution of products gives an indication of the distance and orientation of approach needed for reaction, as well as showing that the event is complete in less than 1 ps.

(b) Attractive and repulsive surfaces

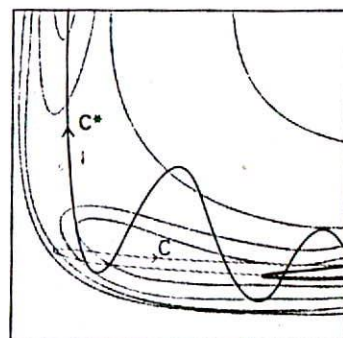
Some reactions are very sensitive to whether the energy has been predigested into a vibrational mode or left as the relative translational kinetic energy of the colliding molecules. For example, if two HI molecules are hurled together with more than twice the activation energy of the reaction, then no reaction occurs if all the energy is translational. For $\text{F} + \text{HCl} \rightarrow \text{Cl} + \text{HF}$, for example, the reaction is about five times as efficient when the HCl is in its first vibrational excited state than when, although HCl has the same total energy, it is in its vibrational ground state.

The origin of these requirements can be found by examining the potential energy surface. Figure 27.22 shows an attractive surface in which the saddle point occurs early in the reaction coordinate. Figure 27.23 shows a repulsive surface in which the saddle point occurs late. A surface that is attractive in one direction is repulsive in the reverse direction.

Consider first the attractive surface. If the original molecule is vibrationally excited, then a collision with an incoming molecule takes the system along C. This path is bottled up in the region of the reactants, and does not take the system to the saddle point. If, however, the same amount of energy is present solely as translational kinetic energy, then the system moves along C^* and travels smoothly over the saddle point into products. We can therefore

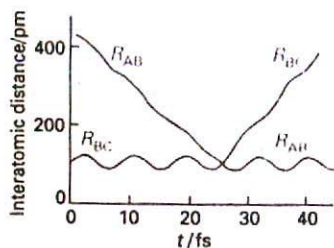


27.22 An attractive potential energy surface. A successful encounter (C^*) involves high translational kinetic energy and results in a vibrationally excited product.



27.23 A repulsive potential energy surface. A successful encounter (C^*) involves initial vibrational excitation and the products have high translational kinetic energy. A reaction that is attractive in one direction is repulsive in the reverse direction.

⁸ There is a subtlety here. In molecular beam work the remarks normally refer to directions in a centre-of-mass coordinate system. The origin of the coordinates is the centre of mass of the colliding reactants, and the collision takes place when the molecules are at the origin. The way in which centre-of-mass coordinates are constructed and the events in them interpreted involves too much detail for our present purposes, but we should bear in mind that 'forward' and 'backward' have unconventional meanings. The details are explained in the books in *Further reading*.



27.24 The calculated trajectories for a reactive encounter between H_A and a vibrating $H_B H_C$ molecule leading to the formation of a vibrating $H_A H_B$ molecule. This direct-mode reaction is between H and H_2 . (M. Karplus, R.N. Porter, and R.D. Sharma, *J. Chem. Phys.* 43, 3258 (1965).)

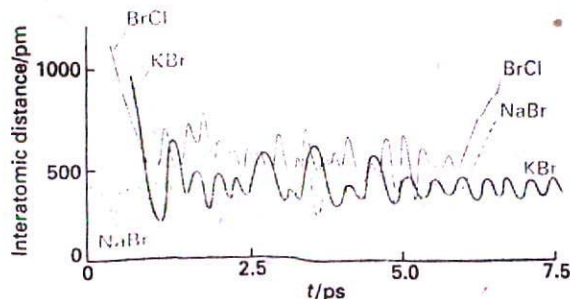
conclude that reactions with attractive potential energy surfaces proceed more efficiently if the energy is in relative translational motion. Moreover, the potential surface shows that once past the saddle point the trajectory runs up the steep wall of the product valley, and then rolls from side to side as it falls to the foot of the valley as the products separate. In other words, the products emerge in a vibrationally excited state.

Now consider the repulsive surface (Fig. 27.23). On trajectory C the collisional energy is largely in translation. As the reactants approach, the potential energy rises. Their path takes them up the opposing face of the valley, and they are reflected back into the reactant region. This path corresponds to an unsuccessful encounter, even though the energy is sufficient for reaction. On C^* some of the energy is in the vibration of the reactant molecule and the motion causes the trajectory to weave from side to side up the valley as it approaches the saddle point. This motion may be sufficient to tip the system round the corner to the saddle point and then on to products. In this case, the product molecule is expected to be in an unexcited vibrational state. Reactions with repulsive potential surfaces can therefore be expected to proceed more efficiently if the excess energy is present as vibrations. This is the case with the $H + Cl_2 \rightarrow HCl + Cl$ reaction, for instance.

(c) Classical trajectories

A clear picture of the reaction event can be obtained using classical mechanics to calculate the trajectories of the atoms taking place in a reaction. Figure 27.24 shows the result of such a calculation of the positions of the three atoms in the reaction $H + H_2 \rightarrow H_2 + H$, the horizontal coordinate now being time and the vertical coordinate the separations. This illustration shows clearly the vibration of the original molecule and the approach of the attacking atom. The reaction itself, the switch of partners, takes place very rapidly and is an example of a direct-mode process. The newly formed molecule shakes, but quickly settles down to steady, harmonic vibration as the expelled atom departs. In contrast, Fig. 27.25 shows an example of a complex-mode process, in which the activated complex survives for an extended period. The reaction in the illustration is the exchange reaction $KCl + NaBr \rightarrow KBr + NaCl$. The tetraatomic activated complex survives for about 5 ps, during which time the atoms make about 15 oscillations before dissociating into products.

Although this kind of calculation gives a good sense of what happens during a reaction, its limitations must be kept in mind. In the first place, a real gas-phase reaction occurs with a wide variety of different speeds and angles of attack. In the second place, the motion of the atoms, electrons, and nuclei is governed by quantum mechanics. The concept of trajectory then fades and is replaced by the unfolding of a wavefunction that represents initially the



27.25 An example of the trajectories calculated for a complex-mode reaction, $KCl + NaBr \rightarrow KBr + NaCl$, in which the collision cluster has a long lifetime. (P. Brumer and M. Karplus, *Faraday Disc. Chem. Soc.* 55, 80 (1973).)

reactants and finally the products. Nevertheless, recognition of these limitations should not be allowed to obscure the fact that recent advances in molecular reaction dynamics have given us a first glimpse of the processes going on at the core of reactions.

Table 27.3 Summary of uses of k

Symbol	Significance
k	Boltzmann constant
k_2	Second-order rate constant
k_2^0	Rate constant at zero ionic strength
k_a, k_b, \dots	Rate constants for individual steps
k'_a, k'_b, \dots	Rate constants for individual reverse steps
k^\ddagger	Rate constant for unimolecular decay of activated complex
K	Equilibrium constant (dimensionless)
K_γ	Ratio of activity coefficients
K^\ddagger	Proportionality constant between $[C^\ddagger]$ and $[A][B]$ (dimensions, 1/concentration)
κ	Transmission coefficient
\bar{K}	When multiplied by p^\ddagger/RT , a type of equilibrium constant but with one vibrational mode discarded (dimensions, 1/concentration)
k_f	Force constant

Checklist of key ideas

Reactive encounters

- collision theory

27.1 Collision theory

- collision density
 like-like collisions (10)
 dissimilar collisions (11)
 energy-dependent reactive collision cross-section (15)
 rate constant from collision theory (16)
 steric factor
 reactive cross-section
 harpoon mechanism

27.2 Diffusion-controlled reactions

- cage effect
 diffusion-controlled limit
 activation-controlled reaction

- rate constant and diffusion coefficient (27)

- rate constant and viscosity (35)

27.3 The material balance equation

- material balance equation (38)

Activated complex theory

- activated complex theory (ACT)

27.4 The reaction coordinate and the transition state

- activated complex
 transition state

27.5 The Eyring equation

- transmission coefficient (45)
 concentration of activated complex (46)
 Eyring equation (55)
 collision of structureless particles (58)
 kinetic isotope effect (60)
 femtochemistry

27.6 Thermodynamic aspects

- Gibbs energy of activation (61)
 entropy of activation (63)
 enthalpy of activation (63)
 steric factor and entropy (67)
 correlation analysis
 linear free energy relation (LFER)
 kinetic salt effect (73)

The dynamics of molecular collisions

27.7 Reactive collisions

- infrared chemiluminescence
 laser-induced fluorescence
 state-to-state cross-section
 state-to-state rate constant (75)

27.8 Potential energy surfaces

- potential energy surface
 saddle point

27.9 Some results from experiments and calculations

- attractive surface
 repulsive surface
 direct mode process
 complex mode process

Further reading

Articles of general interest

- G.M. Fernandez, J.A. Sordo, and T.L. Sordo, Analysis of potential energy surfaces. *J. Chem. Educ.* **65**, 665 (1988).
- K.J. Laidler, Just what is a transition state? *J. Chem. Educ.* **65**, 540 (1988).
- M.A. Smith, The nature of distribution functions for colliding systems: calculation of averaged properties. *J. Chem. Educ.* **70**, 218 (1993).
- H. Maskill, The Arrhenius equation. *Educ. in Chem.* **27**, 111 (1990).
- S.R. Logan, The meaning and significance of "the activation energy" of a chemical reaction. *Educ. in Chem.* **23**, 148 (1986).
- I. Powis, Energy redistribution in unimolecular ion dissociation. *Acc. Chem. Res.* **20**, 179 (1987).
- C.E. Klots, The reaction coordinate and its limitations: an experimental perspective. *Acc. Chem. Res.* **21**, 16 (1988).
- I.W.M. Smith, Vibrational adiabaticity in chemical reactions. *Acc. Chem. Res.* **23**, 101 (1990).
- P.R. Brooks, Spectroscopy of transition region species. *Chem. Rev.* **88**, 407 (1988).
- J. Keizer, Diffusion effects on rapid bimolecular chemical reactions. *Chem. Rev.* **87**, 167 (1987).
- D.W. Lupo and M. Quack, IR-laser photochemistry. *Chem. Rev.* **87**, 181 (1987).
- D.G. Trular, R. Steckler, and M.S. Gordon, Potential energy surfaces for polyatomic reaction dynamics. *Chem. Rev.* **87**, 181 (1987).
- A.H. Zewail, Laser femtochemistry. *Science* **242**, 1645 (1988).
- A.H. Zewail, Femtosecond transition-state dynamics. *Faraday Discuss. Chem. Soc.* **91**, 1 (1991).
- M.S. Child, Molecular reaction dynamics. *Sci. Prog.* **70**, 73 (1986).
- R.W. Carr, Chemical kinetics. In *Encyclopedia of applied physics* (ed. G.L. Trigg), **3**, 345. VCH, New York (1992).

Texts and sources of data and information

- K.J. Laidler, *Chemical kinetics*. Harper & Row, New York (1987).
- G.D. Billing and K.V. Mikkelsen, *Molecular dynamics and chemical kinetics*. Wiley, New York (1996).
- J.I. Steinfeld, J.S. Francisco, and W.L. Hase, *Chemical kinetics and dynamics*. Prentice-Hall, Englewood Cliffs (1989).
- J. Simons, *Energetic principles of chemical reactions*. Jones & Bartlett, Portola Valley (1983).
- R.A. Marcus, Activated complex theory: current status, extensions, and applications. In *Techniques of chemistry* (ed. E.S. Lewis), **6A**, 13. Wiley-Interscience, New York (1974).
- M.J. Blandamer, *Chemical equilibria in solution*. Ellis Horwood/Prentice-Hall, Hemel Hempstead (1992).
- P.C. Jordan, *Chemical kinetics and transport*. Plenum, New York (1979).
- I.W.M. Smith, *Kinetics and dynamics of elementary gas reactions*. Butterworth, London (1980).
- R.G. Gilbert and S.C. Smith, *Theory of unimolecular and recombination reactions*. Blackwell Scientific, Oxford (1990).
- R.B. Bernstein, *Chemical dynamics via molecular beam and laser techniques*. Clarendon Press, Oxford (1982).
- D.M. Hirst, *Potential energy surfaces*. Taylor & Francis, London (1985).
- R.D. Levine and R.B. Bernstein, *Molecular reaction dynamics and chemical reactivity*. Clarendon Press, Oxford (1987).
- R. van Eldik, T. Asano, and W.J. Le Noble, Activation and reaction volumes in solution. 2. *Chem. Rev.* **89**, 549 (1989).

Exercises

- 27.1 (a)** Calculate the collision frequency, z , and the collision density, Z , in ammonia, $R = 190$ pm, at 25°C and 100 kPa. What is the percentage increase when the temperature is raised by 10 K at constant volume?
- 27.1 (b)** Calculate the collision frequency, z , and the collision density, Z , in carbon monoxide, $R = 180$ pm at 25°C and 100 kPa. What is the percentage increase when the temperature is raised by 10 K at constant volume?
- 27.2 (a)** Collision theory demands knowing the fraction of molecular collisions having at least the kinetic energy E_a along the line of flight. What is this fraction when (a) $E_a = 10$ kJ mol $^{-1}$, (b) $E_a = 100$ kJ mol $^{-1}$ at (i) 300 K and (ii) 1000 K?
- 27.2 (b)** Collision theory demands knowing the fraction of molecular collisions having at least the kinetic energy E_a along the line of flight. What is this fraction when (a) $E_a = 15$ kJ mol $^{-1}$, (b) $E_a = 150$ kJ mol $^{-1}$ at (i) 300 K and (ii) 800 K?

- 27.3 (a)** Calculate the percentage increase in the fractions in Exercise 27.2a when the temperature is raised by 10 K.
- 27.3 (b)** Calculate the percentage increase in the fractions in Exercise 27.2b when the temperature is raised by 10 K.
- 27.4 (a)** Use the collision theory of gas-phase reactions to calculate the theoretical value of the second-order rate constant for the reaction $\text{H}_2(\text{g}) + \text{I}_2(\text{g}) \rightarrow 2\text{HI}(\text{g})$ at 650 K, assuming that it is elementary bimolecular. The collision cross-section is 0.36 nm^2 , the reduced mass is $3.32 \times 10^{-27} \text{ kg}$, and the activation energy is 171 kJ mol^{-1} .
- 27.4 (b)** Use the collision theory of gas-phase reactions to calculate the theoretical value of the second-order rate constant for the reaction $\text{D}_2(\text{g}) + \text{Br}_2(\text{g}) \rightarrow 2\text{DBr}(\text{g})$ at 450 K, assuming that it is elementary bimolecular. Take the collision cross-section as 0.30 nm^2 , the reduced mass as 3.930 u , and the activation energy as 200 kJ mol^{-1} .
- 27.5 (a)** A typical diffusion coefficient for small molecules in aqueous solution at 25°C is $5 \times 10^{-9} \text{ m}^2 \text{ s}^{-1}$. If the critical reaction distance is 0.4 nm , what value is expected for the second-order rate constant for a diffusion-controlled reaction?
- 27.5 (b)** Suppose that the typical diffusion coefficient for a reactant in aqueous solution at 25°C is $4.2 \times 10^{-9} \text{ m}^2 \text{ s}^{-1}$. If the critical reaction distance is 0.50 nm , what value is expected for the second-order rate constant for the diffusion-controlled reaction?
- 27.6 (a)** Calculate the magnitude of the diffusion-controlled rate constant at 298 K for a species in (a) water, (b) pentane. The viscosities are $1.00 \times 10^{-3} \text{ kg m}^{-1} \text{ s}^{-1}$, and $2.2 \times 10^{-4} \text{ kg m}^{-1} \text{ s}^{-1}$, respectively.
- 27.6 (b)** Calculate the magnitude of the diffusion-controlled rate constant at 298 K for a species in (a) decylbenzene, (b) concentrated sulfuric acid. The viscosities are 3.36 cP and 27 cP , respectively.
- 27.7 (a)** Calculate the magnitude of the diffusion-controlled rate constant at 298 K for the recombination of two atoms in water, for which $\eta = 0.89 \text{ cP}$. Assuming the concentration of the reacting species is $1.0 \times 10^{-3} \text{ mol L}^{-1}$ initially, how long does it take for the concentration of the atoms to fall to half that value? Assume the reaction is elementary.
- 27.7 (b)** Calculate the magnitude of the diffusion-controlled rate constant at 298 K for the recombination of two atoms in benzene, for which $\eta = 0.601 \text{ cP}$. Assuming the concentration of the reacting species is $1.8 \times 10^{-3} \text{ mol L}^{-1}$ initially, how long does it take for the concentration of the atoms to fall to half that value? Assume the reaction is elementary.
- 27.8 (a)** For the gaseous reaction $\text{A} + \text{B} \rightarrow \text{P}$, the reactive cross-section obtained from the experimental value of the pre-exponential factor is $9.2 \times 10^{-22} \text{ m}^2$. The collision cross-sections of A and B estimated from the transport properties are 0.95 and 0.65 nm^2 , respectively. Calculate the P -factor for the reaction.
- 27.8 (b)** For the gaseous reaction $\text{A} + \text{B} \rightarrow \text{P}$, the reactive cross-section obtained from the experimental value of the pre-exponential factor is $8.7 \times 10^{-22} \text{ m}^2$. The collision cross-sections of A and B estimated from the transport properties are 0.88 and 0.40 nm^2 , respectively. Calculate the P -factor for the reaction.
- 27.9 (a)** Two neutral species, A and B, with diameters 588 pm and 1650 pm , respectively, undergo the diffusion-controlled reaction $\text{A} + \text{B} \rightarrow \text{P}$ in a solvent of viscosity $2.37 \times 10^{-3} \text{ kg m}^{-1} \text{ s}^{-1}$ at 40°C . Calculate the initial rate $d[\text{P}]/dt$ if the initial concentrations of A and B are 0.150 mol L^{-1} and 0.330 mol L^{-1} , respectively.
- 27.9 (b)** Two neutral species, A and B, with diameters 442 pm and 885 pm , respectively, undergo the diffusion-controlled reaction $\text{A} + \text{B} \rightarrow \text{P}$ in a solvent of viscosity 1.27 cP at 20°C . Calculate the initial rate $d[\text{P}]/dt$ if the initial concentrations of A and B are 0.200 mol L^{-1} and 0.150 mol L^{-1} , respectively.
- 27.10 (a)** The reaction of propylxanthate ion in acetic acid buffer solutions has the mechanism $\text{A}^- + \text{H}^+ \rightarrow \text{P}$. Near 30°C the rate constant is given by the empirical expression $k_2 = (2.05 \times 10^{13})e^{-(8681 \text{ K})/T} \text{ L mol}^{-1} \text{ s}^{-1}$. Evaluate the energy and entropy of activation at 30°C .
- 27.10 (b)** The reaction $\text{A}^- + \text{H}^+ \rightarrow \text{P}$ has a rate constant given by the empirical expression $k_2 = (8.72 \times 10^{12})e^{-(6134 \text{ K})/T} \text{ L mol}^{-1} \text{ s}^{-1}$. Evaluate the energy and entropy of activation at 25°C .
- 27.11 (a)** When the reaction in Exercise 27.10a occurs in a dioxane/water mixture which is 30 per cent dioxane by mass, the rate constant fits $k_2 = (7.78 \times 10^{14})e^{-(9134 \text{ K})/T} \text{ L mol}^{-1} \text{ s}^{-1}$ near 30°C . Calculate $\Delta^\ddagger G$ for the reaction at 30°C .
- 27.11 (b)** A rate constant is found to fit the expression $k_2 = (6.45 \times 10^{13})e^{-(5375 \text{ K})/T} \text{ L mol}^{-1} \text{ s}^{-1}$ near 25°C . Calculate $\Delta^\ddagger G$ for the reaction at 25°C .
- 27.12 (a)** The gas-phase association reaction between F_2 and IF_5 is first-order in each of the reactants. The energy of activation for the reaction is 58.6 kJ mol^{-1} . At 65°C the rate constant is $7.84 \times 10^{-3} \text{ kPa}^{-1} \text{ s}^{-1}$. Calculate the entropy of activation at 65°C .
- 27.12 (b)** A gas-phase recombination reaction is first-order in each of the reactants. The energy of activation for the reaction is 49.6 kJ mol^{-1} . At 55°C the rate constant is $0.23 \text{ m}^3 \text{ s}^{-1}$. Calculate the entropy of activation at 55°C .
- 27.13 (a)** Calculate the entropy of activation for a collision between two structureless particles at 300 K , taking $M = 50 \text{ g mol}^{-1}$ and $\sigma = 0.40 \text{ nm}^2$.
- 27.13 (b)** Calculate the entropy of activation for a collision between two structureless particles at 500 K , taking $M = 78 \text{ g mol}^{-1}$ and $\sigma = 0.62 \text{ nm}^2$.
- 27.14 (a)** The pre-exponential factor for the gas-phase decomposition of ozone at low pressures is $4.6 \times 10^{12} \text{ L mol}^{-1} \text{ s}^{-1}$ and its activation energy is 10.0 kJ mol^{-1} . What are (a) the entropy of activation, (b) the enthalpy of activation, (c) the Gibbs energy of activation at 298 K ?
- 27.14 (b)** The pre-exponential factor for a gas-phase decomposition of ozone at low pressures is $2.3 \times 10^{13} \text{ L mol}^{-1} \text{ s}^{-1}$ and its activation energy is 30.0 kJ mol^{-1} . What are (a) the entropy of activation, (b) the enthalpy of activation, (c) the Gibbs energy of activation at 298 K ?

27.15 (a) The base-catalysed bromination of nitromethane- d_3 in water at room temperature (298 K) proceeds 4.3 times more slowly than the bromination of the undeuterated material. Account for this difference. Use $k_f(\text{CH}) = 450 \text{ N m}^{-1}$.

27.15 (b) Predict the order of magnitude of the isotope effect on the relative rates of displacement of (a) ^1H and ^3H , (b) ^{16}O and ^{18}O . Will raising the temperature enhance the difference? Take $k_f(\text{CH}) = 450 \text{ N m}^{-1}$, $k_f(\text{CO}) = 1750 \text{ N m}^{-1}$.

27.16 (a) The rate constant of the reaction $\text{H}_2\text{O}_2(\text{aq}) +$

$\text{I}^-(\text{aq}) + \text{H}^+(\text{aq}) \rightarrow \text{H}_2\text{O}(\text{l}) + \text{HIO}(\text{aq})$ is sensitive to the ionic strength of the aqueous solution in which the reaction occurs. At 25°C , $k = 12.2 \text{ L}^2 \text{ mol}^{-2} \text{ min}^{-1}$ at an ionic strength of 0.0525. Use the Debye-Hückel limiting law to estimate the rate constant at zero ionic strength.

27.16 (b) At 25°C , $k = 1.55 \text{ L}^2 \text{ mol}^{-3} \text{ min}^{-1}$ at an ionic strength of 0.0241 for a reaction in which the rate-determining step involves the encounter of two singly charged cations. Use the Debye-Hückel limiting law to estimate the rate constant at zero ionic strength.

Problems

Numerical problems

27.1 In the dimerization of methyl radicals at 25°C , the experimental pre-exponential factor is $2.4 \times 10^{10} \text{ L mol}^{-1} \text{ s}^{-1}$. What is (a) the reactive cross-section, (b) the P -factor for the reaction if the C-H bond length is 154 pm?

27.2 Nitrogen dioxide reacts bimolecularly in the gas phase to give $2\text{NO} + \text{O}_2$. The temperature dependence of the second-order rate constant for the rate law $d[\text{P}]/dt = k[\text{NO}_2]^2$ is given below. What are the P -factor and the reactive cross-section for the reaction?

T/K	600	700	800	1000
$k/(\text{cm}^3 \text{ mol}^{-1} \text{ s}^{-1})$	4.6×10^2	9.7×10^3	1.3×10^5	3.1×10^6

Take $\sigma = 0.60 \text{ nm}^2$.

27.3 The diameter of the methyl radical is about 308 pm. What is the maximum rate constant in the expression $d[\text{C}_2\text{H}_6]/dt = k[\text{CH}_3]^2$ for second-order recombination of radicals at room temperature? 10 per cent of a 1.0 L sample of ethane at 298 K and 100 kPa is dissociated into methyl radicals. What is the minimum time for 90 per cent recombination?

27.4 The rates of thermolysis of a variety of *cis*- and *trans*-azoalkanes have been measured over a range of temperatures in order to settle a controversy concerning the mechanism of the reaction. In ethanol an unstable *cis*-azoalkane decomposed at a rate that was followed by observing the N_2 evolution, and this led to the rate constants listed below (P.S. Engel and D.J. Bishop, *J. Amer. Chem. Soc.* 97, 6754 (1975)). Calculate the enthalpy, entropy, energy, and Gibbs energy of activation at -20°C .

$\theta/^\circ\text{C}$	-24.82	-20.73	-17.02	-13.00	-8.95
$10^4 \times k/\text{s}^{-1}$	1.22	2.31	4.39	8.50	14.3

27.5 In an experimental study of a bimolecular reaction in aqueous solution, the second-order rate constant was measured at 25°C and at a variety of ionic strengths and the results are tabulated below. It is known that a singly charged ion is involved in the rate-determining step. What is the charge on the other ion involved?

I	0.0025	0.0037	0.0045	0.0065	0.0085
$k/(\text{L mol}^{-1} \text{ s}^{-1})$	1.05	1.12	1.16	1.18	1.26

27.6 The rate constant of the reaction $\text{I}^-(\text{aq}) + \text{H}_2\text{O}_2(\text{aq}) \rightarrow \text{H}_2\text{O}(\text{l}) + \text{IO}^-(\text{aq})$ varies slowly with ionic strength, even though the Debye-Hückel limiting law predicts no

effect. Use the following data from 25°C to find the dependence of $\log k_r$ on the ionic strength:

I	0.0207	0.0525	0.0925	0.1575
$k_r/(\text{L mol}^{-1} \text{ min}^{-1})$	0.663	0.670	0.679	0.694

Evaluate the limiting value of k_r at zero ionic strength. What does the result suggest for the dependence of $\log \gamma$ on ionic strength for a neutral molecule in an electrolyte solution?

27.7 The total cross-sections for reactions between alkali metal atoms and halogen molecules are given in the table below (R.D. Levine and R.B. Bernstein, *Molecular reaction dynamics*, Clarendon Press, Oxford, 72 (1974)). Assess the data in terms of the harpoon mechanism.

σ^*/nm^2	Cl_2	Br_2	I_2
Na	1.24	1.16	0.97
K	1.54	1.51	1.27
Rb	1.90	1.97	1.67
Cs	1.96	2.04	1.95

Electron affinities are approximately 1.3 eV (Cl_2), 1.2 eV (Br_2), and 1.7 eV (I_2), and ionization energies are 5.1 eV (Na), 4.3 eV (K), 4.2 eV (Rb), and 3.9 eV (Cs).

Theoretical problems

27.8 Confirm that eqn 40 is a solution of eqn 39, where $[J]$, is a solution of the same equation but with $k = 0$ and for the same initial conditions.

27.9 Evaluate $[J]^*$ numerically using mathematical software for integration in eqn 40, and explore the effect of increasing reaction rate constant on the spatial distribution of J .

27.10 Estimate the orders of magnitude of the partition functions involved in a rate expression. State the order of magnitude of q_m^T/N_A , q^R , q^V , q^E for typical molecules. Check that in the collision of two structureless molecules the order of magnitude of the pre-exponential factor is of the same order as that predicted by collision theory. Go on to estimate the P -factor for a reaction in which $\text{A} + \text{B} \rightarrow \text{P}$, and A and B are nonlinear triatomic molecules.

27.11 Use the Debye-Hückel limiting law to show that changes in ionic strength can affect the rate of reaction catalysed by H^+ from the ionization of a weak acid. Consider the mechanism: $H^+(aq) + B(aq) \rightarrow P(aq)$, where H^+ comes from the ionization of the weak acid, HA. The weak acid has a fixed concentration. First show that $\log[H^+]$, derived from the ionization of HA, depends on the activity coefficients of ions and thus depends on the ionic strength. Then find the relationship between $\log(\text{rate})$ and $\log[H^+]$ to show that the rate also depends on the ionic strength.

27.12 The major difficulty in applying activated complex theory (and, it must be admitted, in devising straightforward problems to illustrate it) is to decide on the structure of the activated complex and to ascribe appropriate bond strengths and lengths to it. The following exercise gives some familiarity with the difficulties involved, yet leads to a numerical result for a reaction of some interest. Consider the attack of H on D_2 , which is one step in the $H_2 + D_2$ reaction. Suppose that the H atom approaches D_2 from the side and forms a complex in the form of an isosceles triangle. Take the H-D distance as 30 per cent greater than in H_2 (74 pm) and the D-D distance as 20 per cent greater than in H_2 . Let the critical coordinate be the antisymmetric stretching vibration in which one H-D bond stretches as the other shortens. Let all the vibrations be at about 1000 cm^{-1} . Estimate k_2 for this reaction at 400 K using the experimental activation energy of about 35 kJ mol^{-1} .

27.13 Now change the model of the activated complex in Problem 27.12 and make it linear. Use the same estimated molecular bond lengths and vibrational frequencies to calculate k_2 for this choice of model.

27.14 Clearly, there is much scope for modifying the parameters of the models of the activated complex in the last pair of problems. Write and run a program that allows you to vary the structure of the complex and the parameters in a plausible way, and look for a model (or more than one model) that gives a value of k close to the experimental value, $4 \times 10^5\text{ L mol}^{-1}\text{ s}^{-1}$.

27.15 The Eyring equation can also be applied to physical processes. As an example, consider the rate of diffusion of an atom stuck to the surface of a solid. Suppose that in order to move from one site to another it has to reach the top of the barrier where it can vibrate classically in the vertical direction and in one horizontal direction, but vibration along the other horizontal direction takes it into the neighbouring site. Find an expression for the rate of diffusion, and evaluate it for W atoms on a tungsten surface ($E_a = 60\text{ kJ mol}^{-1}$). Suppose that the vibration frequencies at the transition state are (a) the same as, (b) one-half the value for the adsorbed atom. What is the value of the diffusion coefficient D at 500 K? (Take the site separation as 316 pm and $\nu = 1 \times 10^{11}\text{ Hz}$.)

27.16 Suppose now that the adsorbed, migrating species treated in Problem 27.15 is a spherical molecule, and that it can rotate classically as well as vibrate at the top of the barrier, but that at the adsorption site itself it can only vibrate. What effect does this have on the diffusion constant? Take the molecule to be methane, for which $B = 5.24\text{ cm}^{-1}$.

27.17 Show that the intensities of a molecular beam before and after passing through a chamber of length l containing inert scattering atoms are related by $I = I_0 e^{-N\sigma l}$, where σ is the collision cross-section and N the number density of scattering atoms.

27.18 In a molecular beam experiment to measure collision cross-sections it was found that the intensity of a CsCl beam was reduced to 60 per cent of its intensity on passage through CH_2F_2 at $10\ \mu\text{Torr}$, but that when the target was Ar at the same pressure the intensity was reduced only by 10 per cent. What are the relative cross-sections of the two types of collision? Why is one much larger than the other?

Additional problems supplied by Carmen Giunta and Charles Trapp

27.19 T. Gierczak, R.K. Talukdar, S.C. Herndon, G.L. Vaghjiani, and A.R. Ravishankara (*J. Phys. Chem. A* 101, 3125 (1997)) measured the rate constants for the bimolecular gas-phase reaction of methane with the hydroxyl radical in several isotopic variations. From their data, the following Arrhenius parameters can be obtained.

	$A/(\text{L mol}^{-1}\text{ s}^{-1})$	$E_a/(\text{kJ mol}^{-1})$
$CH_4 + OH \rightarrow CH_3 + H_2O$	1.13×10^9	14.1
$CD_4 + OH \rightarrow CD_3 + DOH$	6.0×10^8	17.5
$CH_4 + OD \rightarrow CH_3 + DOH$	1.01×10^9	13.6

Compute the rate constants at 298 K, and interpret the kinetic isotope effects.

27.20 R. Atkinson (*J. Phys. Chem. Ref. Data* 26, 215 (1997)) has reviewed a large set of rate constants relevant to the atmospheric chemistry of volatile organic compounds. The recommended rate constant for the bimolecular association of O_2 with an alkyl radical R at 298 K is $4.7 \times 10^9\text{ L mol}^{-1}\text{ s}^{-1}$ for $R = C_2H_5$ and $8.4 \times 10^9\text{ L mol}^{-1}\text{ s}^{-1}$ for $R = \text{cyclohexyl}$. Assuming no energy barrier, compute the steric factor, P , for each reaction. *Hint*. Obtain collision diameters from collision cross-sections of similar molecules in the *Data section*.

27.21 M. Cyfert, B. Latko, and M. Wawrzeczyk (*Int. J. Chem. Kinet.* 28, 103 (1996)) examined the oxidation of tris(1,10-phenanthroline)iron(II) by periodate in aqueous solution, a reaction that shows autocatalytic behaviour. To assess the kinetic salt effect, they measured rate constants at a variety of concentrations of Na_2SO_4 far in excess of reactant concentrations and reported the following data.

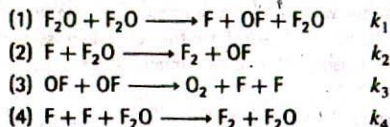
$[Na_2SO_4]/(\text{mol kg}^{-1})$	0.2	0.15	0.1	0.05
$k/(\text{L}^{1/2}\text{ mol}^{-1/2}\text{ s}^{-1})$	0.462	0.430	0.390	0.321
$[Na_2SO_4]/(\text{mol kg}^{-1})$	0.25	0.0125	0.005	
$k/(\text{L}^{1/2}\text{ mol}^{-1/2}\text{ s}^{-1})$	0.283	0.252	0.224	

What can be inferred about the charge of the activated complex of the rate-determining step?

27.22 R.H. Bisby and A.W. Parker (*J. Amer. Chem. Soc.* 117, 5664 (1995)) studied the reaction of photochemically excited duroquinone with the antioxidant α -tocopherol in ethanol. Once the duroquinone was photochemically excited, a bimolecular reaction took place at a rate described as diffusion-limited. (a) Estimate the rate constant for a diffusion-limited reaction in ethanol. (b) The reported rate constant

was $2.77 \times 10^9 \text{ L mol}^{-1} \text{ s}^{-1}$; estimate the critical reaction distance if the sum of diffusion constants is $1 \times 10^{-9} \text{ m}^2 \text{ s}^{-1}$.

27.23 For the thermal decomposition of F_2O by the reaction $2\text{F}_2\text{O}(\text{g}) \rightarrow 2\text{F}_2(\text{g}) + \text{O}_2(\text{g})$, J. Czarnowski and H.J. Schuhmacher (*Chem. Phys. Lett.* 17, 235 (1972)) have suggested the following mechanism:



(a) Using the steady-state approximation, show that this mechanism is consistent with the experimental rate law $-d[\text{F}_2\text{O}]/dt = k[\text{F}_2\text{O}]^2 + k'[\text{F}_2\text{O}]^{3/2}$. (b) The experimentally determined Arrhenius parameters in the range 501–583 K are $A = 7.8 \times 10^{13} \text{ L mol}^{-1} \text{ s}^{-1}$, $E_a/R = 1.935 \times 10^4 \text{ K}$ for k and $A = 2.3 \times 10^{10} \text{ L mol}^{-1} \text{ s}^{-1}$, $E_a/R = 1.691 \times 10^4 \text{ K}$ for k' . At 540 K, $\Delta_f H^\ominus(\text{F}_2\text{O}) = +24.41 \text{ kJ mol}^{-1}$, $D(\text{F}-\text{F}) = 160.6 \text{ kJ mol}^{-1}$, and $D(\text{O}-\text{O}) = 498.2 \text{ kJ mol}^{-1}$. Estimate the bond dissociation energies of the first and second F–O bonds and the Arrhenius activation energy of reaction 2.

27.24 Show that bimolecular reactions between nonlinear molecules are much slower than those between atoms even when the activation

energies of both reactions are equal. Use activated complex theory and make the following assumptions. (1) All vibrational partition functions are close to unity; (2) all rotational partition functions are approximately $1 \times 10^{1.5}$, which is a reasonable order of magnitude number; (3) the translational partition function for each species is 1×10^{26} .

27.25 For the gas-phase reaction $\text{A} + \text{A} \rightarrow \text{A}_2$, the experimental rate constant, k_2 , has been fitted to the Arrhenius equation with the preexponential factor $A = 4.07 \times 10^5 \text{ L mol}^{-1} \text{ s}^{-1}$ at 300 K and an activation energy of $65.43 \text{ kJ mol}^{-1}$. Calculate $\Delta^\ddagger S$, $\Delta^\ddagger H$, $\Delta^\ddagger U$, and $\Delta^\ddagger G$ for the reaction.

27.26 One of the most historically significant studies of chemical reaction rates was that by M. Bodenstein (*Z. physik. Chem.* 29, 295 (1899)) of the gas-phase reaction $2\text{HI}(\text{g}) \rightarrow \text{H}_2(\text{g}) + \text{I}_2(\text{g})$ and its reverse, with rate constants k and k' , respectively. The measured rate constants as a function of temperature are


T/K	647	666	683	700
$k/(22.4 \text{ L mol}^{-1} \text{ min}^{-1})$	0.230	0.588	1.37	3.10
$k'/(22.4 \text{ L mol}^{-1} \text{ min}^{-1})$	0.0140	0.0379	0.0659	0.172
T/K	716	781		
$k/(22.4 \text{ L mol}^{-1} \text{ min}^{-1})$	6.70	105.9		
$k'/(22.4 \text{ L mol}^{-1} \text{ min}^{-1})$	0.375	3.58		

Demonstrate that these data are consistent with the collision theory of bimolecular gas-phase reactions.



28

Processes at solid surfaces



The growth and structure of solid surfaces

- 28.1 Surface growth
- 28.2 Surface composition

The extent of adsorption

- 28.3 Physisorption and chemisorption
- 28.4 Adsorption isotherms
- 28.5 The rates of surface processes

Catalytic activity at surfaces

- 28.6 Adsorption and catalysis
- 28.7 Examples of catalysis

Checklist of key ideas

Further reading

Exercises

Problems

In this chapter we see how solids grow at their surfaces and how the details of the structure and composition of solid surfaces can be determined experimentally. A major part of the material concerns the extent to which a surface is covered and the variation of the extent of coverage with the pressure and temperature. This material is used to discuss how surfaces affect the rate and course of chemical change by acting as the site of catalysis.

Processes at solid surfaces govern the viability of industry both constructively, as in catalysis, and destructively, as in corrosion. Chemical reactions at solid surfaces may differ sharply from reactions in the bulk, for reaction pathways of much lower activation energy may be provided, and hence result in catalysis. The concept of a solid surface has been extended in recent years with the availability of microporous aluminosilicates, the zeolites, in which the surface effectively extends deep inside the solid (Fig. 27.1). Most of the catalysts used in the petrochemical industry are now zeolites.

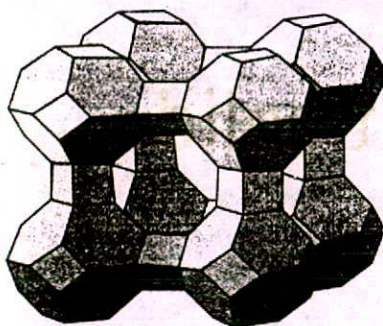
We shall see that acronyms are widely used in surface studies; for convenience, a list of the acronyms used in this text is given at the end of the chapter.

The growth and structure of solid surfaces

In this section we see how surfaces are extended and crystals grow. The attachment of particles to a surface is called **adsorption**. The substance that adsorbs is the **adsorbate** and the underlying material that we are concerned with in this section is the **adsorbent** or **substrate**. The reverse of adsorption is **desorption**.

27.1 Surface growth

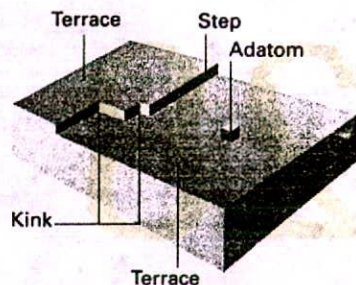
A simple picture of a perfect crystal surface is as a tray of oranges in a grocery store (Fig. 27.2). A gas molecule that collides with the surface can be imagined as a ping-pong ball bouncing erratically over the oranges. The molecule loses energy as it bounces, but it is likely to escape from the surface before it has lost enough kinetic energy to be trapped. The same



28.1 A framework representation showing the general layout of the atoms in a zeolite material. Note the truncated octahedra, the small cubic cages, and the large central cage.



28.2 A schematic diagram of the flat surface of a solid. This primitive model is largely supported by surface-tunnelling microscope images (see Fig. 28.20).



28.3 Some of the kinds of defects that may occur on otherwise perfect terraces. Defects play an important role in surface growth and catalysis.

is true, to some extent, of an ionic crystal in contact with a solution. There is little energy advantage for an ion in solution to discard some of its solvating molecules and stick at an exposed position on the surface.

(a) The role of defects

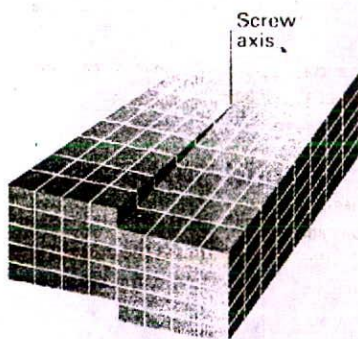
The picture changes when the surface has defects, for then there are ridges of incomplete layers of atoms or ions. A typical type of surface defect is a step between two otherwise flat layers of atoms called terraces (Fig. 28.3). A step defect might itself have defects for it might have kinks. When an atom settles on a terrace it bounces across it under the influence of the intermolecular potential, and might come to a step or a corner formed by a kink. Instead of interacting with a single terrace atom, the molecule now interacts with several, and the interaction may be strong enough to trap it. Likewise, when ions deposit from solution, the loss of the solvation interaction is offset by a strong Coulombic interaction between the arriving ions and several ions at the surface defect.

(b) Dislocations

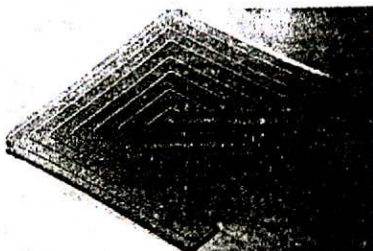
Not all kinds of defect result in sustained surface growth. As the process of settling into ledges and kinks continues, there comes a stage when an entire lower terrace has been covered. At this stage the surface defects have been eliminated, and growth will cease. For continuing growth, a surface defect is needed that propagates as the crystal grows. We can see what form of defect this must be by considering the types of dislocations, or discontinuities in the regularity of the lattice, that exist in the bulk of a crystal. One reason for their formation may be that the crystal grows so quickly that its particles do not have time to settle into states of lowest potential energy before being trapped in position by the deposition of the next layer.

A special kind of dislocation is the screw dislocation shown in Fig. 28.4. Imagine a cut in the crystal, with the particles to the left of the cut pushed up through a distance of one unit cell. The unit cells now form a continuous spiral around the end of the cut, which is called the screw axis. A path encircling the screw axis spirals up to the top of the crystal, and where the dislocation breaks through to the surface it takes the form of a spiral ramp.

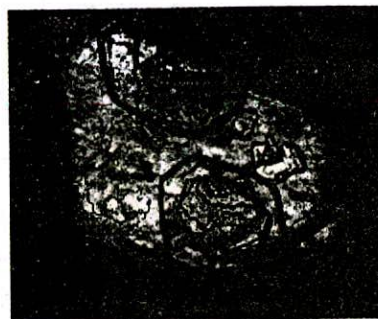
The surface defect formed by a screw dislocation is a step, possibly with kinks, where growth can occur. The incoming particles lie in ranks on the ramp, and successive ranks reform the step at an angle to its initial position. As deposition continues the step rotates around the screw axis, and is not eliminated. Growth may therefore continue indefinitely.



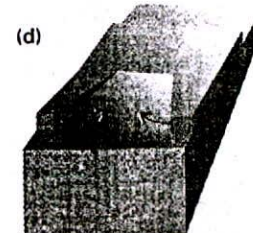
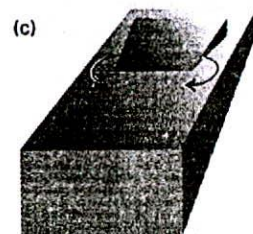
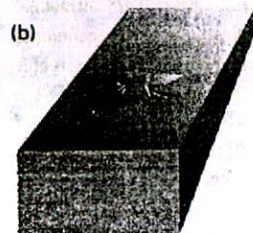
28.4 A screw dislocation occurs where one region of the crystal is pushed up through one or more unit cells relative to another region. The cut extends to the screw axis. As atoms lie along the step, the dislocation rotates round the screw axis, and is not annihilated.



28.5 The spiral growth arising from the propagation of a screw axis is clearly visible in this photograph of an alkane crystal. (B.R. Jennings and V.J. Morris, *Atoms in contact*, Clarendon Press, Oxford (1974); courtesy of Dr A.J. Forty.)



28.6 The spiral growth pattern is sometimes concealed because the terraces are subsequently completed by further deposition. This accounts for the appearance of this cadmium iodide crystal. (H.M. Rosenberg, *The solid state*, Clarendon Press, Oxford (1978).)



28.7 Counter-rotating screw dislocations on the same surface lead to the formation of terraces. Four stages of one cycle of growth are shown here. Subsequent deposition can complete each terrace.

Several layers of deposition may occur, and the edges of the spirals might be cliffs several atoms high (Fig. 28.5).

Propagating spiral edges can also give rise to flat terraces (Fig. 28.6). Terraces are formed if growth occurs simultaneously at neighbouring left- and right-handed screw dislocations (Fig. 28.7). Successive tables of atoms may form as counter-rotating defects collide on successive circuits, and the terraces formed may then fill up by further deposition at their edges to give flat crystal planes.

The rapidity of growth depends on the crystal plane concerned, and the slowest growing faces dominate the appearance of the crystal. This feature is explained in Fig. 28.8, where we see that, although the horizontal face grows forward most rapidly, it grows itself out of existence, and the slower-growing faces survive.

28.2 Surface composition

Under normal conditions, a surface exposed to a gas is constantly bombarded with molecules and a freshly prepared surface is covered very quickly. Just how quickly can be estimated using the kinetic theory of gases and the expression (eqn 24.3) for the collision flux:

$$Z_w = \frac{p}{(2\pi mkT)^{1/2}} \quad (1a)$$

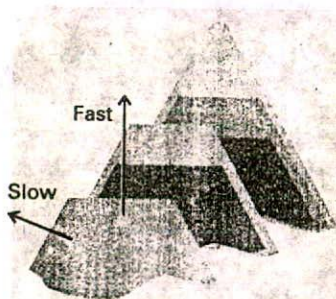
A practical form of this equation is

$$Z_w = \frac{Z_0(p/\text{Pa})}{\{(T/\text{K})(M/(\text{g mol}^{-1}))\}^{1/2}} \quad Z_0 = 2.63 \times 10^{24} \text{ m}^{-2} \text{ s}^{-1} \quad (1b)$$

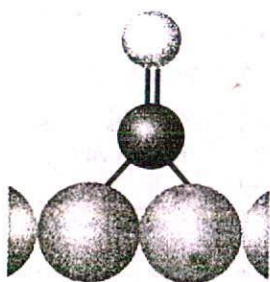
where M is the molar mass of the gas. For air ($M \approx 29 \text{ g mol}^{-1}$) at 1 atm and 25°C the collision flux is $3 \times 10^{27} \text{ m}^{-2} \text{ s}^{-1}$. Because 1 m^2 of metal surface consists of about 10^{19} atoms, each atom is struck about 10^8 times each second. Even if only a few collisions leave a molecule adsorbed to the surface, the time for which a freshly prepared surface remains clean is very short.

(a) High-vacuum techniques

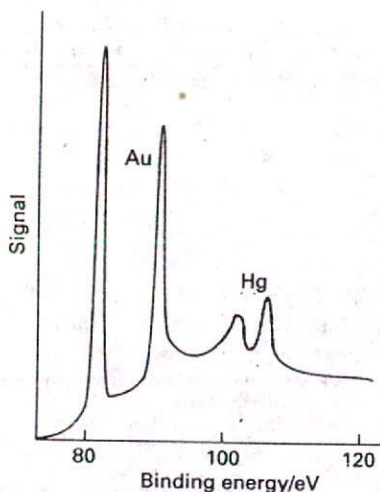
The obvious way to retain cleanliness is to reduce the pressure. When it is reduced to 10^{-4} Pa (as in a simple vacuum system) the collision flux falls to about $10^{18} \text{ m}^{-2} \text{ s}^{-1}$, corresponding to one hit per surface atom in each 0.1 s. Even that is too brief in most experiments, and in ultra-high vacuum (UHV) techniques pressures as low as 10^{-7} Pa (when



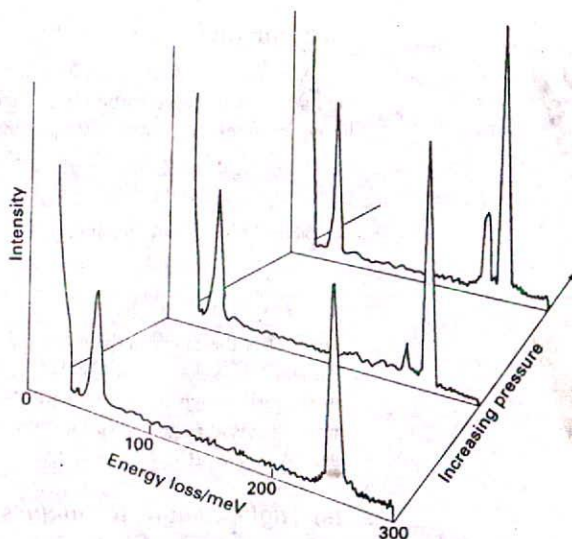
28.8 The slower-growing faces of a crystal dominate its final external appearance. Three successive stages of the growth are shown.



1 Bridge site



28.9 The X-ray photoelectron emission spectrum of a sample of gold contaminated with a surface layer of mercury. (M.W. Roberts and C.S. McKee, *Chemistry of the metal-gas interface*, Oxford (1978).)



28.10 The electron energy-loss spectrum of CO adsorbed on Pt(111). The results for three different pressures are shown, and the growth of the additional peak at about 200 meV (1600 cm^{-1}) should be noted. (Spectra provided by Professor H. Ibach.)

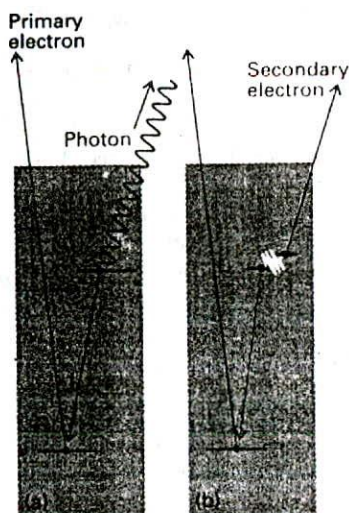
$Z_w = 10^{15}\text{ m}^{-2}\text{ s}^{-1}$) are reached on a routine basis and 10^{-9} Pa (when $Z_w = 10^{13}\text{ m}^{-2}\text{ s}^{-1}$) are reached with special care. These collision fluxes correspond to each surface atom being hit once every 10^5 to 10^6 s, or about once a day.

The layout of a typical UHV apparatus is such that the whole of the evacuated part can be heated to $150\text{--}250^\circ\text{C}$ for several hours to drive gas molecules from the walls. All the taps and seals are usually of metal so as to avoid contamination from greases. The sample is usually in the form of a thin foil, a filament, or a sharp point. Where there is interest in the role of specific crystal planes the sample is a single crystal with a freshly cleaved face. Initial surface cleaning is achieved either by heating it electrically or by bombarding it with accelerated gaseous ions. The latter procedure demands care because ion bombardment can shatter the surface structure and leave it an amorphous jumble of atoms. High-temperature annealing is then required to return the surface to an ordered state.

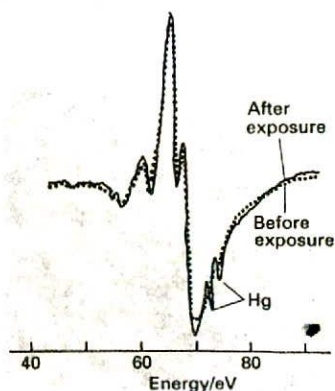
(b) Ionization techniques

Surface composition can be determined by a variety of ionization techniques. The same techniques can be used to detect any remaining contamination after cleaning and to detect layers of material adsorbed later in the experiment. Their common feature is that the escape depth of the electrons, the maximum depth from which ejected electrons come, is in the range $0.1\text{--}1.0\text{ nm}$, which ensures that only surface species contribute.

One technique that may be used is photoelectron spectroscopy (Section 17.8), which in surface studies is normally called photoemission spectroscopy. X-rays or hard ultraviolet ionizing radiation of energy in the range $5\text{--}40\text{ eV}$ may be used, giving rise to the techniques denoted XPS and UPS, respectively. XPS, which examines inner-shell binding energies, is able to fingerprint the materials present (Fig. 28.9). UPS, which examines electrons ejected from valence shells, is more suited to establishing the bonding characteristics and the details of valence shell electronic structures of substances on the surface. Its usefulness is its ability to reveal which orbitals of the adsorbate are involved in the bond to the substrate. For instance,



28.11 When an electron is expelled from a solid, (a) an electron of higher energy may fall into the vacated orbital and emit an X-ray photon to produce X-ray fluorescence. Alternatively, (b) the electron falling into the orbital may give up its energy to another electron, which is ejected in the Auger effect.



28.12 An Auger spectrum of the same sample used for Fig. 28.9 taken before and after deposition of mercury. (M.W. Roberts and C.S. McKee, *Chemistry of the metal-gas interface*, Oxford (1978).)

the principal difference between the photoemission results on free benzene and benzene adsorbed on palladium is in the energies of the π electrons. This difference is interpreted as meaning that the C_6H_6 molecules lie parallel to the surface and are attached to it by their π orbitals. In contrast, pyridine (C_5H_5N) stands more or less perpendicular to the surface, and is attached by a σ bond formed by the nitrogen lone pair.

(c) Energy-loss spectroscopy

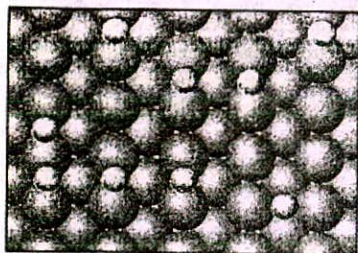
Several kinds of vibrational spectroscopy have been developed to study adsorbates and to show whether dissociation has occurred. Infrared and Raman spectroscopy have been greatly improved by the development of laser and Fourier transform techniques, and have largely overcome the difficulties arising from low intensities on account of the low surface coverages normally encountered under laboratory conditions. **Surface-enhanced Raman scattering (SERS)** makes the Raman technique viable for surface studies despite its intrinsic weakness: the strong enhancement, which can reach a factor of 10^6 on roughened silver surfaces, is due in part to local accumulations of electron density at the features of the roughened surface and at regions where bonding occurs. Raman intensities remain a problem on flat single crystal surfaces, and SERS works for only certain metals.

A hybrid version of photoemission spectroscopy and vibrational spectroscopy is **electron energy-loss spectroscopy (EELS, or HREELS, where HP denotes high resolution)** in which the energy loss suffered by a beam of electrons is monitored when they are reflected from a surface. As in optical Raman spectroscopy, the spectrum of energy loss can be interpreted in terms of the vibrational spectrum of the adsorbate. High resolution and sensitivity are attainable, and the technique is sensitive to light elements (to which X-ray techniques are insensitive). Very tiny amounts of adsorbate can be detected, and one report estimated that about 48 atoms of phosphorus were detected in one sample. As an example, Fig. 28.10 shows the EELS result for CO on the (111) face of a platinum crystal as the extent of surface coverage increases. The main peak arises from CO attached perpendicular to the surface by a single Pt atom. As the coverage increases the neighbouring smaller peak increases in intensity. This peak is due to CO at a bridge site, attached to two Pt atoms, as in (1).

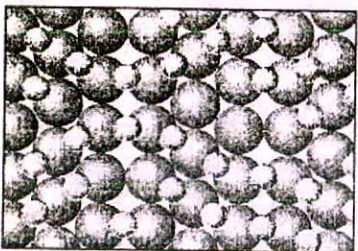
(d) Auger electron spectroscopy

A very important technique, which is widely used in the microelectronics industry, is **Auger electron spectroscopy (AES)**. The Auger effect is the emission of a second electron after high-energy radiation has expelled another. The first electron to depart leaves a hole in a low-lying orbital, and an electron from a higher energy orbital falls into it. The energy this releases may result either in the generation of radiation, which is called **X-ray fluorescence** (Fig. 28.11a) or in the ejection of another electron (Fig. 28.11b). The latter is the secondary electron of the Auger effect. The energies of the secondary electrons are characteristic of the material present, and so the Auger effect effectively takes a fingerprint of the sample (Fig. 28.12). In practice, the Auger spectrum is normally obtained by irradiating the sample with an electron beam of energy in the range 1–5 keV rather than with electromagnetic radiation. In **scanning Auger electron microscopy (SAM)**, the finely focused electron beam is scanned over the surface and a map of composition is compiled; the resolution can reach below about 50 nm.

The technique known as **surface-extended X-ray absorption fine structure spectroscopy (SEXAFS)** makes use of the intense X-radiation from synchrotron sources (Section 16.1a). The technique makes use of the oscillations in X-ray absorbance that are observed on the high-frequency side of the absorption edge (the start of an X-ray absorption band) of a substance. Oscillations arise from a quantum mechanical interference between the wavefunction of a photoejected electron and parts of that electron's

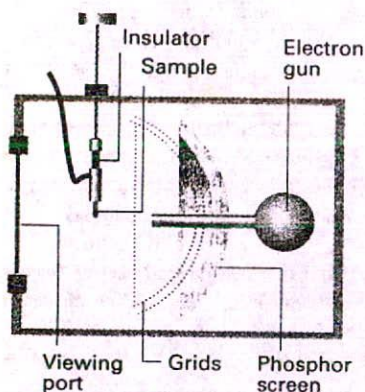


(a)



(b)

28.13 The restructuring of a surface that sometimes accompanies chemisorption. The diagrams illustrate the changes that occur when CO adsorbs on the (111) face of palladium. (a) Up to 0.3 monolayers, the surface structure is unchanged. (b) A metastable structure produced at low temperature when the surface is saturated.



28.14 A schematic diagram of the apparatus used for a LEED experiment. The electrons diffracted by the surface layers are detected by the fluorescence they cause on the phosphor screen.

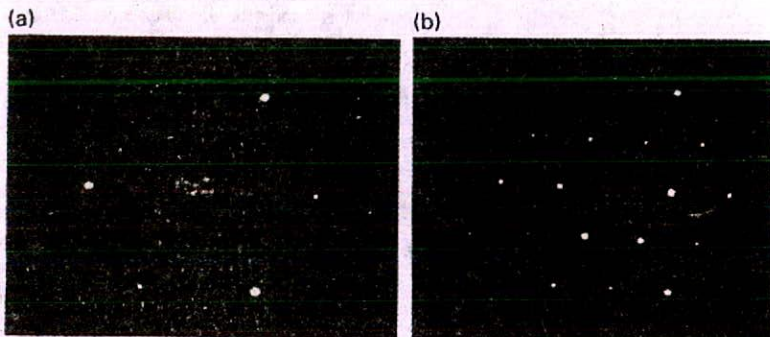
wavefunction that are scattered by neighbouring atoms. If the waves interfere destructively, the photoelectron appears with lower probability and the X-ray absorption is correspondingly less. If the waves interfere constructively, then the photoelectron amplitude is higher, and the photoelectron has a higher probability of appearing; correspondingly, the X-ray absorption is greater. The oscillations therefore contain information about the number and distances of the neighbouring atoms. Such studies show that a solid's surface is much more plastic than had previously been thought, and that it undergoes reconstruction, or structural modification, in response to adsorbates that are present. An example is given in Fig. 28.13, which shows how a palladium surface is reconstructed in different ways and to different extents at different temperatures and with varying surface coverage of CO.

(e) Low-energy electron diffraction

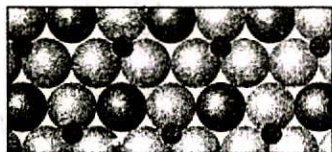
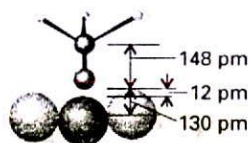
One of the most informative techniques for determining the arrangement of the atoms close to the surface is low-energy electron diffraction (LEED). This technique is essentially electron diffraction (Section 21.10), but the sample is now the surface of a solid. The use of low-energy electrons (with energies in the range 10–200 eV, corresponding to wavelengths in the range 100–400 pm) ensures that the diffraction is caused only by atoms on and close to the surface. The experimental arrangement is shown in Fig. 28.14, and typical LEED patterns, obtained by photographing the fluorescent screen through the viewing port, are shown in Fig. 28.15.

The LEED pattern portrays the two-dimensional structure of the surface. By studying how the diffraction intensities depend on the energy of the electron beam it is also possible to infer some details about the vertical location of the atoms and to measure the thickness of the surface layer, but the interpretation of LEED data is much more complicated than the interpretation of bulk X-ray data. The pattern is sharp if the surface is well-ordered for distances long compared with the wavelength of the incident electrons. In practice, sharp patterns are obtained for surfaces ordered to depths of about 20 nm and more. Diffuse patterns indicate either a poorly ordered surface or the presence of impurities. If the LEED pattern does not correspond to the pattern expected by extrapolation of the bulk surface to the surface, then either a reconstruction of the surface has occurred or there is order in the arrangement of an adsorbed layer.

LEED experiments show that the surface of a crystal rarely has exactly the same form as a slice through the bulk. As a general rule, it is found that metal surfaces are simply truncations of the bulk lattice, but the distance between the top layer of atoms and the one



28.15 LEED photographs of (a) a clean platinum surface and (b) after its exposure to propyne, $\text{CH}_3\text{C}\equiv\text{CH}$. (Photographs provided by Professor G.A. Samorjai.)



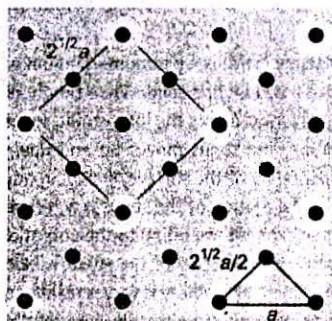
28.16 The structure of a surface close to the point of attachment of $\text{CH}_3\text{C}-$ to the (111) surface of rhodium at 300 K and the changes in positions of the metal atoms that accompany chemisorption.

below is contracted by around 5 per cent. Semiconductors generally have surfaces reconstructed to a depth of several layers. Reconstruction occurs in ionic solids. For example, in lithium fluoride the Li^+ and F^- ions close to the surface apparently lie on slightly different planes. An actual example of the detail that can now be obtained from refined LEED techniques is shown in Fig. 28.16 for $\text{CH}_3\text{C}-$ adsorbed on a (111) plane of rhodium.

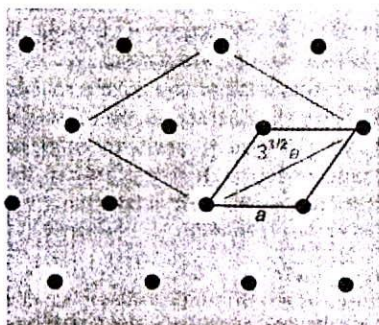
A simple notation has been developed to describe the arrangement of atoms at a surface. An arrangement of atoms corresponding to the bulk unit cell is called the **substrate structure** and is designated (1×1) . Thus, the substrate structure of the (111) face of a metal M would be designated $M(111)-(1 \times 1)$. An adsorbed species A that has the same structure would be denoted $(1 \times 1)-A$. Therefore, a monolayer of oxygen atoms on the (111) face of silicon would be denoted $\text{Si}(111)-(1 \times 1)-\text{O}$.

A surface structure with a unit cell side that is twice as large as the unit cell side of the substrate surface is denoted (2×2) . In general, the relative size would be denoted $(n \times m)$, as illustrated for two common cases in Fig. 28.17. In a number of cases, the surface atoms form a lattice that is rotated with respect to the substrate. A surface structure rotated by 45° , for instance, would be denoted $R45^\circ$, as in $(2^{1/2} \times 2^{1/2})R45^\circ$.

The presence of terraces, steps, and kinks in a surface shows up in LEED patterns, and their surface density (the number of defects in a region divided by the area of the region) can be estimated. The importance of this type of measurement will emerge later. Three examples of how steps and kinks affect the pattern are shown in Fig. 28.18. The samples used were obtained by cleaving a crystal at different angles to a plane of atoms. Only terraces are produced when the cut is parallel to the plane, and the density of steps increases as the angle

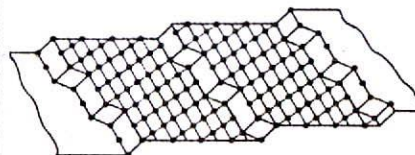
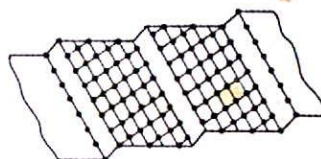


(a)

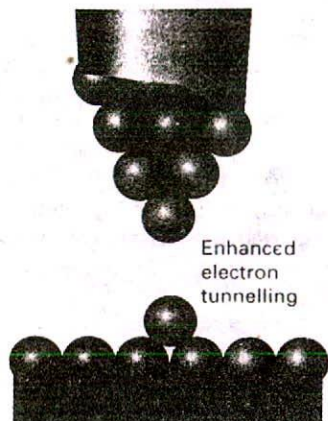


(b)

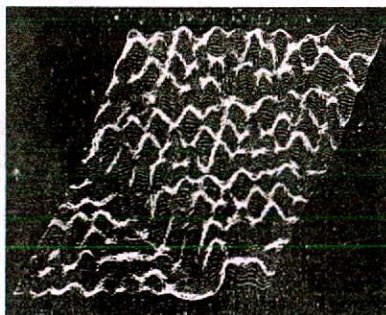
28.17 The designation of two adsorbed surface layers: (a) $(2^{1/2} \times 2^{1/2})R45^\circ$, (b) $(3^{1/2} \times 3^{1/2})R30^\circ$.



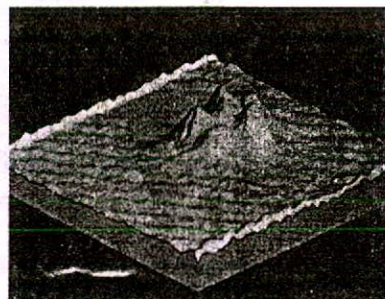
28.18 LEED patterns may be used to assess the defect density of a surface. The photographs correspond to a platinum surface with (a) low defect density, (b) regular steps separated by about six atoms, and (c) regular steps with kinks. (Photographs provided by Professor G.A. Samorjai.)



28.19 A representation of the the tip of a scanning tunnelling microscope and the surface above which it lies. The tunnelling probability for electrons varies exponentially with the separation of the tip from the surface features, so the current (shown here by the green band) is representative of atomic-scale variations of the topography of the surface.



28.20 The type of image that can be obtained with scanning tunnelling microscopy. The sample is of a silicon surface and the cliff is one atom high. (Sang-il Park and C.F. Quate.)



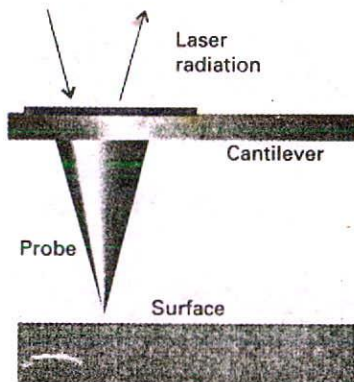
28.21 A scanning tunnelling microscope image of a liquid-crystal molecule (5-nonyl-2-nonyloxyphenylpyrimidine) adsorbed on a graphite surface. (J.S. Foster, et al., *Nature* 338, 137 (1988).)

of the cut increases. The observation of additional structure in the LEED patterns, rather than blurring, shows that the steps are arrayed regularly.

(f) Scanning tunnelling and atomic force microscopy

The central component in scanning tunnelling microscopy (STM) is a platinum-rhodium or tungsten needle, which is scanned across the surface of a conducting solid. When the tip of the needle is brought very close to the surface, electrons tunnel across the intervening space (Fig. 28.19). In the constant-current mode of operation, the stylus moves up and down corresponding to the form of the surface, and the topography of the surface, including any adsorbates, can be mapped on an atomic scale. The vertical motion of the stylus is achieved by fixing it to a piezoelectric cylinder, which contracts or expands according to the potential difference it experiences. In the constant- z mode, the vertical position of the stylus is held constant and the current is monitored. Because the tunnelling probability is very sensitive to the size of the gap (Section 12.3), the microscope can detect tiny, atomic-scale variations in the height of the surface. An example of the kind of image obtained with a clean surface is shown in Fig. 28.20, where the cliff is only one atom high. A spectacular demonstration of the power of the technique for displaying the shape of adsorbed species is shown in Fig. 28.21, which shows a single liquid-crystal molecule adsorbed to a surface.

In atomic force microscopy (AFM) a sharpened stylus attached to a beam is scanned across the surface (Fig. 28.22). The force exerted by the surface and any adsorbate pushes or pulls on the stylus and deflects the beam. The deflection is monitored either by interferometry or by using a laser beam. Because no current is needed between the sample and the probe, the technique can be applied to nonconducting surfaces too.



28.22 A representation of the probe of an atomic force microscope. The probe tapers to a single atom; the deflection of the cantilever beam is monitored by using laser radiation reflected from a small mirror.

(g) Molecular beam techniques

Whereas many important studies have been carried out simply by exposing a surface to a gas, modern work is increasingly making use of molecular beam scattering (MBS). One advantage is that the activity of specific crystal planes can be investigated by directing the beam on to an orientated surface with known step and kink densities (as measured by LEED). Furthermore, if the adsorbate reacts at the surface, the products (and their angular distributions) can be analysed as they are ejected from the surface and pass into a mass

spectrometer. Another advantage is that the time of flight of a particle may be measured and interpreted in terms of its residence time on the surface. In this way a very detailed picture can be constructed of the events taking place during reactions at surfaces.

The extent of adsorption

The extent of surface coverage is normally expressed as the fractional coverage, θ :

$$\theta = \frac{\text{number of adsorption sites occupied}}{\text{number of adsorption sites available}} \quad [2]$$

The fractional coverage is often expressed in terms of the volume of adsorbate adsorbed by $\theta = V/V_{\infty}$, where V_{∞} is the volume of adsorbate corresponding to complete monolayer coverage. The rate of adsorption, $d\theta/dt$, is the rate of change of surface coverage, and can be determined by observing the change of fractional coverage with time.

Among the principal techniques for measuring $d\theta/dt$ are flow methods, in which the sample itself acts as a pump because adsorption removes particles from the gas. One commonly used technique is therefore to monitor the rates of flow of gas into and out of the system: the difference is the rate of gas uptake by the sample. Integration of this rate then gives the fractional coverage at any stage. In flash desorption the sample is suddenly heated (electrically) and the resulting rise of pressure is interpreted in terms of the amount of adsorbate originally on the sample. The interpretation may be confused by the desorption of a compound (for example, WO_3 from oxygen on tungsten). Gravimetry, in which the sample is weighed on a microbalance during the experiment, can also be used, as can radioactive tracers. In the latter case, the radioactivity of the sample is measured after exposure to an isotopically labelled gas.

28.3 Physisorption and chemisorption

Molecules and atoms can attach to surfaces in two ways. In physisorption (an abbreviation of 'physical adsorption'), there is a van der Waals interaction (for example, a dispersion or a dipolar interaction) between the adsorbate and the substrate. Van der Waals interactions have a long range but are weak, and the energy released when a particle is physisorbed is of the same order of magnitude as the enthalpy of condensation. Such small energies can be absorbed as vibrations of the lattice and dissipated as thermal motion, and a molecule bouncing across the surface will gradually lose its energy and finally adsorb to it in the process called accommodation. The enthalpy of physisorption can be measured by monitoring the rise in temperature of a sample of known heat capacity, and typical values are in the region of 20 kJ mol^{-1} (Table 28.1). This small enthalpy change is insufficient to lead to bond breaking, so a physisorbed molecule retains its identity, although it might be distorted by the presence of the surface.

(a) Chemisorption

In chemisorption (an abbreviation of 'chemical adsorption'), the molecules (or atoms) stick to the surface by forming a chemical (usually covalent) bond, and tend to find sites that maximize their coordination number with the substrate. The enthalpy of chemisorption is very much greater than that for physisorption, and typical values are in the region of 200 kJ mol^{-1} (Table 28.2). The distance between the surface and the closest adsorbate atom is also typically shorter for chemisorption than for physisorption. A chemisorbed molecule may be torn apart at the demand of the unsatisfied valencies of the surface atoms, and the existence of molecular fragments on the surface as a result of chemisorption is one reason why solid surfaces catalyse reactions.

Table 28.1* Maximum observed enthalpies of physisorption, $\Delta_{\text{ad}}H^{\ominus}/(\text{kJ mol}^{-1})$

CH_4	-21
H_2	-84
H_2O	-59
N_2	-21

*More values are given in the Data section at the end of this volume.

Table 28.2* Enthalpies of chemisorption, $\Delta_{\text{ad}}H^{\ominus}/(\text{kJ mol}^{-1})$

Adsorbate	Adsorbent (substrate)		
	Cr	Fe	Ni
C_2H_4	-427	-285	-243
CO		-192	
H_2	-188	-134	
NH_3		-188	-155

*More values are given in the Data section.

Except in special cases, chemisorption must be exothermic. A spontaneous process requires $\Delta G < 0$. Because the translational freedom of the adsorbate is reduced when it is adsorbed, ΔS is negative. Therefore, in order for $\Delta G = \Delta H - T\Delta S$ to be negative, ΔH must be negative (that is, the process is exothermic). Exceptions may occur if the adsorbate dissociates and has high translational mobility on the surface. For example, H_2 adsorbs endothermically on glass because there is a large increase of translational entropy accompanying the dissociation of the molecules into atoms that move quite freely over the surface. In its case, the entropy change in the process $H_2(g) \rightarrow 2H(\text{glass})$ is sufficiently positive to overcome the small positive enthalpy change.

The principal test for distinguishing chemisorption from physisorption used to be the enthalpy of adsorption. Values less negative than -25 kJ mol^{-1} were taken to signify physisorption, and values more negative than about -40 kJ mol^{-1} were taken to signify chemisorption. However, this criterion is by no means foolproof, and spectroscopic techniques that identify the adsorbed species are now available.

The enthalpy of adsorption depends on the extent of surface coverage, mainly because the adsorbate particles interact. If the particles repel each other (as for CO on palladium) the adsorption becomes less exothermic (the enthalpy of adsorption less negative) as coverage increases. Moreover, LEED studies show that such species settle on the surface in a disordered way until packing requirements demand order. If the adsorbate particles attract one another (as for O_2 on tungsten), then they tend to cluster together in islands, and growth occurs at the borders. These adsorbates also show order-disorder transitions when they are heated enough for thermal motion to overcome the particle-particle interactions, but not so much that they are desorbed.

28.4 Adsorption isotherms

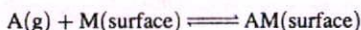
The free gas and the adsorbed gas are in dynamic equilibrium, and the fractional coverage of the surface depends on the pressure of the overlying gas. The variation of θ with pressure at a chosen temperature is called the adsorption isotherm.

(a) The Langmuir isotherm

The simplest physically plausible isotherm is based on three assumptions:

1. Adsorption cannot proceed beyond monolayer coverage.
2. All sites are equivalent and the surface is uniform (that is, the surface is perfectly flat on a microscopic scale).
3. The ability of a molecule to adsorb at a given site is independent of the occupation of neighbouring sites.

The dynamic equilibrium is



with rate constants k_a for adsorption and k_d for desorption. The rate of change of surface coverage due to adsorption is proportional to the partial pressure p of A and the number of vacant sites $N(1 - \theta)$, where N is the total number of sites:

$$\frac{d\theta}{dt} = k_a p N (1 - \theta) \quad (3)$$

The rate of change of θ due to desorption is proportional to the number of adsorbed species, $N\theta$:

$$\frac{d\theta}{dt} = -k_d N \theta \quad (4)$$

At equilibrium there is no net change (that is, the sum of these two rates is zero), and solving for θ gives the Langmuir isotherm:

$$\theta = \frac{Kp}{1 + Kp} \quad K = \frac{k_a}{k_d} \quad (5)$$

Example 28.1 Using the Langmuir isotherm

The data given below are for the adsorption of CO on charcoal at 273 K. Confirm that they fit the Langmuir isotherm, and find the constant K and the volume corresponding to complete coverage. In each case V has been corrected to 1.00 atm.

p/Torr	100	200	300	400	500	600	700
V/cm^3	10.2	18.6	25.5	31.5	36.9	41.6	46.1

Method From eqn 5,

$$Kp\theta + \theta = Kp$$

With $\theta = V/V_\infty$, where V_∞ is the volume corresponding to complete coverage, this expression can be rearranged into

$$\frac{p}{V} = \frac{p}{V_\infty} + \frac{1}{KV_\infty}$$

Hence, a plot of p/V against p should give a straight line of slope $1/V_\infty$ and intercept $1/KV_\infty$.

Answer The data for the plot are as follows:

p/Torr	100	200	300	400	500	600	700
$(p/\text{Torr})/(V/\text{cm}^3)$	9.80	10.8	11.8	12.7	13.6	14.4	15.2

The points are plotted in Fig. 28.23. The (least squares) slope is 0.00904, so $V_\infty = 111 \text{ cm}^3$. The intercept at $p = 0$ is 8.99, so

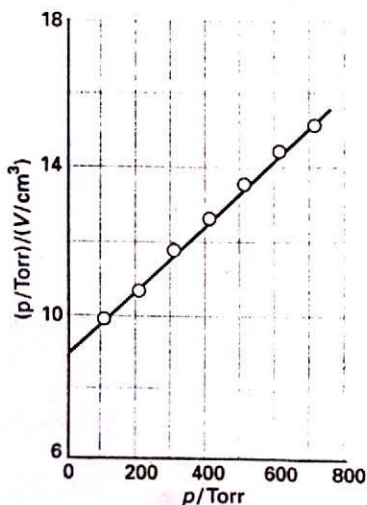
$$K = \frac{1}{(111 \text{ cm}^3) \times (8.99 \text{ Torr cm}^{-3})} = 1.00 \times 10^{-3} \text{ Torr}^{-1}$$

Comment At high surface coverage, the data would deviate from a straight line. The dimensions of K are $1/\text{pressure}$.

Self-test 28.1 Repeat the calculation for the following data:

p/Torr	100	200	300	400	500	600	700
V/cm^3	10.3	19.3	27.3	34.1	40.0	45.5	48.0

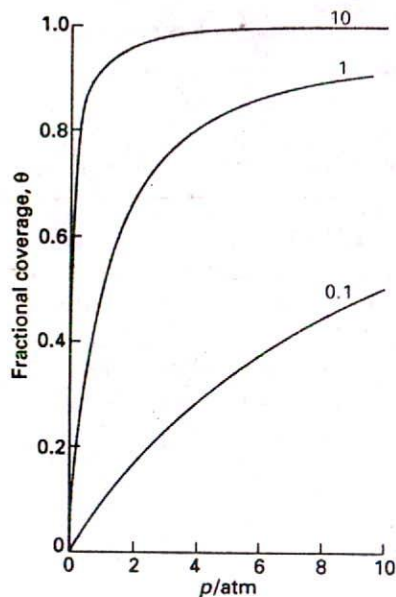
$$[128 \text{ cm}^3, 8.89 \times 10^{-4} \text{ Torr}^{-1}]$$



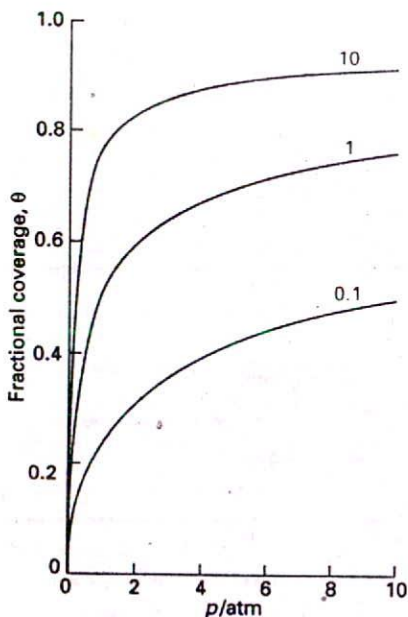
28.23 The plot of the data in Example 28.1. As illustrated here, the Langmuir isotherm predicts that a straight line should be obtained when p/V is plotted against p .

For adsorption with dissociation, the rate of adsorption is proportional to the pressure and to the probability that both atoms will find sites, which is proportional to the square of the number of vacant sites,

$$\frac{d\theta}{dt} = k_a p \{N(1 - \theta)\}^2 \quad (6)$$



28.24 The Langmuir isotherm for dissociative adsorption ($X_2 \rightarrow 2X$) for different values of K .



28.25 The Langmuir isotherm for non-dissociative adsorption for different values of K .

The rate of desorption is proportional to the frequency of encounters of atoms on the surface, and is therefore second-order in the number of atoms present:

$$\frac{d\theta}{dt} = -k_d(N\theta)^2 \quad (7)$$

The condition for no net change leads to the isotherm

$$\theta = \frac{(Kp)^{1/2}}{1 + (Kp)^{1/2}} \quad (8)$$

The surface coverage now depends more weakly on pressure than for non-dissociative adsorption.

The shapes of the Langmuir isotherms with and without dissociation are shown in Fig. 28.24 and Fig. 28.25. The fractional coverage increases with increasing pressure, and approaches 1 only at very high pressure, when the gas is forced on to every available site of the surface. Different curves (and therefore values of K) are obtained at different temperatures, and the temperature dependence of K can be used to determine the isosteric enthalpy of adsorption, $\Delta_{ad}H^\ominus$, the standard enthalpy of adsorption at a fixed surface coverage. To determine this quantity we recognize that K is essentially an equilibrium constant, and then use the van't Hoff equation (eqn 9.24) to write

$$\left(\frac{\partial \ln K}{\partial T}\right)_\theta = \frac{\Delta_{ad}H^\ominus}{RT^2} \quad (9)$$

Example 28.2 Measuring the isosteric enthalpy of adsorption

The data below show the pressures of CO needed for the volume of adsorption (corrected to 1.00 atm and 273 K) to be 10.0 cm³ using the same sample as in Example 28.1. Calculate the adsorption enthalpy at this surface coverage.

T/K	200	210	220	230	240	250
p/Torr	30.0	37.1	45.2	54.0	63.5	73.9

Method The Langmuir isotherm can be rearranged to

$$Kp = \frac{\theta}{1 - \theta}$$

Therefore, when θ is constant,

$$\ln K + \ln p = \text{constant}$$

It follows from eqn 9 that

$$\left(\frac{\partial \ln p}{\partial T}\right)_\theta = -\left(\frac{\partial \ln K}{\partial T}\right)_\theta = -\frac{\Delta_{ad}H^\ominus}{RT^2}$$

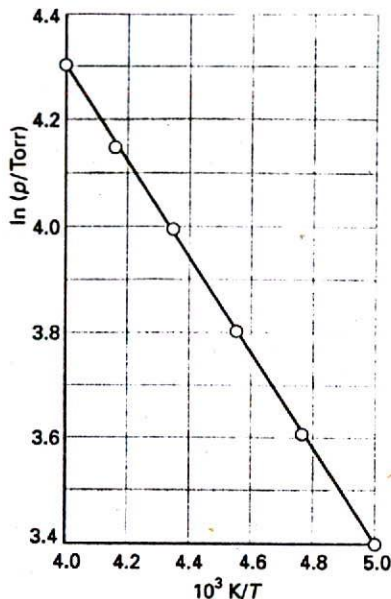
With $d(1/T)/dT = -1/T^2$, this expression rearranges to

$$\left(\frac{\partial \ln p}{\partial(1/T)}\right)_\theta = \frac{\Delta_{ad}H^\ominus}{R}$$

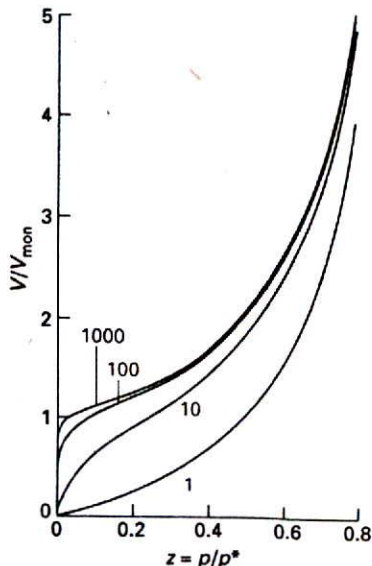
Therefore, a plot of $\ln p$ against $1/T$ should be a straight line of slope $\Delta_{ad}H^\ominus/R$.

Answer We draw up the following table:

T/K	200	210	220	230	240	250
$10^3/(T/K)$	5.00	4.76	4.55	4.35	4.17	4.00
$\ln(p/\text{Torr})$	3.40	3.61	3.81	3.99	4.15	4.30



28.26 The isosteric enthalpy of adsorption can be obtained from the slope of the plot of $\ln p$ against $1/T$, where p is the pressure needed to achieve the specified surface coverage. The data used are from Example 28.2.



28.27 Plots of the BET isotherm for different values of c . The value of V/V_{mon} rises indefinitely because the adsorbate may condense on the covered substrate surface.

The points are plotted in Fig. 28.26. The slope (of the least squares fitted line) is -0.904 , so $\Delta_{\text{ad}}H^\ominus = -(0.902 \times 10^3 \text{ K}) \times R = -7.50 \text{ kJ mol}^{-1}$.

Comment The value of K can be used to obtain a value of $\Delta_{\text{ad}}G^\ominus$, and then that value combined with $\Delta_{\text{ad}}H^\ominus$ to obtain the standard entropy of adsorption.

Self-test 28.2 Repeat the calculation using the following data:

T/K	200	210	220	230	240	250.
p/Torr	32.4	41.9	53.0	66.0	80.0	96.0

[-9.0 kJ mol^{-1}]

(b) The BET isotherm

If the initial adsorbed layer can act as a substrate for further (for example, physical) adsorption then, instead of the isotherm levelling off to some saturated value at high pressures, it can be expected to rise indefinitely. The most widely used isotherm dealing with multilayer adsorption was derived by Stephen Brunauer, Paul Emmett, and Edward Teller, and is called the BET isotherm:

$$\frac{V}{V_{\text{mon}}} = \frac{cz}{(1-z)\{1-(1-c)z\}} \quad z = \frac{p}{p^*} \quad (10)$$

In this expression, p^* is the vapour pressure above a layer of adsorbate that is more than one molecule thick and which resembles a pure bulk liquid, V_{mon} is the volume corresponding to monolayer coverage, and c is a constant which is large when the enthalpy of desorption from a monolayer is large compared with the enthalpy of vaporization of the liquid adsorbate:

$$c = e^{(\Delta_{\text{ad}}H^\ominus - \Delta_{\text{vap}}H^\ominus)/RT} \quad (11)$$

The shapes of BET isotherms are illustrated in Fig. 28.27. They rise indefinitely as the pressure is increased because there is no limit to the amount of material that may condense when multilayer coverage may occur. A BET isotherm is not accurate at all pressures, but it is widely used in industry to determine the surface areas of solids.

Example 28.3 Using the BET isotherm

The data below relate to the adsorption of N_2 on rutile (TiO_2) at 75 K. Confirm that they fit a BET isotherm in the range of pressures reported, and determine V_{mon} and c .

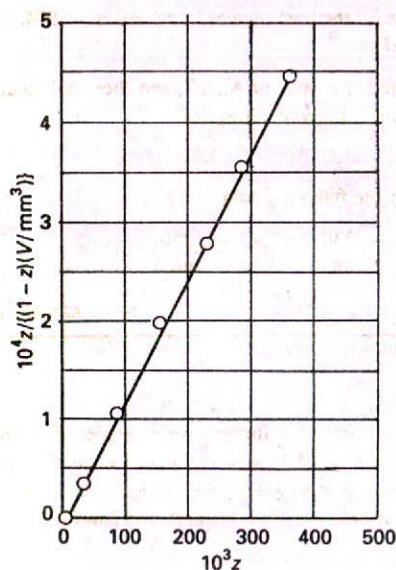
p/Torr	1.20	14.0	45.8	87.5	127.7	164.4	204.7
V/mm^3	601	720	822	935	1046	1146	1254

At 75 K, $p^* = 570 \text{ Torr}$. The volumes have been corrected to 1.00 atm and 273 K and refer to 1.00 g of substrate.

Method Equation 10 can be reorganized into

$$\frac{z}{(1-z)V} = \frac{1}{cV_{\text{mon}}} + \frac{(c-1)z}{cV_{\text{mon}}}$$

It follows that $(c-1)/cV_{\text{mon}}$ can be obtained from the slope of a plot of the expression on the left against z , and cV_{mon} can be found from the intercept at $z = 0$. The results can then be combined to give c and V_{mon} .



28.28 The BET isotherm can be tested, and the parameters determined, by plotting $z/(1-z)V$ against $z = p/p^*$. The data are from Example 28.3.

Answer We draw up the following table:

p/Torr	1.20	14.0	45.8	87.5	127.7	164.4	204.7
$10^3 z$	2.11	24.6	80.4	154	224	288	359
$10^4 z/(1-z)(V/\text{mm}^3)$	0.035	0.350	1.06	1.95	2.76	3.53	4.47

These points are plotted in Fig. 28.28. The least squares best line has an intercept at 0.0406, so

$$\frac{1}{cV_{\text{mon}}} = 4.06 \times 10^{-6} \text{ mm}^{-3}$$

The slope of the line is 1.23×10^{-2} , so

$$\frac{c-1}{cV_{\text{mon}}} = (1.23 \times 10^{-2}) \times 10^3 \times 10^{-4} \text{ mm}^{-3} = 1.23 \times 10^{-3} \text{ mm}^{-3}$$

The solutions of these equations are $c = 303$ and $V_{\text{mon}} = 814 \text{ mm}^3$.

Comment At 1.00 atm and 273 K, 810 mm^3 corresponds to $3.6 \times 10^{-5} \text{ mol}$, or 2.2×10^{19} atoms. Because each atom occupies an area of about 0.16 nm^2 , the surface area of the sample is about 3.5 m^2 .

Self-test 28.3 Repeat the calculation for the following data:

p/Torr	1.20	14.0	45.8	87.5	127.7	164.4	204.7
V/cm^3	235	559	649	719	790	860	950

[370, 615 cm^3]

When $c \gg 1$, the BET isotherm takes the simpler form

$$\frac{V}{V_{\text{mon}}} = \frac{1}{1-z} \quad (12)$$

This expression is applicable to unreactive gases on polar surfaces, for which $c \approx 10^2$ because $\Delta_{\text{des}}H^\ominus$ is then significantly greater than $\Delta_{\text{vap}}H^\ominus$ (eqn 11). The BET isotherm fits experimental observations moderately well over restricted pressure ranges, but it errs by underestimating the extent of adsorption at low pressures and by overestimating it at high pressures.

(c) Other isotherms

An assumption of the Langmuir isotherm is the independence and equivalence of the adsorption sites. Deviations from the isotherm can often be traced to the failure of these assumptions. For example, the enthalpy of adsorption often becomes less negative as θ increases, which suggests that the energetically most favourable sites are occupied first. Various attempts have been made to take these variations into account. The Temkin isotherm,

$$\theta = c_1 \ln(c_2 p) \quad (13)$$

where c_1 and c_2 are constants, corresponds to supposing that the adsorption enthalpy changes linearly with pressure. The Freundlich isotherm

$$\theta = c_1 p^{1/c_2} \quad (14)$$

corresponds to a logarithmic change. Different isotherms agree with experiment more or less well over restricted ranges of pressure, but they remain largely empirical. Empirical, however, does not mean useless for, if the parameters of a reasonably reliable isotherm are

known, reasonably reliable results can be obtained for the extent of surface coverage under various conditions. This kind of information is essential for any discussion of heterogeneous catalysis.

28.5 The rates of surface processes

Figure 28.29 shows how the potential energy of a molecule varies with its distance from the substrate surface. As the molecule approaches the surface its energy falls as it becomes physisorbed into the precursor state for chemisorption. Dissociation into fragments often takes place as a molecule moves into its chemisorbed state, and after an initial increase of energy as the bonds stretch there is a sharp decrease as the adsorbate-substrate bonds reach their full strength. Even if the molecule does not fragment, there is likely to be an initial increase of potential energy as the bonds adjust as the molecule approaches the surface.

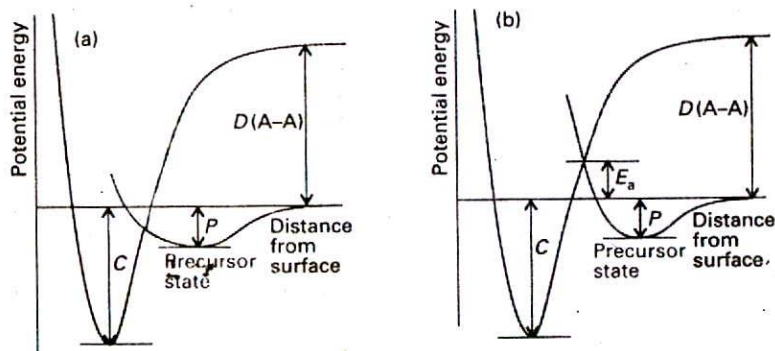
In most cases, therefore, we can expect there to be a potential energy barrier separating the precursor and chemisorbed states. This barrier, though, might be low, and might not rise above the energy of a distant, stationary particle (as in Fig. 28.29a). In this case, chemisorption is not an activated process and can be expected to be rapid. Many gas adsorptions on clean metals appear to be non-activated. In some cases the barrier rises above the zero axis (as in Fig. 28.29b); such chemisorptions are activated and slower than the non-activated kind. An example is H_2 on copper, which has an activation energy in the region of $20\text{--}40\text{ kJ mol}^{-1}$.

One point that emerges from this discussion is that rates are not good criteria for distinguishing between physisorption and chemisorption. Chemisorption can be fast if the activation energy is small or zero, but it may be slow if the activation energy is large. Physisorption is usually fast, but it can appear to be slow if adsorption is taking place on a porous medium.

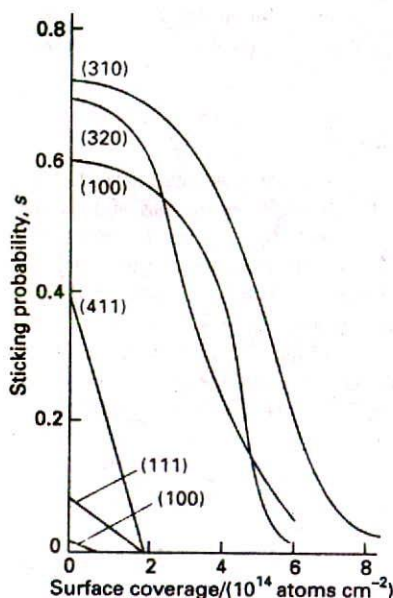
(a) The rate of adsorption

The rate at which a surface is covered by adsorbate depends on the ability of the substrate to dissipate the energy of the incoming particle as thermal motion as it crashes on to the surface. If the energy is not dissipated quickly, the particle migrates over the surface until a vibration expels it into the overlying gas or it reaches an edge. The proportion of collisions with the surface that successfully lead to adsorption is called the sticking probability, s :

$$s = \frac{\text{rate of adsorption of particles by the surface}}{\text{rate of collision of particles with the surface}} \quad [15]$$



28.29 The potential energy profiles for the dissociative chemisorption of an A_2 molecule. In each case, P is the enthalpy of (non-dissociative) physisorption and C that for chemisorption (at $T = 0$). The relative locations of the curves determine whether the chemisorption is (a) not activated or (b) activated.



28.30 The sticking probability of N_2 on various faces of a tungsten crystal and its dependence on surface coverage. Note the very low sticking probability for the (110) and (111) faces. (Data provided by Professor D.A. King.)

The denominator can be calculated from kinetic theory, and the numerator can be measured by observing the rate of change of pressure.

Values of s vary widely. For example, at room temperature CO has s in the range 0.1–1.0 for several d -metal surfaces, but for N_2 on rhenium $s < 10^{-2}$, indicating that more than a hundred collisions are needed before one molecule sticks successfully. Beam studies on specific crystal planes show a pronounced specificity: for N_2 on tungsten, s ranges from 0.74 on the (320) faces down to less than 0.01 on the (110) faces at room temperature. The sticking probability decreases as the surface coverage increases (Fig. 28.30). A simple assumption is that s is proportional to $1 - \theta$, the fraction uncovered, and it is common to write

$$s = (1 - \theta)s_0 \quad (16)$$

where s_0 is the sticking probability on a perfectly clean surface. The results in the illustration do not fit this expression because they show that s remains close to s_0 until the coverage has risen to about 6×10^{13} molecules cm^{-2} , and then falls steeply. The explanation is probably that the colliding molecule does not enter the chemisorbed state at once, but moves over the surface until it encounters an empty site.

(b) The rate of desorption

Desorption is always activated because the particles have to be lifted from the foot of a potential well. A physisorbed particle vibrates in its shallow potential well, and might shake itself off the surface after a short time. The temperature dependence of the first-order rate of departure can be expected to be Arrhenius-like, with an activation energy for desorption, E_d , comparable to the enthalpy of physisorption:

$$k_d = Ae^{-E_d/RT} \quad (17)$$

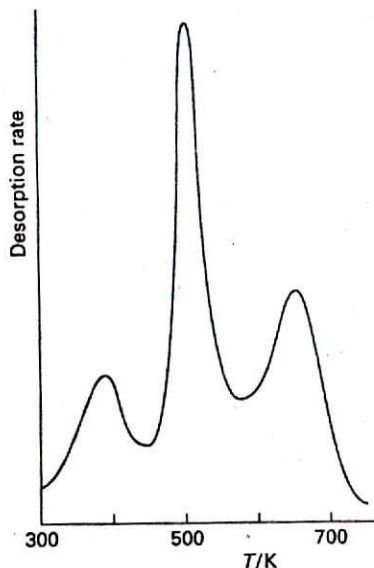
Therefore, the half-life for remaining on the surface has a temperature dependence

$$t_{1/2} = \frac{\ln 2}{k_d} = \tau_0 e^{E_d/RT} \quad \tau_0 = \frac{\ln 2}{A} \quad (18)$$

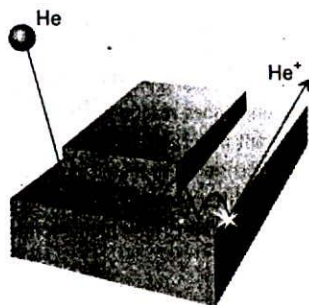
(Note the positive sign in the exponent.) If we suppose that $1/\tau_0$ is approximately the same as the vibrational frequency of the weak particle-surface bond (about 10^{12} Hz) and $E_d \approx 25$ kJ mol^{-1} , then residence half-lives of around 10 ns are predicted at room temperature. Lifetimes close to 1 s are obtained only by lowering the temperature to about 100 K. For chemisorption, with $E_d = 100$ kJ mol^{-1} and guessing that $\tau_0 = 10^{-14}$ s (because the adsorbate-substrate bond is quite stiff), we expect a residence half-life of about 3×10^3 s (about an hour) at room temperature, decreasing to 1 s at about 350 K.

The desorption activation energy can be measured in several ways. However, we must be guarded in its interpretation because it often depends on the fractional coverage, and so may change as desorption proceeds. Moreover, the transfer of concepts such as 'reaction order' and 'rate constant' from bulk studies to surfaces is hazardous, and there are few examples of strictly first-order or second-order desorption kinetics (just as there are few integral-order reactions in the gas phase).

If we disregard these complications, one way of measuring the desorption activation energy is to monitor the rate of increase in pressure when the sample is maintained at a series of temperatures, and to attempt to make an Arrhenius plot. A more sophisticated technique is temperature programmed desorption (TPD) or thermal desorption spectroscopy (TDS). The basic observation is a surge in desorption rate (as monitored by a mass spectrometer) when the temperature is raised linearly to the temperature at which desorption occurs rapidly; but once the desorption has occurred there is no more adsorbate to escape from the surface, so the desorption flux falls again as the temperature continues



28.31 The flash desorption spectrum of H_2 on the (100) face of tungsten. The three peaks indicate the presence of three sites with different adsorption enthalpies and therefore different desorption activation energies. (P.W. Tamm and L.D. Schmidt, *J. Chem. Phys.* 51, 5352 (1969).)



28.32 The events leading to an FIM image of a surface. The He atom migrates across the surface until it is ionized at an exposed atom, when it is pulled off by the externally applied potential. (The bouncing motion is due to the intermolecular potential, not gravity!)

28.33 FIM micrographs showing the migration of Re atoms on rhenium during 3 s intervals at 375 K. (Photographs provided by Professor G. Ehrlich.)

to rise. The TPD spectrum, the plot of desorption flux against temperature, therefore shows a peak, the location of which depends on the desorption activation energy. In the example shown in Fig. 28.31, three maxima are shown, indicating the presence of three sites with different activation energies.

In many cases only a single activation energy (and a single peak in the TPD spectrum) is observed. When several peaks are observed they might correspond to adsorption on different crystal planes or to multilayer adsorption. For instance, Cd atoms on tungsten show two activation energies, one of 18 kJ mol^{-1} and the other of 90 kJ mol^{-1} . The explanation is that the more tightly bound Cd atoms are attached directly to the substrate, and the less strongly bound are in a layer (or layers) above the primary overlayer. Chemisorption cannot normally exceed monolayer coverage because a hydrocarbon gas, for instance, cannot chemisorb on to a surface already covered with its fragments; a metal adsorbate, on the other hand, as in this case, can provide a surface capable of further chemisorption.

Another example of a system showing two desorption activation energies is CO on tungsten, the values being 120 kJ mol^{-1} and 300 kJ mol^{-1} . The explanation is believed to be the existence of two types of metal-adsorbate binding site, one involving a simple M-CO bond, the other adsorption with dissociation into individually adsorbed C and O atoms. In some cases two desorption peaks may occur even though there is only one type of site. This complication arises when there are significant interactions between the adsorbate particles with the result that at low surface coverages the enthalpy of adsorption is significantly different from its value at high coverages.

(c) Mobility on surfaces

A further aspect of the strength of the interactions between adsorbate and substrate is the mobility of the adsorbate. Mobility is often a vital feature of a catalyst's activity, because a catalyst might be impotent if the reactant molecules adsorb so strongly that they cannot migrate. The activation energy for diffusion over a surface need not be the same as for desorption because the particles may be able to move through valleys between potential peaks without leaving the surface completely. In general, the activation energy for migration is about 10–20 per cent of the energy of the surface-adsorbate bond, but the actual value depends on the extent of coverage. The defect structure of the sample (which depends on the temperature) may also play a dominant role because the adsorbed molecules might find it easier to skip across a terrace than to roll along the foot of a step, and these molecules might become trapped in vacancies in an otherwise flat terrace. Diffusion may also be easier across one crystal face than another, and so the surface mobility depends on which lattice planes are exposed.

Diffusion characteristics of an adsorbate can be examined by using STM to follow the change in surface characteristics or by field-ionization microscopy (FIM), which portrays the electrical characteristics of a surface by using the ionization of noble gas atoms to probe the surface (Fig. 28.32). An individual atom is imaged, the temperature is raised, and then lowered after a definite interval. A new image is then recorded, and the new position of the atom measured (Fig. 28.33). A sequence of images shows that the atom makes a random walk across the surface, and the diffusion coefficient, D , can be inferred from the mean

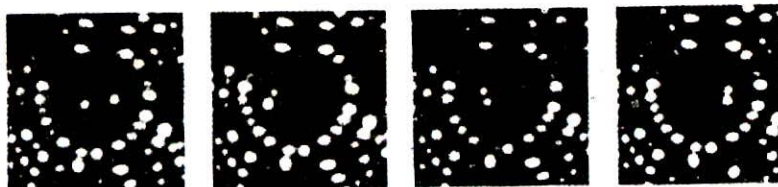


Table 28.3* Activation energies of catalysed reactions

Reaction	Catalyst	$E_a/(\text{kJ mol}^{-1})$
$2\text{HI} \rightarrow \text{H}_2 + \text{I}_2$	None	184
	Au	105
	Pt	59
$2\text{NH}_3 \rightarrow \text{N}_2 + 3\text{H}_2$	None	350
	W	162

*More values are given in the Data section.

distance, d , travelled in an interval τ by using the two-dimensional random walk expression $d = (D\tau)^{1/2}$. The value of D for different crystal planes at different temperatures can be determined directly in this way, and the activation energy for migration over each plane obtained from the Arrhenius-like expression

$$D = D_0 e^{-E_D/RT} \quad (19)$$

where E_D is the activation energy for diffusion. Typical values for W atoms on tungsten have E_D in the range 57–87 kJ mol⁻¹ and $D_0 \approx 3.8 \times 10^{-11} \text{ m}^2 \text{ s}^{-1}$. For CO on tungsten, the activation energy falls from 144 kJ mol⁻¹ at low surface coverage to 88 kJ mol⁻¹ when the coverage is high.

Catalytic activity at surfaces

A catalyst acts by providing an alternative reaction path with a lower activation energy (Table 28.3). It does not disturb the final equilibrium composition of the system, only the rate at which that equilibrium is approached. In this section we shall consider heterogeneous catalysis, in which (as mentioned in the introduction preceding Section 26.6) the catalyst and the reagents are in different phases. For simplicity, we shall consider only gas/solid systems.

Many catalysts depend on the coadsorption of species, the adsorption of two or more species. One consequence of the presence of a second species may be the modification of the electronic structure at the surface of a metal. For instance, partial coverage of d -metal surfaces by alkali metals has a pronounced effect on the electron distribution and reduces the work function of the metal. Such modifiers can act as promoters (to enhance the action of catalysts) or as poisons (to inhibit catalytic action).

28.6 Adsorption and catalysis

Heterogeneous catalysis normally depends on at least one reactant being adsorbed (usually chemisorbed) and modified to a form in which it readily undergoes reaction. Often this modification takes the form of a fragmentation of the reactant molecules. In practice, the active phase is dispersed as very small particles of linear dimension less than 2 nm on a porous oxide support. Shape-selective catalysts, such as the zeolites, which have a pore size that can distinguish shapes and sizes at a molecular scale (recall Fig. 28.1), have high internal specific surface areas, in the range of 100–500 m² g⁻¹.

(a) The Langmuir–Hinshelwood mechanism

In the Langmuir–Hinshelwood mechanism (LH mechanism) of surface-catalysed reactions, the reaction takes place by encounters between molecular fragments and atoms adsorbed on the surface. We therefore expect the rate law to be second-order in the extent of surface coverage:



Insertion of the appropriate isotherms for A and B then gives the reaction rate in terms of the partial pressures of the reactants. For example, if A and B follow Langmuir isotherms, and adsorb without dissociation, so that

$$\theta_A = \frac{K_A p_A}{1 + K_A p_A + K_B p_B} \quad \theta_B = \frac{K_B p_B}{1 + K_A p_A + K_B p_B} \quad (21)$$

then it follows that the rate law is

$$v = \frac{kK_A K_B p_A p_B}{(1 + K_A p_A + K_B p_B)^2} \quad (22)$$

The parameters K in the isotherms and the rate constant k are all temperature-dependent, so the overall temperature dependence of the rate may be strongly non-Arrhenius (in the sense that the reaction rate is unlikely to be proportional to $e^{-E_a/RT}$).

(b) The Eley-Rideal mechanism

In the Eley-Rideal mechanism (ER mechanism) of a surface-catalysed reaction, a gas-phase molecule collides with another molecule already adsorbed on the surface. The rate of formation of product is expected to be proportional to the partial pressure, p_B , of the non-adsorbed gas B and the extent of surface coverage, θ_A , of the adsorbed gas A. It follows that the rate law should be



The rate constant, k , might be much larger than for the uncatalysed gas-phase reaction because the reaction on the surface has a low activation energy and the adsorption itself is often not activated.

If we know the adsorption isotherm for A, we can express the rate law in terms of its partial pressure, p_A . For example, if the adsorption of A follows a Langmuir isotherm in the pressure range of interest, then the rate law would be

$$v = \frac{kK p_A p_B}{1 + K p_A} \quad (24)$$

If A were a diatomic molecule that adsorbed as atoms, we would substitute the isotherm given in eqn 8 instead.

According to eqn 24, when the partial pressure of A is high (in the sense $K p_A \gg 1$) there is almost complete surface coverage, and the rate is equal to $k p_B$. Now the rate-determining step is the collision of B with the adsorbed fragments. When the pressure of A is low ($K p_A \ll 1$), perhaps because of its reaction, the rate is equal to $kK p_A p_B$; now the extent of surface coverage is important in the determination of the rate.

Almost all thermal surface-catalysed reactions are thought to take place by the LH mechanism, but a number of reactions with an ER mechanism have also been identified from molecular beam investigations. For example, the reaction between H(g) and D(ad) to form HD(g) is thought to be by an ER mechanism involving the direct collision and pick-up of the adsorbed D atom by the incident H atom. However, the two mechanisms should really be thought of as ideal limits, and all reactions lie somewhere between the two and show features of each one.

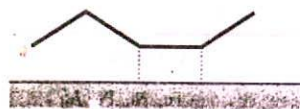
Example 2B.4 Interpreting the kinetics of a catalysed reaction

The decomposition of phosphine (PH_3) on tungsten is first-order at low pressures and zero-order at high pressures. Account for these observations.

Method Write down a plausible rate law in terms of an adsorption isotherm and explore its form in the limits of high and low pressure.

Answer If the rate is supposed to be proportional to the surface coverage, we can write

$$v = k\theta = \frac{kKp}{1 + Kp}$$



6



7

form (6) and then desorb to (7), an isomer of the original molecule. The new alkene would not be formed if the two hydrogen atoms attached simultaneously.

A major industrial application of catalytic hydrogenation is to the formation of edible fats from vegetable and animal oils. Raw oils obtained from sources such as the soya bean have the structure $\text{CH}_2(\text{OOCR})\text{CH}(\text{OOCR}')\text{CH}_2(\text{OOCR}'')$, where R, R', and R'' are long-chain hydrocarbons with several double bonds. One disadvantage of the presence of many double bonds is that the oils are susceptible to atmospheric oxidation, and therefore are liable to become rancid. The geometrical configuration of the chains is responsible for the liquid nature of the oil, and in many applications a solid fat is at least much better and often necessary. Controlled partial hydrogenation of an oil with a catalyst, carefully selected so that hydrogenation is incomplete and so that the chains do not isomerize (finely divided nickel, in fact), is used on a wide scale to produce edible fats. The process, and the industry, is not made any easier by the seasonal variation of the number of double bonds in the oils.

(c) Oxidation

Catalytic oxidation is also widely used in industry and in pollution control. Although in some cases it is desirable to achieve complete oxidation (as in the production of nitric acid from ammonia), in others partial oxidation is the aim. For example, the complete oxidation of propene to carbon dioxide and water is wasteful, but its partial oxidation to propenal (acrolein, $\text{CH}_2=\text{CHCHO}$) is the start of important industrial processes. Likewise, the controlled oxidations of ethene to ethanol, acetaldehyde, and (in the presence of acetic acid or chlorine) to vinyl acetate or vinyl chloride, are the initial stages of very important chemical industries.

Some of these reactions are catalysed by *d*-metal oxides of various kinds. The physical chemistry of oxide surfaces is very complex, as can be appreciated by considering what happens during the oxidation of propene to acrolein on bismuth molybdate. The first stage is the adsorption of the propene molecule with loss of a hydrogen to form the allyl radical, $\text{CH}_2=\text{CHCH}_2$. An O atom in the surface can now transfer to this radical, leading to the formation of acrolein (propenal, $\text{CH}_2=\text{CHCHO}$) and its desorption from the surface. The H atom also escapes with a surface O atom, and goes on to form H_2O , which leaves the surface. The surface is left with vacancies and metal ions in lower oxidation states. These vacancies are attacked by O_2 molecules in the overlying gas, which then chemisorb as O^{2-} ions, so reforming the catalyst. This sequence of events, which is called the **Mars van Krevelen mechanism**, involves great upheavals of the surface, and some materials break up under the stress.

(d) Cracking and reforming

Many of the small organic molecules used in the preparation of all kinds of chemical products come from oil. These small building blocks of polymers, and petrochemicals in general, are usually cut from the long-chain hydrocarbons drawn from the Earth as petroleum. The catalytically induced fragmentation of the long-chain hydrocarbons is called **cracking**, and is often brought about on silica-alumina catalysts. These catalysts act by forming unstable carbocations, which dissociate and rearrange to more highly branched isomers. These branched isomers burn more smoothly and efficiently in internal combustion engines, and are used to produce higher octane fuels.

Catalytic reforming uses a dual-function catalyst, such as a dispersion of platinum and acidic alumina. The platinum provides the metal function, and brings about dehydrogenation and hydrogenation. The alumina provides the acidic function, being able to form carbocations from alkenes. The sequence of events in catalytic reforming shows up very clearly the complications that must be unravelled if a reaction as important as this is to be

understood and improved. The first step is the attachment of the long-chain hydrocarbon by chemisorption to the platinum. In this process first one and then a second H atom is lost, and an alkene is formed. The alkene migrates to a Brønsted acid site, where it accepts a proton and attaches to the surface as a carbocation. This carbocation can undergo several different reactions. It can break into two, isomerize into a more highly branched form, or undergo varieties of ring-closure. Then the adsorbed molecule loses a proton, escapes from the surface, and migrates (possibly through the gas) as an alkene to a metal part of the catalyst where it is hydrogenated. We end up with a rich selection of smaller molecules which can be withdrawn, fractionated, and then used as raw materials for other products.

Table 28.6 Summary of acronyms

AES	Auger electron spectroscopy
AFM	Atomic force microscopy
BET isotherm	Brunauer, Emmett, Teller isotherm
EELS	Electron energy-loss spectroscopy
ER mechanism	Eley-Rideal mechanism
FIM	Field-ionization microscopy
HREELS	High-resolution electron energy-loss spectroscopy
LEED	Low-energy electron diffraction
LH mechanism	Langmuir-Hinshelwood mechanism
MBRS	Molecular beam reactive scattering
MBS	Molecular beam scattering
SAMS	Scanning Auger electron microscopy
SERS	Surface-enhanced Raman scattering
SEXAFS	Surface-extended X-ray absorption fine structure spectroscopy
STM	Scanning tunnelling microscopy
TDS	Thermal desorption spectroscopy
TPD	Temperature programmed desorption
UHV	Ultra-high vacuum technique
UPS	Ultraviolet photoemission spectroscopy
XPS	X-ray photoemission spectroscopy

Checklist of key ideas

The growth and structure of solid surfaces

- adsorption
- adsorbate
- adsorbent
- substrate
- desorption

28.1 Surface growth

- step defect
- terrace
- dislocation
- screw dislocation
- screw axis

28.2 Surface composition

- ultra-high vacuum (UHV) techniques
- escape depth
- photoemission spectroscopy (UPS, XPS)
- surface-enhanced Raman scattering (SERS)
- electron energy-loss spectroscopy (EELS, HREELS)
- Auger electron spectroscopy (AES)
- Auger effect
- X-ray fluorescence

- scanning Auger electron microscopy (SAM)
- surface-extended X-ray absorption fine structure spectroscopy (SEXAFS)
- surface reconstruction
- low-energy electron diffraction (LEED)
- substrate structure notation
- scanning tunnelling microscopy (STM)
- atomic force microscopy (AFM)
- molecular beam scattering (MBS)

The extent of adsorption

- fractional coverage (2)
- rate of adsorption
- flash desorption
- gravimetry

28.3 Physisorption and chemisorption

- physisorption
- accommodation
- chemisorption

28.4 Adsorption isotherms

- adsorption isotherm
- Langmuir isotherm (5)

- | | | | |
|---|--|--|--|
| <input type="checkbox"/> Langmuir isotherm with dissociation (8) | 28.5 The rates of surface processes | <input type="checkbox"/> surface diffusion temperature dependence (19) | <input type="checkbox"/> molecular beam reactive scattering (MBRS) |
| <input type="checkbox"/> isosteric enthalpy of adsorption (9) | <input type="checkbox"/> precursor state | | <input type="checkbox"/> pulsed beams |
| <input type="checkbox"/> Brunauer, Emmett, Teller (BET) isotherm (10) | <input type="checkbox"/> sticking probability (15) | Catalytic activity at surfaces | |
| <input type="checkbox"/> Temkin isotherm (13) | <input type="checkbox"/> half-life for desorption (18) | <input type="checkbox"/> coadsorption | 28.7 Examples of catalysis |
| <input type="checkbox"/> Freundlich isotherm (14) | <input type="checkbox"/> temperature programmed desorption (TPD) | | <input type="checkbox"/> volcano curve |
| | <input type="checkbox"/> thermal desorption spectroscopy (TDS) | 28.6 Adsorption and catalysis | <input type="checkbox"/> hydrogenation |
| | <input type="checkbox"/> field-ionization microscopy (FIM) | <input type="checkbox"/> shape-selective catalyst | <input type="checkbox"/> oxidation |
| | | <input type="checkbox"/> Langmuir-Hinshelwood (LH) mechanism | <input type="checkbox"/> Mars van Krevelen mechanism |
| | | <input type="checkbox"/> Eley-Rideal (ER) mechanism | <input type="checkbox"/> cracking |
| | | | <input type="checkbox"/> reforming |

Further reading

Articles of general interest

- S.T. Oyama and G.A. Samorjai, Homogeneous, heterogeneous, and enzymatic catalysis. *J. Chem. Educ.* 65, 765 (1988).
- N.-F. Zhou, The availability of simple form of Gibbs adsorption equation for mixed surfactants. *J. Chem. Educ.* 66, 137 (1989).
- T.E. Mallouk and H. Lee, Designer solids and surfaces. *J. Chem. Educ.* 67, 829 (1990).
- L. Glasser, The BET isotherm in 3D. *Educ. in Chem.* 25, 178 (1988).
- E. Shustorovich, Chemisorption theory: in search of the elephant. *Acc. Chem. Res.* 21, 183 (1988).
- S.L. Bernasek, State-resolved dynamics of chemical reactions at surfaces. *Chem. Rev.* 87, 91 (1987).
- B.B. Laird and A.D.J. Haymet, The crystal/liquid interface: structure and properties from computer simulation. *Chem. Rev.* 92, 1819 (1992).
- R. Parsons, Electrical double layer: recent experimental and theoretical developments. *Chem. Rev.* 90, 813 (1990).
- E. Schönherr, Crystal growth. In *Encyclopedia of applied physics* (ed. G.L. Trigg), 4, 335. VCH, New York (1992).
- R.R. Corderman, Auger spectroscopy. In *Encyclopedia of applied physics* (ed. G.L. Trigg), 2, 297. VCH, New York (1991).
- F.J. Himpsell and I. Lindau, Photoemission and photoelectron spectra. In *Encyclopedia of applied physics* (ed. G.L. Trigg), 13, 477. VCH, New York (1995).
- N. Beall Fowler, R. Phillips, and A.E. Carlsson, Point and extended defects in crystals. In *Encyclopedia of applied physics* (ed. G.L. Trigg), 14, 317. VCH, New York (1996).
- J.M. Cowley, Electron diffraction. In *Encyclopedia of applied physics* (ed. G.L. Trigg), 5, 405. VCH, New York (1993).

Texts and sources of data and information

- B.C. Gates, *Catalytic chemistry*. Wiley, New York (1992).
- J.M. Thomas and W.J. Thomas, *Principles and practice of heterogeneous catalysis*. VCH, Weinheim (1996).
- G. Ertl, H. Knözinger, and J. Weitkamp, *Handbook of heterogeneous catalysis*. VCH, Weinheim (1997).
- K.L. Mittal (ed.), *Particles on surfaces*, Vol. 3. Plenum, New York (1991).
- V.P. Zhdanov, *Elementary physicochemical processes on solid surfaces*. Plenum, New York (1991).
- S.R. Morrison, *The chemical physics of surfaces*. Plenum, New York (1990).
- J. Israelachvili, *Intermolecular and surface forces*. Academic Press, New York (1985).
- C.H. Bamford and C.F. Tipper (ed.), *Comprehensive chemical kinetics*, Vols 1-26. Elsevier, Amsterdam (1969-1986).
- R.G. Compton (ed.), *Comprehensive chemical kinetics*, Vols 27-33. Elsevier, Amsterdam (1987-1992).
- K. Tamaru, *Dynamic heterogeneous catalysis*. Academic Press, New York (1978).
- A. Zangwill, *Physics at surfaces*. Cambridge University Press (1988).
- J. Vickerman, *Surface analysis: techniques and applications*. Wiley, New York (1997).
- R. Aveyard and D.A. Haydon, *An introduction to the principles of surface chemistry*. Cambridge University Press (1973).
- A.W. Anderson, *Physical chemistry of surfaces*. Wiley-Interscience, New York (1990).
- R.P.H. Gasser, *An introduction to chemisorption and catalysis by metals*. Clarendon Press, Oxford (1985).
- M.W. Roberts and C.S. McKee, *Chemistry of the metal-gas interface*. Clarendon Press, Oxford (1978).

G.A. Somorjai, *Chemistry in two dimensions: surfaces*. Cornell University Press, Ithaca (1981).

G.A. Somorjai, *Surface chemistry and catalysis*. Wiley-Interscience, New York (1994).

G.C. Bond, *Heterogeneous catalysis: principles and applications*. Clarendon Press, Oxford (1986).

M. Boudart and G. Djéga-Mariadassou, *Kinetics of heterogeneous catalysis reactions*. Princeton University Press

Exercises

- 28.1 (a)** Calculate the frequency of molecular collisions per square centimetre of surface in a vessel containing (a) hydrogen, (b) propane at 25°C when the pressure is (i) 100 Pa, (ii) 0.10 μ Torr.
- 28.1 (b)** Calculate the frequency of molecular collisions per square centimetre of surface in a vessel containing (a) nitrogen, (b) methane at 25°C when the pressure is (i) 10.0 Pa, (ii) 0.150 μ Torr.
- 28.2 (a)** What pressure of argon gas is required to produce a collision rate of $4.5 \times 10^{20} \text{ s}^{-1}$ at 425 K on a circular surface of diameter 1.5 mm?
- 28.2 (b)** What pressure of nitrogen gas is required to produce a collision rate of $5.00 \times 10^{19} \text{ s}^{-1}$ at 525 K on a circular surface of diameter 2.0 mm?
- 28.3 (a)** Calculate the average rate at which He atoms strike a Cu atom in a surface formed by exposing a (100) plane in metallic copper to helium gas at 80 K and a pressure of 35 Pa. Crystals of copper are face-centred cubic with a cell edge of 361 pm.
- 28.3 (b)** Calculate the average rate at which He atoms strike an iron atom in a surface formed by exposing a (100) plane in metallic iron to helium gas at 100 K and a pressure of 24 Pa. Crystals of iron are body-centred cubic with a cell edge of 145 pm.
- 28.4 (a)** A monolayer of N_2 molecules (effective area 0.167 nm^2) is adsorbed on the surface of 1.00 g of an $\text{Fe}/\text{Al}_2\text{O}_3$ catalyst at 77 K, the boiling point of liquid nitrogen. Upon warming, the nitrogen occupies 2.86 cm^3 at 0°C and 760 Torr. What is the surface area of the catalyst?
- 28.4 (b)** A monolayer of CO molecules (effective area 0.165 nm^2) is adsorbed on the surface of 1.00 g of an $\text{Fe}/\text{Al}_2\text{O}_3$ catalyst at 77 K, the boiling point of liquid nitrogen. Upon warming, the carbon monoxide occupies 4.25 cm^3 at 0°C and 1.00 bar. What is the surface area of the catalyst?
- 28.5 (a)** The volume of oxygen gas at 0°C and 101 kPa adsorbed on the surface of 1.00 g of a sample of silica at 0°C was 0.284 cm^3 at 142.4 Torr and 1.430 cm^3 at 760 Torr. What is the value of V_{mon} ?
- 28.5 (b)** The volume of gas at 20°C and 1.00 bar adsorbed on the surface of 1.50 g of a sample of silica at 0°C was 1.60 cm^3 , at 52.4 kPa and 2.73 cm^3 at 104 kPa. What is the value of V_{mon} ?
- 28.6 (a)** The enthalpy of adsorption of CO on a surface is found to be -120 kJ mol^{-1} . Is the adsorption physisorption or chemisorption? Estimate the mean lifetime of a CO molecule on the surface at 400 K.
- 28.6 (b)** The enthalpy of adsorption of ammonia on a nickel surface is found to be -155 kJ mol^{-1} . Estimate the mean lifetime of an NH_3 molecule on the surface at 500 K.
- 28.7 (a)** The average time for which an oxygen atom remains adsorbed to a tungsten surface is 0.36 s at 2548 K and 3.49 s at 2362 K. Find the activation energy for desorption. What is the pre-exponential factor for these tightly chemisorbed atoms?
- 28.7 (b)** The chemisorption of hydrogen on manganese is activated, but only weakly so. Careful measurements have shown that it proceeds 35 per cent faster at 1000 K than at 600 K. What is the activation energy for chemisorption?
- 28.8 (a)** The adsorption of a gas is described by the Langmuir isotherm with $K = 0.85 \text{ kPa}^{-1}$ at 25°C. Calculate the pressure at which the fractional surface coverage is (a) 0.15, (b) 0.95.
- 28.8 (b)** The adsorption of a gas is described by the Langmuir isotherm with $K = 0.777 \text{ kPa}^{-1}$ at 25°C. Calculate the pressure at which the fractional surface coverage is (a) 0.20, (b) 0.75.
- 28.9 (a)** A certain solid sample adsorbs 0.44 mg of CO when the pressure of the gas is 26.0 kPa and the temperature is 300 K. The mass of gas adsorbed when the pressure is 3.0 kPa and the temperature is 300 K is 0.19 mg. The Langmuir isotherm is known to describe the adsorption. Find the fractional coverage of the surface at the two pressures.
- 28.9 (b)** A certain solid sample adsorbs 0.63 mg of CO when the pressure of the gas is 36.0 kPa and the temperature is 300 K. The mass of gas adsorbed when the pressure is 4.0 kPa and the temperature is 300 K is 0.21 mg. The Langmuir isotherm is known to describe the adsorption. Find the fractional coverage of the surface at the two pressures.
- 28.10 (a)** For how long on average would an H atom remain on a surface at 298 K if its desorption activation energy were (a) 15 kJ mol^{-1} , (b) 150 kJ mol^{-1} ? Take $\tau_0 = 0.10 \text{ ps}$. For how long on average would the same atoms remain at 1000 K?
- 28.10 (b)** For how long on average would an atom remain on a surface at 400 K if its desorption activation energy were (a) 20 kJ mol^{-1} , (b) 200 kJ mol^{-1} ? Take $\tau_0 = 0.12 \text{ ps}$. For how long on average would the same atoms remain at 800 K?
- 28.11 (a)** A solid in contact with a gas at 12 kPa and 25°C adsorbs 2.5 mg of the gas and obeys the Langmuir isotherm. The enthalpy change when 1.00 mmol of the adsorbed gas is desorbed is $+10.2 \text{ J mol}^{-1}$. What is the equilibrium pressure for the adsorption of 2.5 mg of gas at 40°C?
- 28.11 (b)** A solid in contact with a gas at 8.86 kPa and 25°C adsorbs 4.67 mg of the gas and obeys the Langmuir isotherm. The enthalpy

change when 1.00 mmol of the adsorbed gas is desorbed is +12.2 J. What is the equilibrium pressure for the adsorption of the same mass of gas at 45°C?

28.12 (a) Hydrogen iodide is very strongly adsorbed on gold but only slightly adsorbed on platinum. Assume the adsorption follows the Langmuir isotherm and predict the order of the HI decomposition reaction on each of the two metal surfaces.

28.12 (b) Suppose it is known that ozone adsorbs on a particular surface in accord with a Langmuir isotherm. How could you use the pressure dependence of the fractional coverage to distinguish between adsorption (a) without dissociation, (b) with dissociation into $O + O_2$, (c) with dissociation into $O + O + O$?

28.13 (a) Nitrogen gas adsorbed on charcoal to the extent of $0.921 \text{ cm}^3 \text{ g}^{-1}$ at 490 kPa and 190 K, but at 250 K the same amount of adsorption was achieved only when the pressure was increased to 3.2 MPa. What is the enthalpy of adsorption of nitrogen on charcoal?

28.13 (b) Nitrogen gas adsorbed on a surface to the extent of $1.242 \text{ cm}^3 \text{ g}^{-1}$ at 350 kPa and 180 K, but at 240 K the same amount of adsorption was achieved only when the pressure was increased to 1.02 MPa. What is the enthalpy of adsorption of nitrogen on the surface?

28.14 (a) In an experiment on the adsorption of oxygen on tungsten it was found that the same volume of oxygen was desorbed in 27 min at 1856 K and 2.0 min at 1978 K. What is the activation energy of desorption? How long would it take for the same amount to desorb at (a) 298 K, (b) 3000 K?

28.14 (b) In an experiment on the adsorption of ethene on iron it was found that the same volume of the gas was desorbed in 1856 s at 873 K and 8.44 s at 1012 K. What is the activation energy of desorption? How long would it take for the same amount of ethene to desorb at (a) 298 K, (b) 1500 K?

Problems

Numerical problems

28.1 Nickel is face-centred cubic with a unit cell of side 352 pm. What is the number of atoms per square centimetre exposed on a surface formed by (a) (100), (b) (110), (c) (111) planes? Calculate the frequency of molecular collisions per surface atom in a vessel containing (a) hydrogen, (b) propane at 25°C when the pressure is (i) 100 Pa, (ii) 0.10 μTorr .

28.2 The data below are for the chemisorption of hydrogen on copper powder at 25°C. Confirm that they fit the Langmuir isotherm at low coverages. Then find the value of K for the adsorption equilibrium and the adsorption volume corresponding to complete coverage.

p/Torr	0.19	0.97	1.90	4.05	7.50	11.95
V/cm^3	0.042	0.163	0.221	0.321	0.411	0.471

28.3 The data for the adsorption of ammonia on barium fluoride are reported below. Confirm that they fit a BET isotherm and find values of c and V_{mon} .

(a) $\theta = 0^\circ\text{C}$, $p^* = 3222 \text{ Torr}$:

p/Torr	105	282	492	594	620	755	798
V/cm^3	11.1	13.5	14.9	16.0	15.5	17.3	16.5

(b) $\theta = 18.6^\circ\text{C}$, $p^* = 6148 \text{ Torr}$:

p/Torr	39.5	62.7	108	219	466	555	601	765
V/cm^3	9.2	9.8	10.3	11.3	12.9	13.1	13.4	14.1

28.4 The following data have been obtained for the adsorption of H_2 on the surface of 1.00 g of copper at 0°C. The volume of H_2 below is the volume that the gas would occupy at STP (0°C and 1 atm).

p/atm	0.050	0.100	0.150	0.200	0.250
V/mL	1.22	1.33	1.31	1.36	1.40

Determine the volume of H_2 necessary to form a monolayer and estimate the surface area of the copper sample. The density of liquid hydrogen is 0.0708 g cm^{-3} .

28.5 The designers of a new industrial plant wanted to use a catalyst code-named CR-1 in a step involving the fluorination of butadiene. As a first step in the investigation they determined the form of the adsorption isotherm. The volume of butadiene adsorbed per gram of CR-1 at 15°C varied with pressure as given below. Is the Langmuir isotherm suitable at this pressure?

p/Torr	100	200	300	400	500	600
V/cm^3	17.9	33.0	47.0	60.8	75.3	91.3

Investigate whether the BET isotherm gives a better description of the adsorption of butadiene on CR-1. At 15°C, p^* (butadiene) = 200 kPa. Find V_{mon} and c .

28.6 The adsorption of solutes on solids from liquids often follows a Freundlich isotherm. Check the applicability of this isotherm to the following data for the adsorption of acetic acid on charcoal at 25°C and find the values of the parameters c_1 and c_2 .

[acid]/(mol L ⁻¹)	0.05	0.10	0.50	1.0	1.5
w_a/g	0.04	0.06	0.12	0.16	0.19

w_a is the mass adsorbed per unit mass of charcoal.

28.7 In some catalytic reactions the products may adsorb more strongly than the reacting gas. This is the case, for instance, in the catalytic decomposition of ammonia on platinum at 1000°C. As a first step in examining the kinetics of this type of process, show that the rate of ammonia decomposition should follow

$$\frac{dp_{\text{NH}_3}}{dt} = -k_c \frac{p_{\text{NH}_3}}{p_{\text{H}_2}}$$

in the limit of very strong adsorption of hydrogen. Start by showing that, when a gas J adsorbs very strongly, and its pressure is p_j , the fraction of uncovered sites is approximately $1/Kp_j$. Solve the rate equation for the catalytic decomposition of NH_3 on platinum and show that a plot of $F(t) = (1/t) \ln(p/p_0)$ against $G(t) = (p - p_0)/t$, where p is the pressure of ammonia, should give a straight line from which k_c can be determined. Check the rate law on the basis of the data below, and find k_c for the reaction.

t/s	0	30	60	100	160	200	250
p/Torr	100	88	84	80	77	74	72

Theoretical problems

28.8 The deposition of atoms and ions on a surface depends on their ability to stick, and therefore on the energy changes that occur. As an illustration, consider a two-dimensional square lattice of univalent positive and negative ions separated by 200 pm, and consider a cation approaching the upper terrace of this array from the top of the page. Calculate, by direct summation, its Coulombic interaction when it is in an empty lattice point directly above an anion. Now consider a high step in the same lattice, and let the approaching ion go into the corner formed by the step and the terrace. Calculate the Coulombic energy for this position, and decide on the likely settling point for a deposited cation.

28.9 Although the attractive van der Waals interaction between individual molecules varies as R^{-6} , the interaction of a molecule with a nearby solid (a homogeneous collection of molecules) varies as R^{-3} , where R is its vertical distance above the surface. Confirm this assertion. Calculate the interaction energy between an Ar atom and the surface of solid argon on the basis of a Lennard-Jones (6, 12)-potential. Estimate the equilibrium distance of an atom above the surface.

28.10 Use the Gibbs adsorption isotherm [another name for eqn 23.47], to show that the volume adsorbed per unit area of solid, V_a/σ , is related to the pressure of the gas by $V_a = -(\sigma/RT)(d\mu/d \ln p)$, where μ is the chemical potential of the adsorbed gas.

28.11 If the dependence of the chemical potential of the gas on the extent of surface coverage is known, the Gibbs adsorption isotherm, eqn 23.47, can be integrated to give a relation between V_a and p , as in a normal adsorption isotherm. For instance, suppose that the change in the chemical potential of a gas when it adsorbs is of the form $d\mu = -c_2(RT/\sigma)dV_a$, where c_2 is a constant of proportionality; show that the Gibbs isotherm leads to the Freundlich isotherm in this case.

28.12 Finally we come full circle and return to the Langmuir isotherm. Find the form of $d\mu$ that, when inserted in the Gibbs adsorption isotherm, leads to the Langmuir isotherm.

Additional problems supplied by Carmen Giunta and Charles Trapp

28.13 N.E. Shafer and R.N. Zare in the article 'Through a beer glass darkly' (*Phys. Today* 44, 48 (1991)) observe that the radii of bubbles

ascending from the bottom of a glass of beer increase in size as they rise. The reason is that after the bottle of beer is opened the partial pressure of dissolved CO_2 in the beer is greater than the pressure of CO_2 in the bubble. Assuming that the pressure difference is approximately constant, the change in the number, N , of CO_2 molecules is proportional to the surface area of the bubble, that is, $dN/dt = 4\pi r^2 g$, where g is a constant and r is the time-dependent radius of the bubble. (a) Use the perfect gas law to show that the radius of the bubble increases linearly with time in accordance with $r = r_0 + vt$, where r_0 is the initial radius of the bubble and v is the rate of increase of its radius. Also find an expression for v . (b) Shafer and Zare observe that the velocity and spacing between bubbles in a linear stream of bubbles proceeding from the bottom of the glass increase with height. Their data on radius and height as a function of time, with typical uncertainties are reproduced below.

Time/s	Radius, r/cm	Height, z/cm
0.00	0.017 ± 0.004	0.0 ± 0.2
0.54 ± 0.04	0.020	1.2
1.08	0.026	3.4
2.16	0.025	5.2
2.70	0.030	9.6
3.24	0.031	12.4
3.78	0.034	15.6

Test the goodness of fit of the radius data to the equation. From the fit, determine v and the constant g . Also, find an empirical relation between height and time and difference in height and time.

28.14 A. Akgerman and M. Zardkoobi (*J. Chem. Eng. Data* 41, 185 (1996)) examined the adsorption of phenol from aqueous solution on to fly ash at 20°C. They fitted their observations to a Freundlich isotherm of the form $c_{\text{ads}} = Kc_{\text{sol}}^{1/n}$, where c_{ads} is the concentration of adsorbed phenol and c_{sol} is the concentration of aqueous phenol. Among the data reported are the following.

$c_{\text{sol}}/(\text{mg g}^{-1})$	8.26	15.63	25.43	31.74	40.00
$c_{\text{ads}}/(\text{mg g}^{-1})$	4.4	19.2	35.2	52.0	67.2

Determine the constants K and n . What further information would be necessary in order to express the data in terms of fractional coverage, θ ?

28.15 C. Huang and W.P. Cheng (*J. Colloid Interface Sci.* 188, 270 (1997)) examined the adsorption of the hexacyanoferrate(III) ion, $[\text{Fe}(\text{CN})_6]^{3-}$, on $\gamma\text{-Al}_2\text{O}_3$ from aqueous solution. They modelled the adsorption with a modified Langmuir isotherm, obtaining the following values of K at pH 6.5.

T/K	283	298	308	318
$10^{11}K$	2.642	2.078	1.286	1.085

Determine the isosteric enthalpy of adsorption, $\Delta_{\text{ads}}H^\ominus$, at this pH. The researchers also reported $\Delta_{\text{ads}}S^\ominus = +146 \text{ J K}^{-1} \text{ mol}^{-1}$ under these conditions. Determine $\Delta_{\text{ads}}G^\ominus$.

28.16 M.-G. Olivier and R. Jadot (*J. Chem. Eng. Data* 42, 230 (1997)) studied the adsorption of butane on silica gel. They report the following amounts of absorption (in moles per kilogram of silica gel) at 303 K.

p/kPa	31.00	38.22	53.03	76.38	101.97
$n/(\text{mol kg}^{-1})$	1.00	1.17	1.54	2.04	2.49
p/kPa	130.47	165.06	182.41	205.75	219.91
$n/(\text{mol kg}^{-1})$	2.90	3.22	3.30	3.35	3.36

Fit these data to a Langmuir isotherm, and determine the value of n that corresponds to complete coverage and the constant K .

28.17 In a study relevant to automobile catalytic converters, C.E. Wartnaby, A. Stuck, Y.Y. Yeo, and D.A. King (*J. Phys. Chem.* 100, 12483 (1996)) measured the enthalpy of adsorption of CO, NO, and O₂ on initially clean platinum 110 surfaces. They report $\Delta_{\text{ads}}H^\ominus$ for NO to be -160 kJ mol^{-1} . How much more strongly adsorbed is NO at 500°C than at 400°C?

28.18 The following data were obtained for the extent of adsorption, s , of acetone (propanone) on charcoal from an aqueous solution of concentration c at 18°C.

$c/(\text{mmol L}^{-1})$	15.0	23.0	42.0	84.0	165	390	800
$s/(\text{mmol acetone/g charcoal})$	0.60	0.75	1.05	1.50	2.15	3.50	5.10

Which isotherm fits this data best, Langmuir, Freundlich, or Temkin?

28.19 The removal or recovery of volatile organic compounds (VOCs) from exhaust gas streams is an important process in environmental engineering. Activated carbon has long been used as an adsorbent in this process, but the presence of moisture in the stream reduces its effectiveness. M.-S. Chou and J.-H. Chiou (*J. Envir. Engrg.* ASCE 123, 437(1997)) have studied the effect of moisture content on the adsorption capacities of granular activated carbon (GAC) for normal hexane and cyclohexane in air streams. From their data for dry streams, shown in the table below, they conclude that GAC obeys a Langmuir type model in which $q_{\text{VOC,RH=0}} = abc_{\text{VOC}}/(1 + bc_{\text{VOC}})$, where $q_{\text{VOC}} = m_{\text{VOC}}/m_{\text{GAC}}$, RH is the relative humidity, a is the maximum adsorption capacity, b is the affinity parameter, and c is the concentration in parts per million (ppm).

c/ppm	$q_{\text{VOC,RH=0}}(\text{cyclohexane})$				
	33.6°C	41.5°C	57.4°C	76.4°C	99°C
200	0.080	0.069	0.052	0.042	0.027
500	0.093	0.083	0.072	0.056	0.042
1000	0.101	0.088	0.076	0.063	0.045
2000	0.105	0.092	0.083	0.068	0.052
3000	0.112	0.102	0.087	0.072	0.058

(a) By linear regression of $1/q_{\text{VOC,RH=0}}$ against $1/c_{\text{VOC}}$, test the goodness of fit and determine values of a and b . (b) The parameters a and b can be related to $\Delta_{\text{ad}}H$, the enthalpy of adsorption, and $\Delta_{\text{h}}H$, the difference in activation energy for adsorption and desorption of the VOC molecules, through Arrhenius type equations: $a = k_a e^{-\Delta_{\text{ad}}H/RT}$; $b = k_b e^{-\Delta_{\text{h}}H/RT}$. Test the goodness of fit of the data to these equations and obtain values for k_a , k_b , $\Delta_{\text{ad}}H$, and $\Delta_{\text{h}}H$. (c) What interpretation might you give to k_a and k_b ?

28.20 M.-S. Chou and J.-H. Chiou (*J. Envir. Engrg.*, ASCE 123, 437 (1997)) have studied the effect of moisture content on the adsorption capacities of granular activated carbon (GAC, Norit PK 1-3) for the volatile organic compounds (VOCs) normal hexane and cyclohexane in air streams. The following table shows the adsorption capacities ($q_{\text{water}} = m_{\text{water}}/m_{\text{GAC}}$) of GAC for pure water from moist air streams as a function of relative humidity (RH) in the absence of VOCs at 41.5°C.

RH	0.00	0.26	0.49	0.57	0.80	1.00
q_{water}	0.00	0.026	0.072	0.091	0.161	0.229

The authors conclude that the data at this and other temperatures obey a Freundlich type isotherm, $q_{\text{water}} = k(\text{RH})^{1/n}$. (a) Test this hypothesis for their data at 41.5°C and determine the constants k and n . (b) Why might VOCs obey the Langmuir model, but water the Freundlich model? (c) When both water vapour and cyclohexane were present in the stream the values given in the table below were determined for the ratio $r_{\text{VOC}} = q_{\text{VOC}}/q_{\text{VOC,RH=0}}$ at 41.5°C.

RH	0.00	0.10	0.25	0.40	0.53	0.76	0.81
r_{VOC}	1.00	0.98	0.91	0.84	0.79	0.67	0.61

The authors propose that these data fit the equation $r_{\text{VOC}} = 1 - q_{\text{water}}$. Test their proposal and determine values for k and n and compare to those obtained in part (b) for pure water. Suggest reasons for any differences.

28.21 The release of petroleum products by leaky underground storage tanks is a serious threat to clean ground water. BTEX compounds (benzene, toluene, ethylbenzene, and xylenes) are of primary concern due to their ability to cause health problems at low concentrations. D.S. Kershaw, B.C. Kulik, and S. Pamukcu (*J. Geotech. Et Geoenvir. Engrg.* 123, 324 (1997)) have studied the ability of ground tyre rubber to sorb (adsorb and absorb) benzene and *o*-xylene. Though sorption involves more than surface interactions, sorption data is usually found to fit one of the adsorption isotherms. In this study, the authors have tested how well their data fit the linear ($q = Kc_{\text{eq}}$), Freundlich ($q = K_F c_{\text{eq}}^{1/n}$), and Langmuir ($q = K_L M c_{\text{eq}}/(1 + K_L c_{\text{eq}})$) type isotherms, where q is the mass of solvent sorbed per gram of ground rubber (in milligrams per gram), the K s and M are empirical constants, c_{eq} the equilibrium concentration of contaminant in solution (in milligrams per litre). (a) Determine the units of the empirical constants. (b) Determine which of the isotherms best fits the data in the table below for the sorption of benzene on ground rubber.

$c_{\text{eq}}/(\text{mg L}^{-1})$	97.10	36.10	10.40	6.51	6.21	2.48
$q/(\text{mg g}^{-1})$	7.13	4.60	1.80	1.10	0.55	0.31

(c) Compare the sorption efficiency of ground rubber to that of granulated activated charcoal which, for benzene has been shown to obey the Freundlich isotherm in the form $q = 1.0c_{\text{eq}}^{1.6}$ with coefficient of determination $R^2 = 0.94$.



29

Dynamic electrochemistry

Processes at electrodes



- 29.1 The electrical double layer
- 29.2 The rate of charge transfer
- 29.3 Polarization

Electrochemical processes

- 29.4 Electrolysis
- 29.5 The characteristics of working cells

Power production and corrosion

- 29.6 Fuel cells and secondary cells
- 29.7 Corrosion

Checklist of key ideas

Further reading

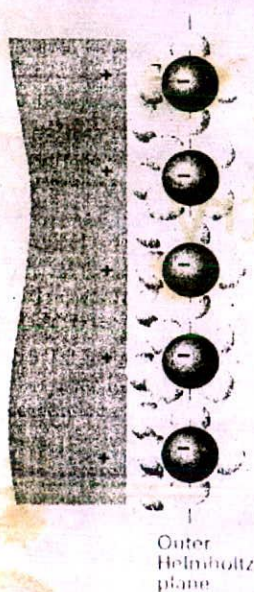
Exercises

Problems

In this final chapter we examine one more example of chemical change, that resulting from the transfer of electrons at electrodes. The approach we adopt is largely phenomenological and draws on the thermodynamic language inspired by activated complex theory. First, a model of a solution–electrode interface is constructed, and that model is used to derive a relation between the current density at the electrode and the overpotential, the difference between the electrode potential when a current is flowing and when it is not. The variation of current with overpotential can be used to infer details of the mechanism responsible for the redox process at the electrode. The Butler–Volmer equation can also be used to analyse the behaviour of working cells and to demonstrate how their electric potential when they are in use differs from the zero-current value. The same approach can be used to analyse the kinetics of reactions that are responsible for corrosion, and point the way to methods of decreasing its rate.

The economic consequences of electrochemistry are almost incalculable. Most of the modern methods of generating electricity are inefficient, and the development of fuel cells could revolutionize our production and deployment of energy. Today we produce energy inefficiently to produce goods that then decay by corrosion. Each step of this wasteful sequence could be improved by discovering more about the kinetics of electrochemical processes. Similarly, the techniques of organic and inorganic electrosynthesis, where an electrode is an active component of an industrial process, depend on a detailed knowledge of the factors affecting their rates.

Much of electrochemistry depends on processes that occur at the interface of an electrode and an ionic solution, and the kinetic problem examined in this chapter is the rate at which reducible or oxidizable species—in short, electroactive species—can gain or lose electrons. A measure of this rate is the current density, j , the charge flux through a region (the electric current divided by the area of the region). Most of the discussion that follows is concerned with the properties that control the current density and its consequences.



29.1 A simple model of the electrical double layer treats it as two rigid planes of charge, one plane, the outer Helmholtz plane (OHP), being due to the ions with their solvating molecules, the other being that on the electrode itself.

Processes at electrodes

When only equilibrium properties are of interest, there is no need to know the details of the charge separation responsible for the potential difference at an interface (just as we do not need to propose a reaction mechanism when discussing equilibria). However, a description of the interface is essential when we are interested in the rate of charge transfer.

29.1 The electrical double layer

An electrode becomes positively charged relative to the solution nearby if electrons leave the electrode and decrease the local cation concentration. The most primitive model of the interface is as an electrical double layer, which consists of a sheet of positive charge at the surface of the electrode and a sheet of negative charge next to it in the solution (or vice versa).

(a) The structure of the double layer

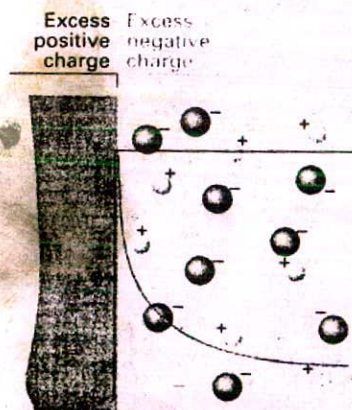
A more detailed picture of the interface can be constructed by speculating about the arrangement of ions and electric dipoles in the solution. In the Helmholtz model of the double layer the solvated ions range themselves along the surface of the electrode but are held away from it by their hydration spheres (Fig. 29.1). The location of the sheet of ionic charge, which is called the outer Helmholtz plane (OHP), is identified as the plane running through the solvated ions. In a refinement of this model, ions that have discarded their solvating molecules and have become attached to the electrode surface by chemical bonds are regarded as forming the inner Helmholtz plane (IHP). The Helmholtz model ignores the disrupting effect of thermal motion, which tends to break up and disperse the rigid outer plane of charge. In the Gouy-Chapman model of the diffuse double layer, the disordering effect of thermal motion is taken into account in much the same way as the Debye-Hückel model describes the ionic atmosphere of an ion (Section 10.2c) with the latter's single central ion replaced by an infinite, plane electrode.

Figure 29.2 shows how the local concentrations of cations and anions differ in the Gouy-Chapman model from their bulk concentrations. Ions of opposite charge cluster close to the electrode, and ions of the same charge are repelled from it. The modification of the local concentrations near an electrode implies that it might be misleading to use activity coefficients characteristic of the bulk to discuss the thermodynamic properties of ions near the interface. This is one of the reasons why measurements in dynamic electrochemistry are almost always done using a large excess of supporting electrolyte (for example, a 1 M solution of a salt, an acid, or a base). Under such conditions, the activity coefficients are almost constant because the inert ions dominate the effects of local changes caused by any reactions taking place.¹

Neither the Helmholtz nor the Gouy-Chapman model is a very good representation of the structure of the double layer. The former overemphasizes the rigidity of the local solution; the latter underemphasizes its structure. The two are combined in the Stern model, in which the ions closest to the electrode are constrained into a rigid Helmholtz plane while outside that plane the ions are dispersed as in the Gouy-Chapman model.

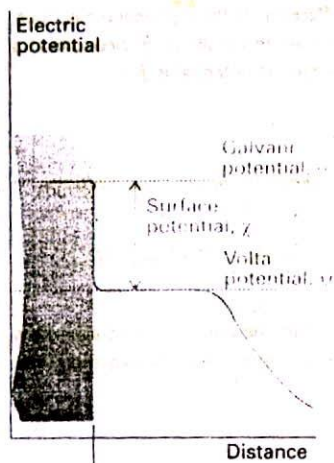
(b) The electric potential at the double layer

The potential at the interface can be analysed by imagining the separation of the electrode from the solution, but with the charges of the metal and the solution frozen in position. A positive test charge at great distances from the isolated electrode experiences a Coulomb



29.2 The Gouy-Chapman model of the electrical double layer treats the outer region as an atmosphere of counter-charge, similar to the Debye-Hückel theory of ion atmospheres.

¹ The use of a concentrated solution also minimizes ion migration effects and ohmic losses.



29.3 The variation of potential with distance from an electrode that has been separated from the electrolyte solution without there being an adjustment of charge. A similar diagram applies to the separated solution.

potential that varies inversely with distance (Fig. 29.3). As the test charge approaches the electrode it enters a region where the potential varies more slowly. This change in behaviour can be traced to the fact that the surface charge is not point-like but is spread over an area. At about 100 nm from the surface the potential varies only slightly with distance, and its value in this region is called the Volta potential, or the outer potential, ψ . As the test charge is taken through the skin of electrons on the surface of the electrode, the potential it experiences changes until the probe reaches the inner, bulk metal environment, where the potential is called the Galvani potential, ϕ . The difference between the Galvani and Volta potentials is called the surface potential, χ .

A similar sequence of changes of potential is observed as a positive test charge is brought up to and through the solution surface. The potential changes to its Volta value as the charge approaches the charged medium, then to its Galvani value as the probe is taken into the bulk.

Now consider bringing the electrode and solution back together again but without any change of charge distribution. The potential difference between points in the bulk metal and the bulk solution is the Galvani potential difference, $\Delta\phi$. Apart from a constant, this Galvani potential difference is the electrode potential that was at the centre of our discussion in Chapter 10. We shall ignore the constant, and identify changes in $\Delta\phi$ with changes in electrode potential.

Justification 29.1

To demonstrate the relation between $\Delta\phi$ and E , consider the cell $\text{Pt}|\text{H}_2(\text{g})|\text{H}^+(\text{aq})||\text{M}^+(\text{aq})|\text{M}(\text{s})$ and the half-reactions



The Gibbs energies of these two half-reactions can be expressed in terms of the chemical potentials, μ , of all the species. However, we must take into account the fact that the species are present in phases with different electric potentials. Thus, a cation in a region of positive potential has a higher chemical potential (is chemically more active in a thermodynamic sense) than in a region of zero potential.

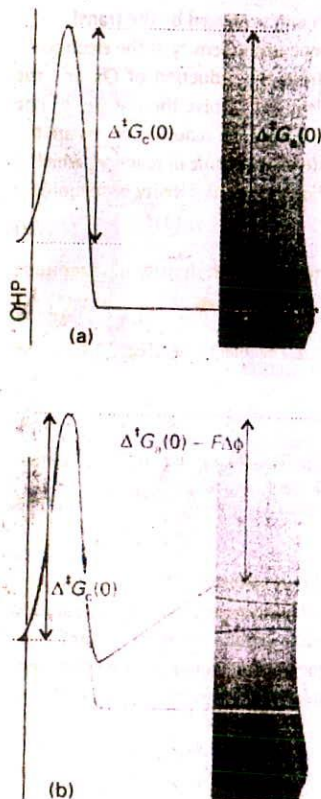
The contribution of an electric potential to the chemical potential is calculated by noting that the electrical work of adding a charge ze to a region where the potential is ϕ is $ze\phi$, and therefore that the work per mole is $zF\phi$, where F is the Faraday constant. Because at constant temperature and pressure the maximum electrical work can be identified with the change in Gibbs energy (Section 10.2c), the difference in chemical potential of an ion with and without the electric potential present is $zF\phi$. The chemical potential of an ion in the presence of an electric potential is called its electrochemical potential, $\bar{\mu}$. It follows that

$$\bar{\mu} = \mu + zF\phi \quad [1]$$

where μ is the chemical potential of the species when the potential is zero. When $z = 0$ (a neutral species), the electrochemical potential is equal to the chemical potential.

To express the Gibbs energy for the half-reactions in terms of the electrochemical potentials of the species we note that the cations M^+ are in the solution where the Galvani potential is ϕ_S and the electrons are in the electrode where it is ϕ_M . It follows that

$$\begin{aligned} \Delta_r G_R &= \bar{\mu}(\text{M}) - \{\bar{\mu}(\text{M}^+) + \bar{\mu}(\text{e}^-)\} \\ &= \mu(\text{M}) - \{\mu(\text{M}^+) + F\phi_S + \mu(\text{e}^-) - F\phi_M\} \\ &= \mu(\text{M}) - \mu(\text{M}^+) - \mu(\text{e}^-) + F\Delta\phi_R \end{aligned}$$



29.7 When the transition state resembles a species that has undergone oxidation, the cathodic current activation Gibbs energy is almost unchanged but the anodic current activation Gibbs energy is strongly affected. (a) Zero potential difference; (b) nonzero potential difference.

increased. If the transition state is reactant-like (represented by the peak of the reaction profile being close to the outer plane of the double layer in Fig. 29.7), then $\Delta^\ddagger G_c$ is independent of $\Delta\phi$. In a real system, the transition state has an intermediate resemblance to these extremes (Fig. 29.8) and the activation Gibbs energy for reduction may be written as

$$\Delta^\ddagger G_c = \Delta^\ddagger G_c(0) + \alpha F\Delta\phi \quad (12)$$

The parameter α is called the (cathodic) transfer coefficient, and lies in the range 0 to 1. Experimentally, α is often found to be about 0.5.

Now consider the oxidation reaction, $\text{Red} + e^- \rightarrow \text{Ox}$ and its reaction profile. Similar remarks apply. In this case, Red discards an electron to the electrode, so the extra work is zero if the transition state is reactant-like (represented by a peak close to the electrode, Fig. 29.6). The extra work is the full $-F\Delta\phi$ if it resembles the product (the peak close to the outer plane, Fig. 29.7). In general (Fig. 29.8), the activation Gibbs energy for this anodic process is

$$\Delta^\ddagger G_a = \Delta^\ddagger G_a(0) - (1 - \alpha)F\Delta\phi \quad (13)$$

The two activation Gibbs energies can now be inserted in place of the values used in eqn 10 with the result that

$$j = FB_a[\text{Red}]e^{-\Delta^\ddagger G_c(0)/RT}e^{-(1-\alpha)F\Delta\phi/RT} - FB_c[\text{Ox}]e^{-\Delta^\ddagger G_a(0)/RT}e^{-\alpha F\Delta\phi/RT} \quad (14)$$

This is an explicit, if complicated, expression for the net current density in terms of the potential difference.

The appearance of eqn 14 can be simplified. First, in a purely cosmetic step we write

$$f = \frac{F}{RT} \quad (15)$$

Next, we identify the individual cathodic and anodic current densities:

$$\left. \begin{aligned} j_a &= FB_a[\text{Red}]e^{-\Delta^\ddagger G_c(0)/RT}e^{(1-\alpha)f\Delta\phi} \\ j_c &= FB_c[\text{Ox}]e^{-\Delta^\ddagger G_a(0)/RT}e^{-\alpha f\Delta\phi} \end{aligned} \right\} j = j_a - j_c \quad (16)$$

Example 29.1 Calculating the current density

Calculate the change in cathodic current density at an electrode when the potential difference changes from 1.0 V to 2.0 V at 25°C.

Method Equation 16 can be used to express the ratio of cathodic current densities j'_c and j_c when the potential differences are $\Delta\phi'$ and $\Delta\phi$. Then insert a typical value of α (namely, $\frac{1}{2}$) and the data.

Answer The ratio is

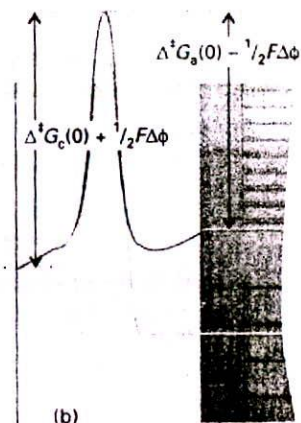
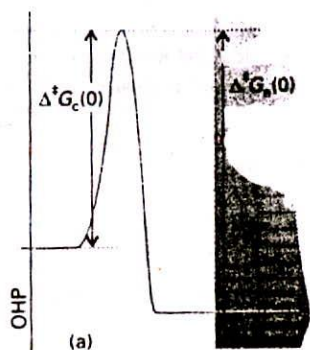
$$\frac{j'_c}{j_c} = e^{-\alpha f(\Delta\phi' - \Delta\phi)}$$

So, with $\alpha = \frac{1}{2}$ and $\Delta\phi' - \Delta\phi = 1.0$ V,

$$\alpha f \times (\Delta\phi' - \Delta\phi) = \frac{1}{2} \times (9.6485 \times 10^4 \text{ C mol}^{-1}) \times (1.0 \text{ V}) / (8.3145 \text{ J K}^{-1} \text{ mol}^{-1}) \times (298 \text{ K}) = 19.47$$

(At this stage, we are preserving an unwarranted number of significant figures.) Hence,

$$\frac{j'_c}{j_c} = e^{-19.47} = 4 \times 10^{-9}$$



29.9 When the transition state is intermediate in its resemblance to reduced and oxidized species, as represented here by a peak located at an intermediate position as measured by α (with $0 < \alpha < 1$), both activation Gibbs energies are affected; here, $\alpha \approx 0.5$.

Comment This huge change in current density occurs for a very mild and easily applied change of conditions. We can appreciate why the change is so great by realizing that a change of potential difference by 1 V changes the activation Gibbs energy by $(1 \text{ V}) \times F$, or about 50 kJ mol^{-1} , which has an enormous effect on the rates.

Self-test 29.1 Calculate the change in anodic current density under the same circumstances.

$$(j'_a/j_a = 3 \times 10^8)$$

If the cell is balanced against an external source, the difference in Galvani potential, $\Delta\phi$, can be identified as the (zero-current) electrode potential, E , and we can write⁵

$$j_c = F B_{\text{red}} [\text{Red}]_e e^{-\Delta^\ddagger G_c(0)/RT} e^{(1-\alpha)FE}$$

$$j_a = F B_{\text{ox}} [\text{Ox}]_e e^{-\Delta^\ddagger G_a(0)/RT} e^{-\alpha FE} \quad (17)$$

When these equations apply, there is no net current at the electrode (as the cell is balanced), and so the two current densities must be equal. From now on we denote them both as j_0 , which is called the exchange current density.

When the cell is producing current (that is, when a load is connected between the electrode being studied and a second counter-electrode) the electrode potential changes from its zero-current value, E , to its working value, E' , and the difference is the overpotential, η :

$$\eta = E' - E \quad (18)$$

Hence, $\Delta\phi$ changes to

$$\Delta\phi = E' + \eta \quad (19)$$

It follows that the two current densities become

$$j_c = j_0 e^{(1-\alpha)F\eta} \quad j_a = j_0 e^{-\alpha F\eta} \quad (20)$$

Then from eqn 14 we obtain the Butler-Volmer equation:

$$j = j_0 \left\{ e^{(1-\alpha)F\eta} - e^{-\alpha F\eta} \right\} \quad (21)$$

The Butler-Volmer equation is the basis of all that follows.

(d) The low overpotential limit

When the overpotential is so small that $f\eta \ll 1$ (in practice, η less than about 0.01 V) the exponentials in eqn 21 can be expanded by using $e^x = 1 + x + \dots$ to give

$$j = j_0 \{ 1 + (1-\alpha)f\eta + \dots - (1 - \alpha f\eta + \dots) \} \approx j_0 f\eta \quad (22)$$

This equation shows that the current density is proportional to the overpotential, so at low overpotentials the interface behaves like a conductor that obeys Ohm's law. When there is a small positive overpotential the current is anodic ($j > 0$ when $\eta > 0$), and when the overpotential is small and negative the current is cathodic ($j < 0$ when $\eta < 0$). The relation can also be reversed to calculate the potential difference that must exist if a current density j has been established by some external circuit:

$$\eta = \frac{RT}{F j_0} j \quad (23)$$

The importance of this interpretation will become clear below.

⁵ We assume the standard state is the same for the zero-current electrode potential. Strictly speaking, they differ slightly, but this difference can be regarded as absorbed into the constant B .

consumption of electroactive species close to the electrode results in a concentration gradient; diffusion of the species towards the electrode from the bulk is slow and may become rate-determining. A larger overpotential is then needed to produce a given current. This effect is called concentration polarization and its contribution to the total overpotential is called the polarization overpotential, η^c .

Consider a case for which the concentration polarization dominates all the rate processes and a redox couple of the type M^{z+} , M . Under zero-current conditions, when the net current density is zero, the electrode potential is related to the activity, a , of the ions in the solution by the Nernst equation (eqn 10.45):

$$E = E^\ominus + \frac{RT}{zF} \ln a \quad (28)$$

As remarked earlier, electrode kinetics are normally studied using a large excess of support electrolyte so as to keep the mean activity coefficients approximately constant. Therefore, the constant activity coefficient in $a = \gamma c$ may be absorbed into E , and we write the formal potential, E^\ominus , of the electrode as

$$E^\ominus = E^\ominus + \frac{RT}{zF} \ln \gamma \quad (29)$$

Then the electrode potential is

$$E = E^\ominus + \frac{RT}{zF} \ln c \quad (30)$$

When the cell is producing current, the active ion concentration at the OHP changes to c' and the electrode potential changes to

$$E' = E^\ominus + \frac{RT}{zF} \ln c' \quad (31)$$

The concentration overpotential is therefore

$$\eta^c = E' - E = \frac{RT}{zF} \ln \left(\frac{c'}{c} \right) \quad (32)$$

We now suppose that the solution has its bulk concentration, c , up to a distance δ from the outer Helmholtz plane; and then falls linearly to c' at the plane itself. This Nernst diffusion layer is illustrated in Fig. 29.11. The thickness of the Nernst layer (which is typically 0.1 mm, and strongly dependent on the condition of hydrodynamic flow due to any stirring or convective effects) is quite different from that of the electrical double layer (which is typically less than 1 nm, and unaffected by stirring). The concentration gradient through the Nernst layer is

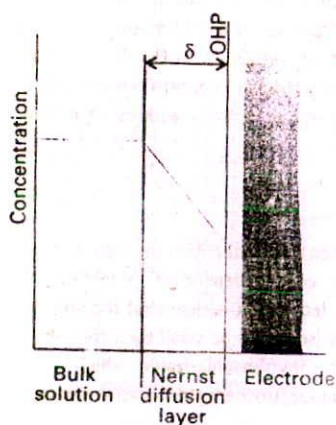
$$\frac{dc}{dx} = \frac{c' - c}{\delta} \quad (33)$$

This gradient gives rise to a flux of ions towards the electrode, which replenishes the cations as they are reduced. The (molar) flux, J , is proportional to the concentration gradient, and according to Fick's law (Section 24.3)

$$J = -D \left(\frac{\partial c}{\partial x} \right) \quad (34)$$

Therefore, the particle flux towards the electrode is

$$J = D \frac{c - c'}{\delta} \quad (35)$$



29.11 In a simple model of the Nernst diffusion layer there is a linear variation in concentration between the bulk and the outer Helmholtz plane; the thickness of the layer depends strongly on the state of flow of the fluid.

The cathodic current density towards the electrode is the product of the particle flux and the charge per mole of ions, zF :

$$j = zFJ = zFD \frac{c - c'}{\delta} \quad (36)$$

The maximum rate of diffusion across the Nernst layer occurs when the gradient is steepest, which is when $c' = 0$. This concentration occurs when an electron from an ion that diffuses across the layer is snapped over the activation barrier and on to the electrode. No flow of current can exceed the limiting current density, j_{lim} , which is given by

$$j_{\text{lim}} = zFJ_{\text{lim}} = \frac{zFDc}{\delta} \quad (37)$$

Example 29.3 Estimating the limiting current density

Estimate the limiting current density at 298 K for an electrode in a 0.10 M Cu^{2+} (aq) unstirred solution in which the thickness of the diffusion layer is about 0.3 mm.

Method To use eqn 37, estimate D from the ionic conductivity $\lambda = 107 \text{ S cm}^2 \text{ mol}^{-1}$ (Table 24.4) and the Nernst-Einstein equation (eqn 24.72).

Answer Because $\lambda = z^2 F^2 D / RT$, eqn 37 may be written

$$j_{\text{lim}} = \frac{cRT\lambda}{zF\delta}$$

Therefore, with $\delta = 0.3 \text{ mm}$, $c = 0.10 \text{ mol L}^{-1}$, $z = 2$, and $T = 298 \text{ K}$, we obtain $j_{\text{lim}} = 5 \text{ mA cm}^{-2}$. The result implies that the current towards an electrode of area 1 cm^2 electrode cannot exceed 5 mA in this (unstirred) solution.

Self-test 29.3 Evaluate the limiting current density for an $\text{Ag(s)}|\text{Ag}^+(\text{aq})$ electrode in a 0.010 M $\text{Ag}^+(\text{aq})$ solution at 298 K. Take $\delta = 0.03 \text{ mm}$.

[5 mA cm⁻²]

It follows from eqn 36 that the concentration c' is related to the current density at the double layer by

$$c' = c - \frac{j\delta}{zFD} \quad (38)$$

Hence, as the current density is increased, the concentration falls below the bulk value. However, this decline in concentration is small when the diffusion constant is large, for then the ions are very mobile and can quickly replenish any ions that have been removed.

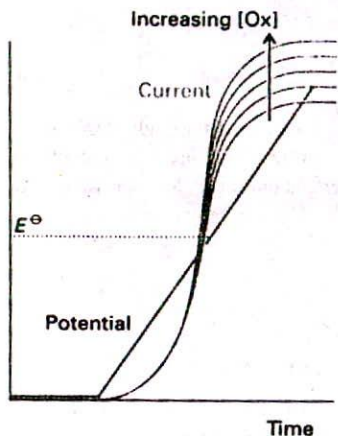
Finally, we substitute eqn 38 into eqn 32 and obtain the following expressions for the overpotential in terms of the current density, and vice versa:

$$\eta^c = \frac{RT}{zF} \ln \left(1 - \frac{j\delta}{zFD} \right) \quad (39)$$

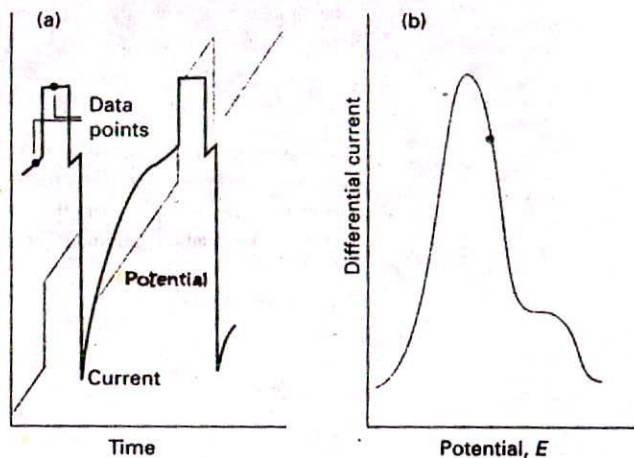
$$j = \frac{zFD}{\delta} (1 - e^{zF\eta^c})$$

(b) Voltammetry

The kinetics of electrode processes can be studied by **voltammetry**, in which the current is monitored as the potential of the electrode is changed, and by **chronopotentiometry**, in



29.12 The change of potential with time and the resulting current/potential curve in a linear-sweep voltammetry experiment. The limiting value of the current density is proportional to the concentration of electroactive species (for instance, [Ox]) in solution.



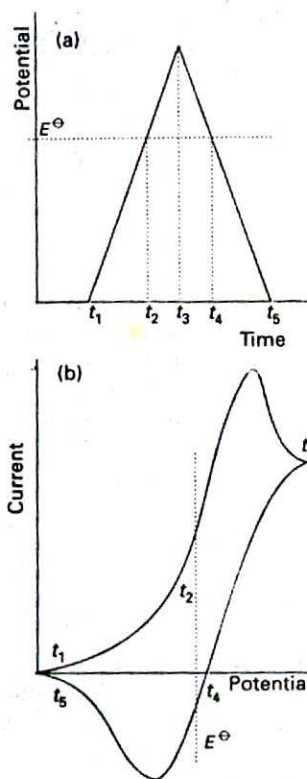
29.13 A differential pulse polarography experiment. (a) The potential is swept linearly as a mercury droplet grows on the end of a capillary dipping into the sample, and then pulsed as shown by the green line. The resulting current is shown as the black line, and is sampled at the two points shown. (b) The data output is obtained as the difference of the currents at the two sampled points.

which the potential is monitored as the current flow is changed. Voltammetry may also be used to identify species present in solution and to determine their concentration.

The kind of output from linear-sweep voltammetry is illustrated in Fig. 29.12. Initially the absolute value of the potential is low, and the cathodic current is due to the migration of ions in the solution. However, as the potential approaches the reduction potential of the reducible solute, the cathodic current grows. Soon after the potential exceeds the reduction potential the current rises to a plateau at which it has its limiting value (as specified in eqn 37). This limiting current is proportional to the molar concentration of the species, so that concentration can be determined from the height of the plateau above the extrapolated baseline. In differential pulse voltammetry the current is monitored before and after a pulse of potential is applied, and the processed output is the slope of a curve like that obtained by linear-sweep voltammetry (Fig. 29.13). The area under the curve (in effect, the integral of the derivative displayed in the illustration) is proportional to the concentration of the species.

In cyclic voltammetry the potential is applied in a sawtooth manner to the working electrode and the current is monitored. A typical cyclic voltammogram is shown in Fig. 29.14. The shape of the curve is initially like that of a linear-sweep experiment, but after the absolute value of the potential begins to fall there is a rapid change in current on account of the high concentration of oxidizable species close to the electrode that were generated on the reductive sweep. When the potential is close to the value required to oxidize the reduced species, there is a substantial anodic current until all the oxidation is complete, and the current returns to zero.

When the reduction reaction at the electrode can be reversed, as in the case of the $[\text{Fe}(\text{CN})_6]^{3-}/[\text{Fe}(\text{CN})_6]^{4-}$ couple, the cyclic voltammogram is almost symmetric about the standard potential of the couple (as in Fig. 29.14b). The scan is initiated with $[\text{Fe}(\text{CN})_6]^{3+}$ present in solution and, as the potential approaches E^\ominus for the couple, the $[\text{Fe}(\text{CN})_6]^{3-}$ near the electrode is reduced and current begins to flow. As the potential continues to change, the cathodic current begins to decline again because all the $[\text{Fe}(\text{CN})_6]^{3-}$ near the electrode has been reduced and the current reaches its limiting value. The potential is now returned linearly to its initial value, and the reverse series of events occurs with the $[\text{Fe}(\text{CN})_6]^{4-}$



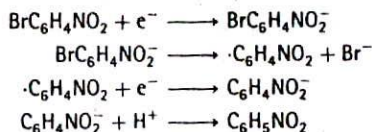
29.14 (a) The change of potential with time and (b) the resulting current/potential curve in a cyclic voltammetry experiment.

produced during the forward scan now undergoing oxidation. The peak of current lies on the other side of E^\ominus , so the species present and its standard potential can be identified, as indicated in the illustration, by noting the locations of the two peaks.

The overall shape of the curve gives details of the kinetics of the electrode process and the change in shape as the rate of change of potential is altered gives information on the rates of the processes involved. For example, the matching peak on the return phase of the sawtooth change of potential may be missing, which indicates that the oxidation (or reduction) is irreversible. The appearance of the curve may also depend on the timescale of the sweep for, if the sweep is too fast, some processes might not have time to occur. This style of analysis is illustrated in the following example.

Example 29.4 Analysing a cyclic voltammetry experiment

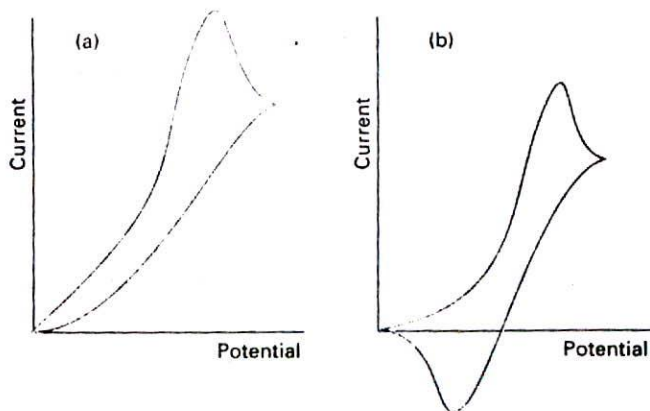
The electroreduction of *p*-bromonitrobenzene in liquid ammonia is believed to occur by the following mechanism:



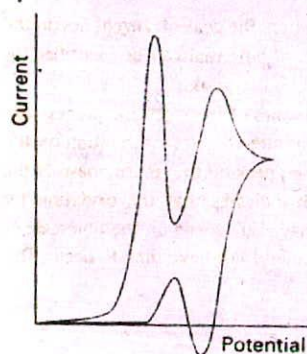
Suggest the likely form of the cyclic voltammogram expected on the basis of this mechanism.

Method Decide which steps are likely to be reversible on the timescale of the potential sweep: such processes will give symmetrical voltammograms. Irreversible processes will give unsymmetrical shapes as reduction (or oxidation) might not occur. However, at fast sweep rates, an intermediate might not have time to react, and a reversible shape will be observed.

Answer At slow sweep rates, the second reaction has time to occur, and a curve typical of a two-electron reduction will be observed, but there will be no oxidation peak on the second half of the cycle because the product, $\text{C}_6\text{H}_5\text{NO}_2$, cannot be oxidized (Fig. 29.15a). At fast sweep rates, the second reaction does not have time to take place before oxidation of the $\text{BrC}_6\text{H}_4\text{NO}_2^-$ intermediate starts to occur during the reverse scan, so the voltammogram will be typical of a reversible one-electron reduction (Fig. 29.15b).

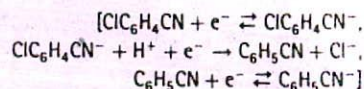


29.15 (a) When a non-reversible step in a reaction mechanism has time to occur, the cyclic voltammogram may not show the reverse oxidation or reduction peak. (b) However, if the rate of sweep is increased, the return step may be caused to occur before the irreversible step has had time to intervene, and a typical 'reversible' voltammogram is obtained.



29.16 The cyclic voltammogram referred to in Self-test 29.5.

Self-test 29.5 Suggest an interpretation of the cyclic voltammogram shown in Fig. 29.16. The electroactive material is $\text{ClC}_6\text{H}_4\text{CN}$ in acid solution; after reduction to $\text{ClC}_6\text{H}_4\text{CN}^-$, the radical anion may form $\text{C}_6\text{H}_5\text{CN}$ irreversibly.



Electrochemical processes

To induce current to flow through an electrolytic cell and bring about a non-spontaneous cell reaction, the applied potential difference must exceed the zero-current potential by at least the cell overpotential. The cell overpotential is the sum of the overpotentials at the two electrodes and the ohmic drop (iR_s , where R_s is the internal resistance of the cell) due to the current through the electrolyte. The additional potential needed to achieve a detectable rate of reaction may need to be large when the exchange current density at the electrodes is small. For similar reasons, a working galvanic cell generates a smaller potential than under zero-current conditions. In this section we see how to cope with both aspects of the overpotential.

29.4 Electrolysis

The rate of gas evolution or metal deposition during electrolysis can be estimated from the Butler-Volmer equation and tables of exchange current densities. The exchange current density depends strongly on the nature of the electrode surface, and changes in the course of the electrodeposition of one metal on another. A very crude criterion is that significant evolution or deposition occurs only if the overpotential exceeds about 0.6 V.

Example 29.5 Estimating the relative rates of electrolysis

Derive an expression for the relative rates of electrodeposition and hydrogen evolution in a solution in which both may occur.

Method We can calculate the ratio of the cathodic currents by using eqn 26. For simplicity, assume equal transfer coefficients.

Answer From eqn 26, where j' is the current density for electrodeposition and j is that for hydrogen evolution, and j'_0 and j_0 are the corresponding exchange current densities.

$$\frac{j'}{j} = \frac{j'_0}{j_0} e^{(\eta - \eta')/aF}$$

Comment This equation shows that metal deposition is favoured by a large exchange current density and relatively high hydrogen evolution overvoltage (so $\eta - \eta'$ is positive and large). Note that $\eta < 0$ for a cathodic process, $-\eta' > 0$.

Self-test 29.6 Deduce an expression for the ratio when the hydrogen evolution is limited by transport across a diffusion layer.

$$[j'/j = (\delta j'_0/cFD)e^{-a\eta'/F}]$$

A glance at Table 29.1 shows the wide range of exchange current densities for a metal/hydrogen electrode. The most sluggish exchange currents occur for lead and mercury, and the value of 1 pA cm^{-2} corresponds to a monolayer of atoms being replaced in about 5 y. For such systems, a high overpotential is needed to induce significant hydrogen evolution. In contrast, the value for platinum (1 mA cm^{-2}) corresponds to a monolayer being replaced in 0.1 s, so gas evolution occurs for a much lower overpotential.

The exchange current density also depends on the crystal face exposed. For the deposition of copper on copper, the (100) face has $j_0 = 1 \text{ mA cm}^{-2}$, so for the same overpotential the (100) face grows at 2.5 times the rate of the (111) face, for which $j_0 = 0.4 \text{ mA cm}^{-2}$.

29.5 The characteristics of working cells

We expect the cell potential to decrease as current is generated because it is then no longer working reversibly and can therefore do less than maximum work.

(a) The potentials of working cells

We shall consider the cell $M|M^+(aq)||M^{++}(aq)|M'$ and ignore all the complications arising from liquid junctions. The working potential of the cell is

$$E' = \Delta\phi_R - \Delta\phi_L \quad (40)$$

Because the working potential differences differ from their zero-current values by overpotentials, we can write

$$\Delta\phi_X = E_X + \eta_X \quad (41)$$

where X is L or R for the left or right electrode, respectively. The working cell potential is therefore

$$E' = E + \eta_R - \eta_L \quad (42)$$

with E the zero-current cell potential. We should subtract from this expression the ohmic potential difference IR_s , where R_s is the cell's internal resistance:

$$E' = E + \eta_R - \eta_L - IR_s \quad (43)$$

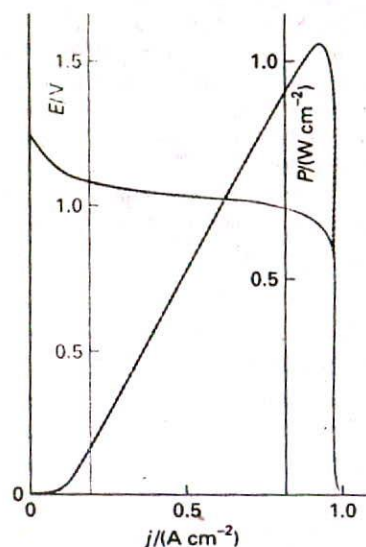
The ohmic term is a contribution to the cell's irreversibility—it is a thermal dissipation term—so the sign of IR_s is always such as to reduce the potential in the direction of zero.

The overpotentials in eqn 43 can be calculated from the Butler-Volmer equation for a given current, I , being drawn. We shall simplify the equations by supposing that the areas, A , of the electrodes are the same, that only one electron is transferred in the rate-determining steps at the electrodes, that the transfer coefficients are both $\frac{1}{2}$, and that the high-overpotential limit of the Butler-Volmer equation may be used. Then from eqns 26 and 43 we find

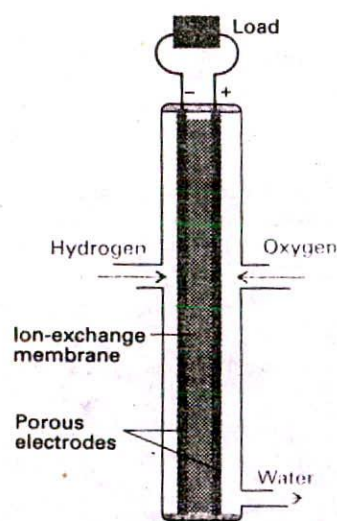
$$E' = E - IR_s - \frac{4RT}{F} \ln \left(\frac{I}{Aj} \right) \quad \bar{j} = (j_{0L}j_{0R})^{1/2} \quad (44)$$

where j_{0L} and j_{0R} are the exchange current densities for the two electrodes.

The concentration overpotential also reduces the cell potential. If we use the Nernst diffusion layer model for each electrode, the total change of potential arising from



29.17 The dependence of the potential of a working cell on the current being drawn (green line) and the corresponding power output (grey line) calculated by using eqns 46 and 47, respectively. Notice the sharp decline in power just after the maximum.



29.18 A single cell of a hydrogen/oxygen fuel cell. In practice, a battery of many cells is used.

concentration polarization is given by eqn 39 as

$$E' = E - \frac{RT}{zF} \ln \left\{ \left(1 - \frac{I}{Aj_{\text{lim,L}}} \right) \left(1 - \frac{I}{Aj_{\text{lim,R}}} \right) \right\} \quad (45)$$

This contribution can be added to the one in eqn 44 to obtain a full (but still very approximate) expression for the cell potential when a current I is being drawn:

$$E' = E - IR_s - \frac{2RT}{zF} \ln g(I) \quad (46)$$

$$g(I) = \left(\frac{I}{A\bar{j}} \right)^{2\alpha} \left\{ \left(1 - \frac{I}{Aj_{\text{lim,L}}} \right) \left(1 - \frac{I}{Aj_{\text{lim,R}}} \right) \right\}^{-1/2}$$

This equation depends on a lot of parameters, but an example of its general form is given in Fig. 29.17. Notice the very steep decline of working potential when the current is high and close to the limiting value for one of the electrodes.

(b) The power output of working cells

Because the power, P , supplied by a working cell is IE' , from eqn 46 we can write

$$P = IE - I^2 R_s - \frac{2IRT}{zF} \ln g(I) \quad (47)$$

The first term on the right is the power that would be produced if the cell retained its zero-current potential when delivering current. The second term is the power generated uselessly as heat as a result of the resistance of the electrolyte. The third term is the reduction of the potential at the electrodes as a result of drawing current.

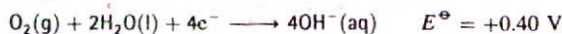
The general dependence of power output on the current drawn is shown in Fig. 29.17 as the grey line. Notice how maximum power is achieved just before the concentration polarization quenches the cell's performance. Information of this kind is essential if the optimum conditions for operating electrochemical devices are to be found and their performance improved.

Power production and corrosion

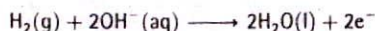
The thermodynamics of galvanic cells were treated in Chapter 10. In this section we consider some kinetic considerations relating to power production and the processes responsible for corrosion.

29.6 Fuel cells and secondary cells

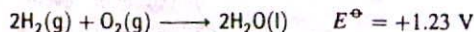
A fuel cell operates like a conventional galvanic cell with the exception that the reactants are supplied from outside rather than forming an integral part of its construction. A fundamental and important example of a fuel cell is the hydrogen/oxygen cell (Fig. 29.18). One of the electrolytes used is concentrated aqueous potassium hydroxide maintained at 200°C and 20–40 atm; the electrodes may be porous nickel in the form of sheets of compressed powder. The cathode reaction is the reduction



and the anode reaction is the oxidation



For the corresponding reduction, $E^\ominus = -0.83 \text{ V}$. Because the overall reaction



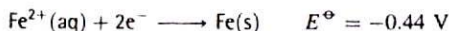
is exothermic as well as spontaneous, it is less favourable thermodynamically at 200°C than at 25°C, so the cell potential is lower at the higher temperature. However, the increased pressure compensates for the increased temperature and, at 200°C and 40 atm, $E \approx +1.2$ V.

One advantage of the hydrogen/oxygen system is the large exchange current density of the hydrogen reaction. Unfortunately, the oxygen reaction has an exchange current density of only about 0.1 nA cm^{-2} , which limits the current available from the cell. One way round the difficulty is to use a catalytic surface (to increase j_0) with a large surface area. One type of highly developed fuel cell has phosphoric acid as the electrolyte and operates with hydrogen and air at about 200°C; the hydrogen is obtained from a reforming reaction on natural gas. The power output of batteries of such cells has reached the order of 10 MW. Cells with molten carbonate electrolytes at about 600°C can make use of natural gas directly. Solid-state electrolytes are also used. They include one version in which the electrolyte is a solid polymeric ionic conductor at about 100°C, but in current versions it requires very pure hydrogen to operate successfully. Solid ionic conducting oxide cells operate at about 1000°C and can use hydrocarbons directly as fuel.

Electric storage cells operate as galvanic cells while they are producing electricity but as electrolytic cells while they are being charged by an external supply. The lead-acid battery is an old device, but one well suited to the job of starting cars (and the only one available). During charging the cathode reaction is the reduction of Pb^{2+} and its deposition as lead on the lead electrode. Deposition occurs instead of the reduction of the acid to hydrogen because the latter has a low exchange current density on lead. The anode reaction during charging is the oxidation of Pb(II) to Pb(IV) , which is deposited as the oxide PbO_2 . On discharge, the two reactions run in reverse. Because they have such high exchange current densities the discharge can occur rapidly, which is why the lead battery can produce large currents on demand.

29.7 Corrosion

A thermodynamic warning of the likelihood of corrosion is obtained by comparing the standard potentials of the metal reduction, such as

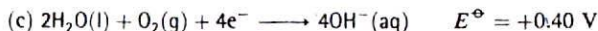


with the values for one of the following half-reactions:

In acidic solution:



In basic solution:

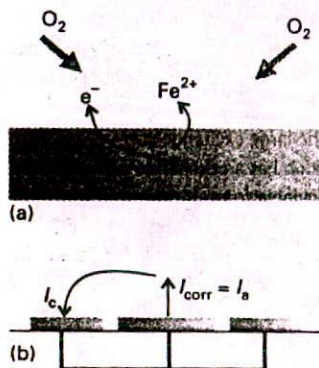


Because all three redox couples have standard potentials more positive than $E^\ominus(\text{Fe}^{2+}/\text{Fe})$, all three can drive the oxidation of iron to iron(II). The electrode potentials we have quoted are standard values, and they change with the pH of the medium. For the first two:

$$E(\text{a}) = E^\ominus(\text{a}) + \frac{RT}{F} \ln a(\text{H}^+) = -(0.059 \text{ V})\text{pH}$$

$$E(\text{b}) = E^\ominus(\text{b}) + \frac{RT}{F} \ln a(\text{H}^+) = 1.23 \text{ V} - (0.059 \text{ V})\text{pH}$$

These expressions let us judge at what pH the iron will have a tendency to oxidize (see Chapter 10). A thermodynamic discussion of corrosion, however, only indicates whether a tendency to corrode exists. If there is a thermodynamic tendency, we must examine the



29.19 (a) A simple version of the corrosion process is that of a droplet of water, which is oxygen-rich near its boundary with air. The oxidation of the iron takes place in the region away from the oxygen because the electrons are transported through the metal. (b) The process may be modelled as a short-circuited electrochemical cell.

kinetics of the processes involved to see whether the process occurs at a significant rate.

(a) The rate of corrosion

A model of a corrosion system is shown in Fig. 29.19a. It can be taken to be a drop of slightly acidic (or basic) water containing some dissolved oxygen in contact with the metal. The oxygen at the edges of the droplet, where the O_2 concentration is higher, is reduced by electrons donated by the iron over an area A . Those electrons are replaced by others released elsewhere as $Fe \rightarrow Fe^{2+} + 2e^-$. This oxidative release occurs over an area A' under the oxygen-deficient inner region of the droplet. The droplet acts as a short-circuited galvanic cell (Fig. 29.19b).

The rate of corrosion is measured by the current of metal ions leaving the metal surface in the anodic region. This flux of ions gives rise to the corrosion current, I_{corr} , which can be identified with the anodic current, I_a . We show in the *Justification* below that the corrosion current is related to the cell potential of the corrosion couple by

$$I_{\text{corr}} = \bar{j}_0 \bar{A} e^{E/4} \quad \bar{j}_0 = (j_0 j'_0)^{1/2}, \quad \bar{A} = (AA')^{1/2} \quad (48)$$

Justification 29.2

Because any current emerging from the anodic region must find its way to the cathodic region, the cathodic current, I_c , and the anodic current, I_a must both be equal to the corrosion current. In terms of the current densities at the oxidation and reduction sites, j and j' , respectively, we can write

$$I_{\text{corr}} = jA = j'A' = (jj'AA')^{1/2} = \bar{j}\bar{A} \quad \bar{j} = (jj')^{1/2}, \quad \bar{A} = (AA')^{1/2} \quad (49)$$

The Butler-Volmer equation is now used to express the current densities in terms of overpotentials. For simplicity we assume that the overpotentials are large enough for the high-overpotential limit (eqn 26) to apply, that polarization overpotential can be neglected, that the rate-determining step is the transfer of a single electron, and that the transfer coefficients are $\frac{1}{2}$. We also assume that, since the droplet is so small, there is negligible potential difference between the cathode and anode regions of the solution. Moreover, because it is short-circuited by the metal, the potential of the metal is the same in both regions, and so the potential difference between the metal and the solution is the same in both regions too; it is denoted $\Delta\phi_{\text{corr}}$. The overpotentials in the two regions are therefore

$$\eta = \Delta\phi_{\text{corr}} - \Delta\phi \quad \eta' = \Delta\phi_{\text{corr}} - \Delta\phi'$$

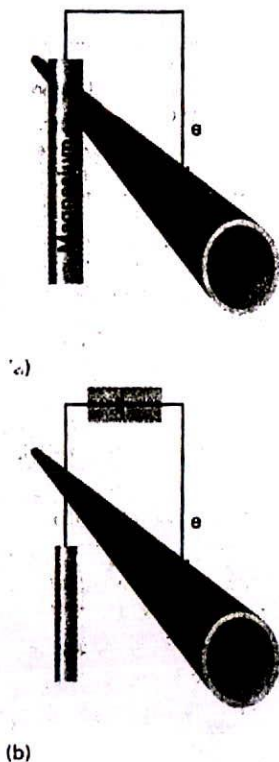
and the current densities are

$$j = j_0 e^{\eta/2} = j_0 e^{f\Delta\phi_{\text{corr}}/2} e^{-f\Delta\phi/2}$$

$$j' = j'_0 e^{-\eta'/2} = j'_0 e^{-f\Delta\phi_{\text{corr}}/2} e^{f\Delta\phi'/2}$$

These expressions can be substituted into the expression for I_{corr} and $\Delta\phi' - \Delta\phi$ replaced by the difference of electrode potentials E to give eqn 48.

Several conclusions can be drawn from eqn 48. First, the rate of corrosion depends on the surfaces exposed: if either A or A' is zero, then the corrosion current is zero. This interpretation points to a trivial, yet often effective, method of slowing corrosion: cover the surface with a coating, such as paint. Paint also increases the effective solution resistance between the cathode and anode patches on the surface. Second, for corrosion reactions with similar exchange current densities, the rate of corrosion is high when E is large. That is, rapid corrosion can be expected when the oxidizing and reducing couples have widely differing electrode potentials.



29.20 (a) In cathodic protection an anode of a more strongly reducing metal is sacrificed to maintain the integrity of the protected object (for example, a pipeline, bridge, or boat). (b) In impressed current cathodic protection electrons are supplied from an external cell so that the object itself is not oxidized. The dotted lines depict the completed circuit through the soil.

The effect of the exchange current density on the corrosion rate can be seen by considering the specific case of iron in contact with acidified water. Thermodynamically, either hydrogen or oxygen reduction reaction (a) or (b) on p. 875 is effective. However, the exchange current density of reaction (b) on iron is only about $10^{-14} \text{ A cm}^{-2}$, whereas for (a) it is $10^{-6} \text{ A cm}^{-2}$. The latter therefore dominates kinetically, and iron corrodes by hydrogen evolution in acidic solution.

(b) The inhibition of corrosion

Several techniques for inhibiting corrosion are available. Coating the surface with an impermeable layer, such as paint, may prevent the access of damp air. Unfortunately, this protection fails disastrously if the paint becomes porous. The oxygen then has access to the exposed metal and corrosion continues beneath the paintwork. Another form of surface coating is provided by galvanizing, the coating of an iron object with zinc. Because the latter's standard potential is -0.76 V , which is more negative than that of the iron couple, the corrosion of zinc is thermodynamically favoured and the iron survives (the zinc survives because it is protected by a hydrated oxide layer). In contrast, tin plating leads to a very rapid corrosion of the iron once its surface is scratched and the iron exposed because the tin couple ($E^\ominus = -0.14 \text{ V}$) oxidizes the iron couple ($E^\ominus = -0.44 \text{ V}$). Some oxides are inert kinetically in the sense that they adhere to the metal surface and form an impermeable layer over a fairly wide pH range. This passivation, or kinetic protection, can be seen as a way of decreasing the exchange currents by sealing the surface. Thus, aluminium is inert in air even though its standard potential is strongly negative (-1.66 V).

Another method of protection is to change the electric potential of the object by pumping in electrons that can be used to satisfy the demands of the oxygen reduction without involving the oxidation of the metal. In cathodic protection, the object is connected to a metal with a more negative standard potential (such as magnesium, -2.36 V). The magnesium acts as a sacrificial anode, supplying its own electrons to the iron and becoming oxidized to Mg^{2+} in the process (Fig. 29.20a). A block of magnesium replaced occasionally is much cheaper than the ship, building, or pipeline for which it is being sacrificed. In impressed-current cathodic protection (Fig. 29.20b) an external cell supplies the electrons and eliminates the need for iron to transfer its own.

Checklist of key ideas

current density

Processes at electrodes

29.1 The electrical double layer

- electrical double layer
- Helmholtz model
- outer Helmholtz plane (OHP)
- inner Helmholtz plane (IHP)
- Gouy-Chapman model
- diffuse double layer
- Stern model
- Volta potential
- outer potential
- Galvani potential

surface potential

electrochemical potential (1)

29.2 The rate of charge transfer

- product flux
- rate of heterogeneous reaction (5)
- cathodic current density
- anodic current density
- transfer coefficient (12)
- exchange current density
- overpotential (18)
- Butler-Volmer equation (21)
- low overpotential limit

(22, 23)

high overpotential limit (25, 27)

Tafel plot

working electrode

reference electrode

29.3 Polarization

- non-polarizable electrode
- polarizable electrode
- concentration polarization
- polarization overpotential
- formal potential (29)
- Nernst diffusion layer
- limiting current density (37)

voltammetry

chronopotentiometry

linear-sweep voltammetry

differential pulse voltammetry

cyclic voltammetry

rate processes in voltammetry

Electrochemical processes

cell overpotential

29.4 Electrolysis

gas evolution and metal deposition

29.5 The characteristics of working cells

- potential of a working cell (46)
 power output (47)

Power production and corrosion**29.6 Fuel cells and secondary cells**

- hydrogen-oxygen fuel cell

- storage cells

29.7 Corrosion

- thermodynamic tendency
 corrosion current

- galvanizing
 cathodic protection
 sacrificial anode
 impressed-current cathodic protection

Further reading

Articles of general interest

R.M. Wightman and D.O. Wipf, High-speed cyclic voltammetry. *Acc. Chem. Res.* **23**, 64 (1990).

A.T. Hubbard, Electrochemistry at well-characterized surfaces. *Chem. Rev.* **88**, 633 (1988).

R. Parsons, Electrical double layer: recent experimental and theoretical developments. *Chem. Rev.* **90**, 813 (1990).

R. Adžić and E.B. Yeager, Electrochemistry. In *Encyclopedia of applied physics* (ed. G.L. Trigg), **5**, 223. VCH, New York (1993).

Texts and sources of data and information

J. Koryta, *Ions, electrodes, and membranes*. Wiley, New York (1991).

R.G. Compton (ed.), *Comprehensive chemical kinetics*. Elsevier, Amsterdam (1987-92).

J.O'M. Bockris, B.E. Conway, and R.E. White (ed.), *Modern aspects of electrochemistry*, Vol. 22. Plenum, New York (1992).

C.D.S. Tuck, *Modern battery construction*. Ellis Horwood, New York (1991).

D. Linden (ed.) *Handbook of batteries and cells*. McGraw-Hill, New York (1984).

D.R. Crow, *Principles and applications of electrochemistry*. Chapman & Hall, London (1988).

A.J. Bard and L.R. Faulkner, *Electrochemical techniques: fundamentals and applications*. Wiley-Interscience, New York (1979).

J.O'M. Bockris and S.U.M. Khan, *Surface electrochemistry: a molecular level approach*. Plenum, New York (1993).

M.G. Fontanna and R.W. Staehle (ed.), *Advances in corrosion science and technology*. Plenum, New York (1980).

Exercises

29.1 (a) The Helmholtz model of the electrical double layer is equivalent to a parallel plate capacitor. Hence the potential difference across the double layer is given by $\Delta\phi = \sigma d/\epsilon$, where d is the distance between the plates and σ is the surface charge density. Assuming that this model holds for concentrated salt solutions calculate the magnitude of the electric field at the surface of silica in 5.0 M NaCl(aq) if the surface charge density is 0.10 C m^{-2} .

29.1 (b) Refer to the preceding exercise. Calculate the magnitude of the electric field at the surface of silica in 4.5 M NaCl(aq) if the surface charge density is 0.12 C m^{-2} .

29.2 (a) The transfer coefficient of a certain electrode in contact with M^{3+} and M^{4+} in aqueous solution at 25°C is 0.39. The current density is found to be 55.0 mA cm^{-2} when the overvoltage is 125 mV. What is the overvoltage required for a current density of 75 mA cm^{-2} ?

29.2 (b) The transfer coefficient of a certain electrode in contact with M^{2+} and M^{3+} in aqueous solution at 25°C is 0.42. The current density is found to be 17.0 mA cm^{-2} when the overvoltage is 105 mV. What is the overvoltage required for a current density of 72 mA cm^{-2} ?

29.3 (a) Determine the exchange current density from the information given in Exercise 29.2a.

29.3 (b) Determine the exchange current density from the information given in Exercise 29.2b.

29.4 (a) To a first approximation, significant evolution or deposition in occurs in electrolysis only if the overpotential exceeds about 0.6 V. To illustrate this criterion determine the effect that increasing the overpotential from 0.40 V to 0.60 V has on the current density in the electrolysis of 1.0 M NaOH(aq), which is 1.0 mA cm^{-2} at 0.4 V and 25°C . Take $\alpha = 0.5$.

29.4 (b) Determine the effect that increasing the overpotential from 0.50 V to 0.60 V has on the current density in the electrolysis of 1.0 M NaOH(aq), which is 1.22 mA cm^{-2} at 0.50 V for a particular electrode and 25°C . Take $\alpha = 0.50$.

29.5 (a) Use the data in Table 29.1 for the exchange current density and transfer coefficient for the reaction $2\text{H}^+ + 2\text{e}^- \rightarrow \text{H}_2$ on nickel at 25°C to determine what current density would be needed to obtain an overpotential of 0.20 V as calculated from (a) the Butler-Volmer equation, and (b) the Tafel equation. Is the validity of the Tafel approximation affected at higher overpotentials (of 0.4 V and more)?

29.5 (b) Use the data in Table 29.1 for the exchange current density and transfer coefficient for the reaction $\text{Fe}^{3+} + \text{e}^- \rightarrow \text{Fe}^{2+}$ on platinum at 25°C to determine what current density would be needed to obtain an

overpotential of 0.30 V as calculated from (a) the Butler-Volmer equation, and (b) the Tafel equation. Is the validity of the Tafel approximation affected at higher overpotentials (of 0.4 V and more)?

29.6 (a) Estimate the limiting current density at an electrode in which the concentration of Ag^+ ions is 2.5 mmol L^{-1} at 25°C . The thickness of the Nernst diffusion layer is 0.40 mm. The ionic conductivity of Ag^+ at infinite dilution and 25°C is $6.19 \text{ mS m}^2 \text{ mol}^{-1}$.

29.6 (b) Estimate the limiting current density at an electrode in which the concentration of Mg^{2+} ions is 1.5 mmol L^{-1} at 25°C . The thickness of the Nernst diffusion layer is 0.32 mm. The ionic conductivity of Mg^{2+} at infinite dilution and 25°C is $10.60 \text{ mS m}^2 \text{ mol}^{-1}$.

29.7 (a) A $0.10 \text{ M CdSO}_4(\text{aq})$ solution is electrolysed between a cadmium cathode and a platinum anode with a current density of 1.00 mA cm^{-2} . The hydrogen overpotential is 0.60 V. What will be the concentration of Cd^{2+} ions when evolution of H_2 just begins at the cathode? Assume all activity coefficients are unity.

29.7 (b) A $0.10 \text{ M FeSO}_4(\text{aq})$ solution is electrolysed between a magnesium cathode and a platinum anode with a current density of 1.50 mA cm^{-2} . The hydrogen overpotential is 0.60 V. What will be the concentration of Fe^{2+} ions when evolution of H_2 just begins at the cathode? Assume all activity coefficients are unity.

29.8 (a) A typical exchange current density, that for H^+ discharge at platinum, is 0.79 mA cm^{-2} at 25°C . What is the current density at an electrode when its overpotential is (a) 10 mV, (b) 100 mV, (c) -0.50 V ? Take $\alpha = 0.5$.

29.8 (b) The exchange current density for a $\text{Pt}|\text{Fe}^{3+}, \text{Fe}^{2+}$ electrode is 2.5 mA cm^{-2} . The standard potential of the electrode is $+0.77 \text{ V}$. Calculate the current flowing through an electrode of surface area 1.0 cm^2 as a function of the potential of the electrode. Take unit activity for both ions.

29.9 (a) Suppose that the electrode potential is set at 1.00 V. The exchange current density is $6.0 \times 10^{-4} \text{ A cm}^{-2}$ and $\alpha = 0.50$. Calculate the current density for the ratio of activities $a(\text{Fe}^{3+})/a(\text{Fe}^{2+})$ in the range 0.1 to 10.0 and at 25°C .

29.9 (b) Suppose that the electrode potential is set at 0.50 V. Calculate the current density for the ratio of activities $a(\text{Cr}^{3+})/a(\text{Cr}^{2+})$ in the range 0.1 to 10.0 and at 25°C .

29.10 (a) What overpotential is needed to sustain a current density of 20 mA cm^{-2} at a $\text{Pt}|\text{Fe}^{3+}, \text{Fe}^{2+}$ electrode in which both ions are at a mean activity $a = 0.10$?

29.10 (b) What overpotential is needed to sustain a current density of 15 mA cm^{-2} at a $\text{Pt}|\text{Ce}^{4+}, \text{Ce}^{3+}$ electrode in which both ions are at a mean activity $a = 0.010$? Take $j_0 = 6.0 \times 10^{-4} \text{ A cm}^{-2}$, $\alpha = 0.50$.

29.11 (a) How many electrons or protons are transported through the double layer in each second when the $\text{Pt}, \text{H}_2|\text{H}^+$, $\text{Pt}|\text{Fe}^{3+}, \text{Fe}^{2+}$, and $\text{Pb}, \text{H}_2|\text{H}^+$ electrodes are at equilibrium at 25°C ? Take the area as 1.0 cm^2 in each case. Estimate the number of times each second a single atom on the surface takes part in a electron transfer event, assuming an electrode atom occupies about $(280 \text{ pm})^2$ of the surface.

29.11 (b) How many electrons or protons are transported through the double layer in each second when the $\text{Cu}, \text{H}_2|\text{H}^+$ and $\text{Pt}|\text{Ce}^{4+}, \text{Ce}^{3+}$ electrodes are at equilibrium at 25°C ? Take the area

as 1.0 cm^2 in each case. Estimate the number of times each second a single atom on the surface takes part in a electron transfer event, assuming an electrode atom occupies about $(260 \text{ pm})^2$ of the surface.

29.12 (a) What is the effective resistance at 25°C of an electrode interface when the overpotential is small? Evaluate it for 1.0 cm^2 (a) $\text{Pt}, \text{H}_2|\text{H}^+$, (b) $\text{Hg}, \text{H}_2|\text{H}^+$ electrodes.

29.12 (b) Evaluate the effective resistance at 25°C of an electrode interface for 1.0 cm^2 (a) $\text{Pb}, \text{H}_2|\text{H}^+$, (b) $\text{Pt}|\text{Fe}^{2+}, \text{Fe}^{3+}$ electrodes.

29.13 (a) State what happens when a platinum electrode in an aqueous solution containing both Cu^{2+} and Zn^{2+} ions at unit activity is made the cathode of an electrolysis cell.

29.13 (b) State what happens when a platinum electrode in an aqueous solution containing both Fe^{2+} and Ni^{2+} ions at unit activity is made the cathode of an electrolysis cell.

29.14 (a) What are the conditions that allow a metal to be deposited from aqueous acidic solution before hydrogen evolution occurs significantly at 293 K? Why may silver be deposited from aqueous silver nitrate?

29.14 (b) The overpotential for hydrogen evolution on cadmium is about 1 V at current densities of 1 mA cm^{-2} . Why may cadmium be deposited from aqueous cadmium sulfate?

29.15 (a) The exchange current density for H^+ discharge at zinc is about 50 pA cm^{-2} . Can zinc be deposited from a unit activity aqueous solution of a zinc salt?

29.15 (b) The standard potential of the $\text{Zn}^{2+}|\text{Zn}$ electrode is -0.76 V at 25°C . The exchange current density for H^+ discharge at platinum is 0.79 mA cm^{-2} . Can zinc be plated on to platinum at that temperature? (Take unit activities.)

29.16 (a) Can magnesium be deposited on a zinc electrode from a unit activity acid solution at 25°C ?

29.16 (b) Can iron be deposited on a copper electrode from a unit activity acid solution at 25°C ?

29.17 (a) Calculate the maximum (zero-current) potential difference of a nickel-cadmium cell, and the maximum possible power output when 100 mA is drawn at 25°C .

29.17 (b) Calculate the maximum (zero-current) potential difference of a lead-acid cell, and the maximum possible power output when 100 mA is drawn at 25°C .

29.18 (a) Calculate the thermodynamic limit to the zero-current potential of fuel cells operating on (a) hydrogen and oxygen, (b) methane and air. Use the Gibbs energy information in the *Data section*, and take the species to be in their standard states at 25°C .

29.18 (b) Calculate the thermodynamic limit to the zero-current potential of fuel cells operating on propane and air. Use the Gibbs energy information in the *Data section*, and take the species to be in their standard states at 25°C .

29.19 (a) Which of the following metals has a thermodynamic tendency to corrode in moist air at $\text{pH} = 7$: Fe, Cu, Pb, Al, Ag, Cr, Co? Take as a criterion of corrosion a metal ion concentration of at least $10^{-6} \text{ mol L}^{-1}$.

29.19 (b) Which of the following metals has a thermodynamic tendency to corrode in moist air at pH = 7: Ni, Cd, Mg, Ti, Mn? Take as a criterion of corrosion a metal ion concentration of at least $10^{-6} \text{ mol L}^{-1}$.

29.20 (a) The corrosion current density j_{corr} at an iron anode is

1.0 A m^{-2} . What is the corrosion rate in millimetres per year? Assume uniform corrosion.

29.20 (b) The corrosion current density j_{corr} at a zinc anode is 2.0 A m^{-2} . What is the corrosion rate in millimetres per year? Assume uniform corrosion.

Problems

Numerical problems

29.1 In an experiment on the Pt|H₂|H⁺ electrode in dilute H₂SO₄ the following current densities were observed at 25°C. Evaluate α and j_0 for the electrode.

η/mV	50	100	150	200	250
$j/(\text{mA cm}^{-2})$	2.66	8.91	29.9	100	335

How would the current density at this electrode depend on the overpotential of the same set of magnitudes but of opposite sign?

29.2 The standard potentials of lead and tin are -126 mV and -136 mV respectively at 25°C, and the overvoltages for their deposition are close to zero. What should their relative activities be in order to ensure simultaneous deposition from a mixture?

29.3 The limiting current density for the reaction $\text{I}_3^- + 2\text{e}^- \rightarrow 3\text{I}^-$ at a platinum electrode is $28.9 \text{ } \mu\text{A cm}^{-2}$ when the concentration of KI is $6.6 \times 10^{-4} \text{ mol L}^{-1}$ and the temperature 25°C. The diffusion coefficient of I_3^- is $1.14 \times 10^{-9} \text{ m}^2 \text{ s}^{-1}$. What is the thickness of the diffusion layer?

29.4 The maximum theoretical efficiency of a fuel cell may be defined as $\epsilon = |\Delta_r G / \Delta_r H| = |vFE / \Delta_r H|$. However, as indicated in eqn 46, the potential of a working cell is reduced from the zero-current potential. In a hydrogen/oxygen fuel cell with platinum electrodes operating at 373 K, the exchange current densities are $j_a = 100 \text{ mA m}^{-2}$ and $j_c = 3.00 \text{ mA m}^{-2}$. Calculate the efficiency of the cell when operated at a current density of 300 mA m^{-2} with internal resistance of $0.500 \text{ } \Omega \text{ m}^{-2}$. Assume $\alpha \approx 0.5$ and $j/j_{\text{lim}} \approx 0.5$ for both electrodes and assume $E = E^\ominus$. Compare the resulting value to the theoretical maximum efficiency of the cell and to the theoretical maximum efficiency of a heat engine that uses the combustion of hydrogen and oxygen and operates between 373 K and 673 K.

29.5 Estimating the power output and potential of a cell under operating conditions is very difficult, but eqn 47 summarizes, in an approximate way, some of the parameters involved. As a first step in manipulating this expression, identify all the quantities that depend on the ionic concentrations. Express E in terms of the concentration and conductivities of the ions present in the cell. Estimate the parameters for Zn|ZnSO₄(aq)||CuSO₄(aq)|Cu. Take electrodes of area 5 cm^2 separated by 5 cm . Ignore both potential differences and resistance of the liquid junction. Take the concentration as 1 mol L^{-1} , the temperature 25°C, and neglect activity coefficients. Plot E as a function of the current drawn. On the same graph, plot the power output of the cell. What current corresponds to maximum power?

29.6 Consider a cell in which the current is activation-controlled. Show that the current for maximum power can be estimated by plotting $\log(I/I_0)$ and $c_1 - c_2 I$ against I (where $I_0 = A^2 j_a j_c$ and c_1 and c_2 are constants), and looking for the point of intersection of the curves. Carry through this analysis for the cell in Problem 29.5 ignoring all concentration overpotentials.

29.7 Estimate the magnitude of the corrosion current for a patch of zinc of area 0.25 cm^2 in contact with a similar area of iron in an aqueous environment at 25°C. Take the exchange current densities as $1 \text{ } \mu\text{A cm}^{-2}$ and the local ion concentrations as $1 \text{ } \mu\text{mol L}^{-1}$.

29.8 The corrosion potential of iron immersed in a de-aerated acidic solution of pH = 3 is -0.720 V as measured at 25°C relative to the standard calomel electrode with potential 0.2802 V . A Tafel plot of cathodic current density against overpotential yields a slope of 18 V^{-1} and the hydrogen ion exchange current density $j_0 = 0.10 \text{ } \mu\text{A cm}^{-2}$. Calculate the corrosion rate in milligrams of iron per square centimetre per day ($\text{mg cm}^{-2} \text{ d}^{-1}$).

Theoretical problems

29.9 If $\alpha = \frac{1}{2}$, an electrode interface is unable to rectify alternating current because the current density curve is symmetrical about $\eta = 0$. When $\alpha \neq \frac{1}{2}$, the magnitude of the current density depends on the sign of the overpotential, and so some degree of 'faradaic rectification' may be obtained. Suppose that the overpotential varies as $\eta = \eta_0 \cos \omega t$. Derive an expression for the mean flow of current (averaged over a cycle) for general α ; and confirm that the mean current is zero when $\alpha = \frac{1}{2}$. In each case work in the limit of small η_0 but to second-order in $\eta_0 F/RT$. Calculate the mean direct current at 25°C for a 1.0 cm^2 hydrogen-platinum electrode with $\alpha = 0.38$ when the overpotential varies between $\pm 10 \text{ mV}$ at 50 Hz.

29.10 Now suppose that the overpotential is in the high overpotential region at all times even though it is oscillating. What waveform will the current across the interface show if it varies linearly and periodically (as a sawtooth waveform) between η_- and η_+ around η_0 ? Take $\alpha = \frac{1}{2}$.

29.11 Derive an expression for the current density at an electrode where the rate process is diffusion-controlled and η_c is known. Sketch the form of j/j_L as a function of η . What changes occur if anion currents are involved?

Additional problems supplied by Carmen Giunta and Charles Trapp

29.12 The rate of deposition of iron, v , on the surface of an iron electrode from an aqueous solution of Fe^{2+} has been studied as a function of potential, E , relative to the standard hydrogen electrode, by J. Konya (*J. Electroanal. Chem.* 84, 83 (1977)). The values in the table below are based on the data obtained with an electrode of surface area 9.1 cm^2 in contact with a solution of concentration $1.70 \mu\text{mol L}^{-1}$ in Fe^{2+} . (a) Assuming unit activity coefficients, calculate the zero current potential of the Fe^{2+}/Fe cathode and the overpotential at each value of the working potential. (b) Calculate the cathodic current density, j_c , from the rate of deposition of Fe^{2+} for each value of E . (c) Examine the extent to which the data fit the Tafel equation and calculate the exchange current density.

$v/(\text{pmol s}^{-1})$	1.47	2.18	3.11	7.26
$-E/\text{mV}$	702	727	752	812

29.13 The thickness of the diffuse double layer according to the Gouy-Chapman model is given by eqn 23.43. Use this equation to calculate and plot the thickness as a function of concentration and electrolyte type at 25°C . For examples, choose aqueous solutions of NaCl and Na_2SO_4 , ranging in concentration from 0.1 to 100 mmol L^{-1} .

29.14 V.V. Losev and A.P. Pchel'nikov (*Soviet Electrochem.* 6, 34 (1970)) obtained the following current-voltage data for an indium anode relative to a standard hydrogen electrode at 293 K.

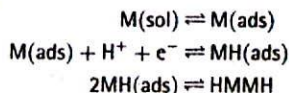
E/V	0.388	0.365	0.350	0.335
$j/(\text{A m}^{-2})$	0	0.590	1.438	3.507

Use these data to calculate the transfer coefficient and the exchange current density. What is the cathodic current density when the potential is 0.365 V?

29.15 The redox reactions of quinones have been the subject of many studies over the years and they continue to be of interest to electrochemists. A relatively recent study is that of E. Kariv, J. Hermolin, and E. Gileadi (*Electrochim. Acta* 16, 1437 (1971)) on methone (1,1-dimethyl-3,5-cyclohexanedione). The current-voltage data for the reduction of this compound (M) in anhydrous butanol on a mercury electrode are:

$-E/\text{V}$	1.50	1.58	1.63	1.72	1.87	1.98	≥ 2.10
$j/(\text{A m}^{-2})$	10	30	50	100	200	250	290

(a) How well do these data fit the empirical Tafel equation? (b) The authors postulate that the reduction product is the dimer HMMH formed by the following mechanism:



The affixes sol and ads refer to species in solution and on the surface of the electrode, respectively. Does this mechanism help to explain the current-voltage data?

29.16 The classic study of the hydrogen overpotential is that of H. Bowden and T. Rideal (*Proc. Roy. Soc.* A120, 59 (1928)), who measured the overpotential for H_2 evolution with a mercury electrode in dilute aqueous solutions of H_2SO_4 at 25°C . Determine the exchange current density and transfer coefficient, α , from their data:

$j/(\text{mA m}^{-2})$	2.9	6.3	28	100	250	630	1650	3300
η/V	0.60	0.65	0.73	0.79	0.84	0.89	0.93	0.96

Explain any deviations from the result expected from the Tafel equation.

MicroProjects Part 3:

Prepared by M. Cady and C. A. Trapp

3.1 Diffusion studies

(a) Show that, for the initial and boundary conditions $c(x, t) = c(x, 0) = c_0$, ($0 < x < \infty$) and $c(0, t) = c_s$ ($0 \leq t < \infty$) where c_0 and c_s are constants, the concentration, $c(x, t)$, of a species is given by

$$c(x, t) = c_0 + (c_s - c_0) \{1 - \operatorname{erf}(\xi)\} \quad \xi(x, t) = \frac{x}{(4Dt)^{1/2}}$$

where $\operatorname{erf}(\xi)$ is the error function (eqn 12.46) and the concentration $c(x, t)$ evolves by diffusion from the yz -plane of constant concentration, such as might occur if a condensed phase is absorbing a species from a gas phase. Draw graphs of concentration profiles at several different times of your choice for the diffusion of oxygen into water at 298 K (when $D = 2.10 \times 10^{-9} \text{ m}^2 \text{ s}^{-1}$) on a spatial scale comparable to passage of oxygen from lungs through alveoli into the blood. Use $c_0 = 0$ and set c_s equal to the solubility of oxygen in water.

(b) Draw graphs of vertical (x) iron concentration, $c(x, t)$, profiles for 5, 10, 15, and 20 h after filling a very wide iron container with molten aluminium at 1273 K, when $D = 2.000 \times 10^{-8} \text{ m}^2 \text{ s}^{-1}$. Assume that the iron dissolves at a steady rate so that the mass flux of iron, $J(x, t)$ with $x \geq 0$, is constant at the iron-aluminium interface, with $J(0, t) = J_0$. In this case, the solution of the diffusion equation is

$$\frac{c(x, t)}{J_0} = \left(\frac{t}{\pi D}\right)^{1/2} e^{-x^2/4Dt} - \frac{x}{2D} \operatorname{erfc}(\xi)$$

where $\operatorname{erfc}(\xi)$ is the complementary error function, $\operatorname{erfc}(\xi) = 1 - \operatorname{erf}(\xi)$. Determine J_0 when $c(3 \text{ cm}, 24 \text{ h}) = 1.2 \text{ mmol L}^{-1}$.

(c) Is it possible that diffusion is the mechanism by which a volatile liquid, like a perfume, becomes distributed around the air of a room? List several situations for which diffusion is important.

3.2 Conductivities of weak (1,1)-electrolyte solutions

A dilute solution of a weak (1,1)-electrolyte contains both neutral ion pairs and ions in equilibrium ($AB \rightleftharpoons A^+ + B^-$). At higher concentrations, or in media of low relative permittivity, the ion pairs may associate with simple ions to form triple ions of the form ABA^+ and BAB^- .

(a) Prove that, in the model for which only ion pairs and simple ions are present, molar conductivities are related to the degree of ionization by the equations

$$\frac{1}{\Lambda_m} = \frac{1}{\Lambda_\alpha} + \frac{(1-\alpha)\Lambda_m}{(\alpha\Lambda_\alpha)^2} \quad \Lambda_\alpha = \lambda_+ + \lambda_- = \Lambda_m^\circ - \mathcal{K}(\alpha c)^{1/2}$$

where Λ_m° is the molar conductivity at infinite dilution and \mathcal{K} is the constant in Kohlrausch's law (eqn 24.31).

(b) The following table contains molar conductivities at 298 K for aqueous iodic acid solutions (R.M. Fuoss and C.A. Kraus, *J. Am. Chem. Soc.* 55, 476 (1933)).

$c/(\text{mmol L}^{-1})$	0.068 517	0.096 291	0.144 572	0.168 284	0.233 308
$\Lambda_m/(\text{S cm}^2 \text{ mol}^{-1})$	389.02	389.02	388.31	388.62	388.31
$c/(\text{mmol L}^{-1})$	0.286 320	0.399 158	0.465 172	0.648 686	0.710 642
$\Lambda_m/(\text{S cm}^2 \text{ mol}^{-1})$	388.04	387.46	387.00	386.12	385.76
$c/(\text{mmol L}^{-1})$	0.986 010	1.023 35	1.436 15	1.494 29	1.528 09
$\Lambda_m/(\text{S cm}^2 \text{ mol}^{-1})$	384.54	384.31	382.20	382.36	382.26
$c/(\text{mmol L}^{-1})$	1.730 67	2.103 23	2.111 08	3.007 36	3.040 44
$\Lambda_m/(\text{S cm}^2 \text{ mol}^{-1})$	380.92	380.09	380.06	376.58	376.77
$c/(\text{mmol L}^{-1})$	5.384 53	5.479 88			
$\Lambda_m/(\text{S cm}^2 \text{ mol}^{-1})$	370.33	370.13			

Develop an extrapolation method to evaluate Λ_m° . Determine the degree of ionization and the mean activity coefficient at each concentration. Calculate the acidity constant. When evaluating the mean activity coefficient, assume the extended Debye-Hückel law of the form

$$-\log \gamma_{\pm} = \frac{A_\gamma(\alpha c)^{1/2}}{1 + B_\gamma(\alpha c)^{1/2}}$$

with $A_\gamma = 0.5044 (\text{mol L}^{-1})^{-1/2}$ and $B_\gamma = 0.0153 (\text{mol L}^{-1})^{-1/2}$. Assume that $\gamma_{AB} = 1$.

(c) The simple ion model in (a) is a basis for a description of the molar conductivities of (b). However, this is not always the case. As an example of the failure of the simple ion model, consider the following molar conductivities for solutions of tetrabutylammonium tetrafluoroborate in 15 mole per cent phenanthrene in anisole, a solvent with a low electric permittivity (A.P. Abott and D.J. Schiffrin, *J. Chem. Soc. Faraday Trans.*, 86, 1453 (1990)).

$c^{1/2}/(\text{mol L}^{-1})^{1/2}$	0.0115	0.0220	0.0278	0.0470	0.0992
$\Lambda_m/(\text{S cm}^2 \text{ mol}^{-1})$	0.0433	0.0341	0.0333	0.0389	0.0705
$c^{1/2}/(\text{mol L}^{-1})^{1/2}$	0.186	0.476	0.844	1.006	1.178
$\Lambda_m/(\text{S cm}^2 \text{ mol}^{-1})$	0.173	0.964	1.51	1.42	1.20

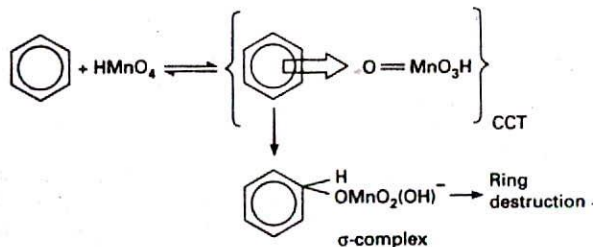
Draw a graph of Λ_m versus $c^{1/2}$. In what range of concentrations might the simple ion model describe conductivities adequately? At what approximate concentration does triple ion formation become important and how does triple ion formation affect conductivity? What happens at high concentrations? Why?

3.3 Destructive oxidation of arenes

The destructive oxidation of alkylarenes by aqueous permanganate may occur by attack upon the alkyl group or by attack upon the aromatic ring. In perchloric acid solution at $\text{pH} \geq 3$ it is thought that permanganate anion attack upon the alkyl group predominates. However, at $\text{pH} \leq 0.3$ permanganic acid attack upon the ring prevails. In this problem, data that concerns the ring oxidation alone will be presented and analysed. A proposed mechanism for the ring

Change

destruction envisions successive formation of a charge-transfer complex (CCT) and a σ -complex as shown below.



This mechanism suggests that reaction activation energies for a homologous series of alkylarenes might be multilinear (that is, $f(x,y) = c_1x + c_2y + c_3$) in both basicity constants (K_b) and ionization energies (I).

(a) Prove that, if the multilinear hypothesis is correct, the rate constant k is given by

$$\Delta \text{pk}(T) = \frac{aT_0 \Delta \text{pk}_b^0 (cT - 1)}{T(cT_0 - 1)} - \frac{b\Delta I}{RT \ln 10}$$

where $\Delta \text{pk} = \text{pk} - \text{pk}_{\text{ref}}$, $\Delta \text{pk}_b = \text{pk}_b - \text{pk}_{b,\text{ref}}$, and $\Delta I = I - I_{\text{ref}}$; 'ref' values are those for a chosen reference compound within the series and K_b^0 is the basicity constant at T_0 . The parameters a , b , and c are temperature-independent properties which may be treated as regression parameters and determined by fitting the equation to experimental rate constants. Assume that $\Delta(\Delta S_b) = c\Delta(\Delta H_b)$, where c is independent of temperature and $\Delta(\Delta X) = \Delta X - \Delta X_{\text{ref}}$. Specify any other assumption that you make.

(b) At 20, 30, 40, 50, 60, and 70°C, $k/(10^{-2} \text{ L mol}^{-1} \text{ s}^{-1}) = 0.86, 2.5, 5.4, 13, 47, \text{ and } 59$, respectively, for 1,4-dimethylbenzene. Determine A and E_a . Derive equations for $\Delta^\ddagger H$ and $\Delta^\ddagger S$ that are appropriate for solution kinetics and calculate their values.

(c) The table below contains kinetic properties for a homologous series (E.S. Rudakov, V.L. Lobachev, and E.V. Zaichuk, *Kinetics and Catalysis* 37, 500 (1996)). The Arrhenius parameters were determined with rate constants measured at the same temperatures as those of (b). Determine the values of a , b , and c using methylbenzene as the reference compound. Develop a graphical method for evaluating the validity of the multilinear hypothesis.

Arene	$\log(A/(\text{L mol}^{-1} \text{ s}^{-1}))$	$E_a/(\text{kJ mol}^{-1})$	pk_b at 273 K	I/eV
benzene	12.5	104	9.2	9.25
methylbenzene	11.4	84	6.3	8.82
1,2-dimethylbenzene	11.2	76	5.3	8.56
1,3-dimethylbenzene	10.5	68	3.2	8.56
1,4-dimethylbenzene	Part b	Part b	5.7	8.44
mesitylene	10.0	56	0.4	8.40
pseudocumene	10.5	62	2.9	8.27
durene	10.6	56	2.2	8.02

3.4 Kinetics of a bromine substitution reaction

Here we consider the reaction $\text{SiCl}_3\text{H}(\text{g}) + \text{Br}_2(\text{g}) \rightarrow \text{SiCl}_3\text{Br}(\text{g}) + \text{HBr}(\text{g})$. The temperature dependence of this reaction has been studied by measuring the degree of conversion, $\alpha(t)$, for initial mixtures of 4.0 volume percentage trichlorosilane and 10.0 volume percentage bromine in helium at 1 bar. The data at four different temperatures are as follows.

$\alpha(160^\circ\text{C}, t) = 0.044$ at 6.07 min; 0.057 at 7.87 min; 0.076 at 10.00 min

$\alpha(180^\circ\text{C}, t) = 0.137$ at 2.72 min; 0.188 at 3.91 min; 0.228 at 5.03 min; 0.273 at 6.67 min; 0.302 at 8.06 min

$\alpha(200^\circ\text{C}, t) = 0.281$ at 1.39 min; 0.395 at 2.16 min; 0.516 at 3.36 min; 0.612 at 5.04 min

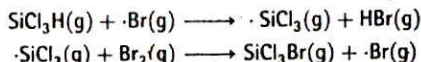
$\alpha(220^\circ\text{C}, t) = 0.592$ at 0.67 min; 0.734 at 1.22 min; 0.866 at 2.16 min

For these reactants it is thought that the dissociation reaction $\text{Br}_2(\text{g}) \rightarrow 2\text{Br}(\text{g})$ is at equilibrium and that, from 300–700 K, the equilibrium constant for the dissociation, can be approximated as $K = 10^{5.1} e^{-C/RT}$, where $C = 190.2 \text{ kJ mol}^{-1}$ and K is expressed in terms of concentrations in moles per cubic centimetre (mol cm^{-3}). No wall effects were observed. Reactions of HBr were discounted and no hexachlorodisilane was observed.

(a) Presume a rate law of the form $d[\text{SiCl}_3\text{Br}]/dt = k[\text{SiCl}_3\text{H}]^a[\text{Br}_2]^b$ and determine the reaction orders a and b .

(b) Determine the rate constant $k(T)$ for each of the four data sets. Evaluate the activation parameters.

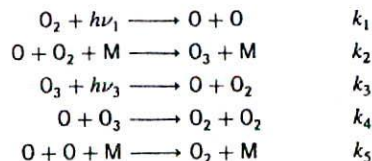
(c) Show that the proposed mechanism



is compatible with the experimental rate law.

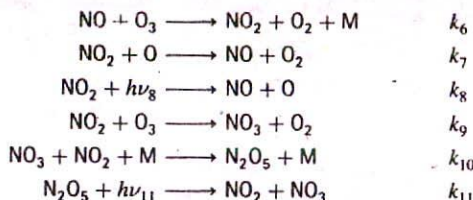
3.5 Photochemical ozone production

The photochemical formation of ozone is a very complex process in the Earth's atmosphere. To simplify the description, consider the experiment in which pure oxygen at 10 Torr and 298 K is exposed to measurable frequencies and intensities of UV radiation. According to the Chapman model, the following elementary reactions contribute to ozone production. (M is a collision partner that must be part of the elementary reaction so as to conserve angular momentum.)



(a) Look up the values of k_2 , k_4 , and k_5 in a source such as the *CRC Handbook of chemistry and physics*. The rate constants k_1 and k_3 depend upon the radiation conditions; assume values of $1.0 \times 10^{-8} \text{ s}^{-1}$ and 0.016 s^{-1} , respectively. Write the rate expressions for the concentration of each chemical species. Assume that the UV radiation is turned on at $t=0$, and solve the rate expressions for the concentration of all species as a function of time over a period of 4 h. Examine relevant concentrations in the very early time period $t < 0.1 \text{ s}$. You will need a software package for solving a set of differential equations and you will find that this set is 'stiff'. Stiff differential equations have at least two rate constants that have widely different values and relate to processes that contribute to the process on very different time scales. The solution to such equations usually requires that the total time period be broken into two or more and solved separately: one may be very short, another very long. State all assumptions. Is there any ozone present initially? Why must the pressure be low and the UV radiation intensities high for the production of ozone? Draw graphs of the time variations of both atomic oxygen and ozone on both the very short and the long time scales. What is the percentage of ozone after 4.0 h of irradiation?

(b) To study the effect of trace amounts of nitrogen dioxide of initial concentration $1.0 \times 10^{12} \text{ molecules cm}^{-3}$, at least the following set of elementary reactions must be added to the Chapman model.



Assume that the values of k_8 and k_{11} are $1.0 \times 10^{-4} \text{ s}^{-1}$ and $1.0 \times 10^{-7} \text{ s}^{-1}$, respectively, and look up the other rate constants in a reference source. Write the rate expressions for the concentration of all chemical species. Solve the set of equations for a time period that allows comparison with the experiment having no nitrogen oxides (a). State all assumptions. Is the ozone production affected in the very early, intermediate, and late time periods? Draw graphs of the time evolution of all chemical species on the relevant time scales. What are your comparative conclusions?

3.6 Autocatalytic mechanisms

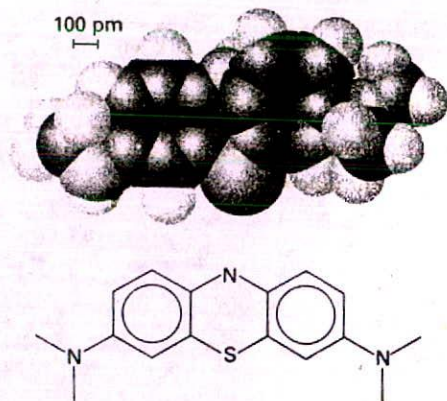
(a) The Lotka-Volterra mechanism may be viewed as being a simple description of the predator-prey relationship with A representing the favourable environmental and nutritional conditions for the prey population, X and Y representing the prey and predator populations, respectively, and B representing predator death. Solve this predator-prey model for the normalized populations of both predator and prey for a 20 year period. Draw graphs for the evolution of the normalized populations. What is the approximate period of the observed oscillations? Why do the oscillations occur? Draw a graph that portrays the limit cycle. What obvious feature of population analysis is missing from this model? In your computations use $k_a = 1 \text{ y}$, $k_b = 1 \text{ y}$, $k_c = 2 \text{ y}$ and the initial normalized conditions $[\text{prey}]_0 = 1$,

$[\text{predator}]_0 = 0.5$. Assume that the environment is unaffected by either species and remains in the normalized steady-state $[\text{environ}] = 1$ throughout the period.

(b) Identify the attractor of Brusselator species when the normalized initial state is $[A]_0 = 1$, $[B]_0 = 1$, $[X]_0 = 30$, and $[Y]_0 = 0.5$. The rate constants are $k_a = 10$, $k_b = 0.01$, $k_c = 0.01$, and $k_d = 10$ in normalized (or 'reduced') units. Assume that A and B are systematically fed into the system so that their concentrations remain constant.

3.7 Adsorption isotherms

A series of experiments designed to measure the adsorption of methylene blue on activated carbon (J.H. Potgieter, *J. Chem. Ed.* **68**, 349 (1991)) uses 100.0 mL of 25.0 mg L^{-1} methylene blue solution. The respective amounts of activated carbon placed in solution were $m/\text{mg} = 1, 5, 10, 12.5, 25, 30$, and 100. After equilibration the corresponding methylene blue concentrations were found to be $c/(\text{mg L}^{-1}) = 19.9, 10.8, 4.2, 3.5, 1.0, 0.70$, and 0.20. Write the equations for the Langmuir and Freundlich adsorption isotherms in a form that is suitable for adsorption from solution. The equations should use concentration, c , and mass fraction adsorbed, x , where x is the mass of solute adsorbed divided by the mass of adsorbent. Perform suitable linear regression fits of the isotherms and critically evaluate the suitability of each fit; compare the statistics of the fits and provide evidence that one or the other is the better fit. Give a critique of the evidence. In addition to the linear relationship suggested in Section 28.4a, write the Langmuir isotherm equation in a form for which x^{-1} versus c^{-1} is expected to be linear and perform the regression analysis. The regression statistics should include the correlation coefficient, the standard deviation or the coefficient of variation, the standard deviation of the intercept, and the standard deviation of the slope. Determine the maximum value of the mass fraction, x_{max} , for this activated carbon sample and use this property to estimate the specific surface area of the adsorbent. The model of methylene blue shown below has the C,N,S frame drawn to scale and can be used to estimate the area occupied by the cation.



3.8 The polarization curve and Tafel plots

Consider a one-electron transfer process for which the transfer is rate-determining.

(a) Draw a graph that shows the dependence of the relative current densities j_a/j_0 , j_c/j_0 , and j'/j_0 on the overpotential. This is the polarization curve. How does variation of the transfer coefficient affect the polarization curve?

(b) Draw a Tafel plot that shows both anodic and cathodic current densities for the platinum electrode process $\text{Ce}^{4+} + \text{e}^- \rightarrow \text{Ce}^{3+}$. Assume that the electron transfer is rate-determining. Explain the graphical methodology for using a Tafel plot of experimental data for evaluation of both the transfer coefficient and the exchange current density. Draw a graph that illustrates the methodology.

3.9 Stationary electrode, reversible voltammetry

The analytic description of reversible redox kinetics at a stationary electrode is well established (R.S. Nicholson and I. Shain, *Anal. Chem.* **36**, 706 (1964)). For a linear-sweep voltammetry experiment with a constant potential scan rate, v , from E_{initial} , the equation for current

density at a flat, non-reactive electrode with linear diffusion to and from the electrode is:

$$j(x) = zF c_{\text{Ox}} (\pi D_{\text{Ox}} z f v)^{1/2} \chi(x)$$

where $x = (E_{\text{initial}} - E)z f$, $f = RT/F$, and

$$\chi(x) = \frac{1}{\pi x^{1/2}(1 + \gamma\theta)} + \frac{1}{4\pi} \int_0^x \frac{1}{(x-y)^{1/2} \cosh^2\left(\frac{1}{2}\{\ln(\gamma\theta) - y\}\right)} dy$$

$$\gamma = \left(\frac{D_{\text{Ox}}}{D_{\text{Red}}}\right)^{1/2} \quad \theta = e^{f(E_{\text{initial}} - E)}$$

Far from the electrode, the bulk concentrations are c_{Ox} and $c_{\text{Red}} = 0$; at the electrode $j_{\text{Ox}} = -j_{\text{Red}}$.

(a) Simulate the reversible electron transfer voltammogram for $\text{Ti}^{3+}/\text{Ti}^{2+}$ reduction. Use $c_{\text{Ox}} = 1.0 \times 10^{-4} \text{ mol L}^{-1}$ and $v = 10 \text{ mV s}^{-1}$. Discuss the physical/chemical properties that cause the variations of the current density revealed by the simulation. How do the values of D_{Ox} and v affect the voltammogram?

(b) Let E_{pc} be the voltammogram peak cathodic potential. Show that both $E_{\text{pc}} \approx E^{\circ'} - (28.5 \text{ mV})/z$ and $E_{\text{p}/2} - E_{\text{pc}} \approx 56.5 \text{ mV}$. List all the experimental criteria for reversibility that are suggested by this simulation. $E_{\text{p}/2}$ is the potential at which $j = \frac{1}{2}j(E_{\text{pc}})$ and $E^{\circ'}$ is the standard formal potential at the ionic strength of the solution.